Nonlinear Dynamics of Poly(hydroxyalkanoate) Production in *Ralstonia eutropha* and *Rhodospirillum rubrum*

Dissertation

zur Erlangung des akademischen Grades

Doktoringenieur (Dr.-Ing.)

von Dipl.-Ing. André Franz

geb. am 02. Juni 1978 in Wriezen

genehmigt durch die
Fakultät für Elektrotechnik und Informationstechnik
der
Otto-von-Guericke-Universität Magdeburg

Gutachter: Prof. Dr.-Ing. Achim Kienle
Prof. Dr. Hartmut Grammel
Prof. Dr.-Ing. Andreas Kremling

Promotionskolloqium am: 24. April 2015

Abstract

This thesis is concerned with the mathematical modeling of the synthesis and metabolization of poly(3-hydroxybutyrate) in microorganisms. Focus is on the bacterium *Ralstonia eutropha* and an outlook is given for the bacterium *Rhodospirillum rubrum*. Poly(3-hydroxybutyrate) is a biopolymer and is synthesized by many organisms as cell-internal carbon and energy storage material.

Previous models in literature usually neglect metabolization of the storage material and/or the cell internal regulation. In the present work, the cell internal regulation was taken into account by choosing a cybernetic modeling approach. This approach was also extended to cell internal metabolites with slow dynamics. For the estimation of model parameters and validation of the model, suitable, experiments were carried out that include both the synthesis and metabolization of the biopolymer. With a nonlinear model analysis it was shown that the metabolization of the storage material plays an important role for the system dynamics.

In a further step model reductions were discussed and evaluated. On the basis of a reduced model, population balance models have been developed which explicitly take the differences in the polymer contents between the individual cells into account. By integrating the cybernetic modeling approach in the population dynamic modeling, the cell internal regulation could be considered.

By conducting own experiments it could also be shown that the wild-type strain H16 of the organism *R. eutropha* is able to grow on glucose as a single substrate without prior mutagenic treatment. This is in contradiction to previous literature. Only a prolonged incubation with high glucose concentration is needed to induce growth on glucose.

Kurzfassung

Die vorliegende Dissertation beschäftigt sich mit der mathematischen Modellierung der Synthese und der Metabolisierung von Polyhydroxybuttersäure in Mikroorganismen. Im Fokus steht hierbei das Bakterium *Ralstonia eutropha*. In einem Ausblick wird die Anwendung der entwickelten Methoden auf das Bakterium *Rhodospirillum rubrum* diskutiert. Polyhydroxybuttersäure ist ein Biopolymer und wird von vielen Organismen als zellinterner Kohlenstoff- und Energiespeicher angelegt.

Bisherige Modelle in der Literatur vernachlässigen in der Regel die Metabolisierung des Speicherstoffes und/oder die zellinterne Regulation. In der vorliegenden Arbeit wurde die zellinterne Regulation durch die Wahl eines kybernetischen Modellierungsansatzes berücksichtigt. Dieser Ansatz wurde zudem so erweitert, dass zellinterne Metabolite berücksichtigt werden können. Für die Parametrisierung und Validierung des Modells wurden geeignete Experimente durchgeführt, die sowohl den Aufbau als auch die Metabolisierung des Biopolymers beinhalten. Mit einer nichtlinearen Analyse wurde das Modell auf Mehrfachstationäritäten hin untersucht und es konnte gezeigt werden, dass die Metabolisierung des Speicherstoffes eine wichtige Rolle in der Systemdynamik spielt.

In einem weiteren Schritt wurden Modellreduktionen diskutiert und bewertet. Auf Grundlage eines reduzierten Modells, wurden populationsdynamische Modelle formuliert, welche explizit die Unterschiede in den Polymergehalten zwischen den einzelnen Zellen berücksichtigen. Diese Unterschiede in den Polymergehalten wurden experimentell mit Hilfe der Durchflusszytometrie bestimmt und mit dem populationsdynamischen Modell verglichen. Durch die Integration des kybernetischen Modellierungsansatz in die populationsdynamische Modellierung konnte auch hier die zellinterne Regulation berücksichtigt werden.

Durch die Durchführung eigener Experimente konnte außerdem gezeigt werden, dass der Wildtyp Stamm H 16 des Organismus *R. eutropha* in der Lage ist, auf Glucose als Einzelsubstrat zu wachsen, auch ohne vorherige mutagene Behandlung. Lediglich eine verlängerte Inkubation mit hohen Glucose Konzenrationen ist dazu notwendig.

Acknowledgment

First and foremost I would like to thank Prof. Achim Kienle for giving me the opportunity to join his research team at the Max Planck Institute and also for his guidance and support during this time. He also gave me the space and time to follow own courses enabling many insights and findings.

I would like to thank Prof. Hartmut Grammel and Prof. Andreas Kremling for their time and effort reviewing this thesis and for their helpfull comments and ideas for future directions.

I would like to thank my collegues for the pleasant working environment and the fruitful and interesting discussions.

I would like to thank Ruxandra Rehner and Hartmut Grammel for their support and input for my work in the laboratory. They gave me many insights and I have learned a lot.

I would also like to thank the team of the mechanical workshop for their fast and excellent support. No matter what mechanical problems arose in the lab, they always found a solution.

Many of my collegues became good friends to me, especially the people from the office S3.18. I would like to thank you for the great time.

And last but not least I would like to thank my own little family for your love and support.

Contents

List of Figures

List of Tables

Glossary

Abbreviations

AM	Active mode
BODIPY	Boron-dipyrromethene
CDW	Cell dry weight
CM	Cybernetic model
DAPI	4',6-Diamidin-2-phenylindol
DNA	Deoxyribonucleic acid
EM	Elementary mode
FSC	Forward scatter
GM	Generating mode
HCM	Hybrid cybernetic model
MYA	Metabolic yield analysis
RNA	Ribonucleic acid
ROI	Return on investment
PBS	Phosphate buffered saline
PHA	Polyhydroxyalkanoate
P(3HA)	Poly(3-hydroxyalkanoate)
P(3HB)	Poly(3-hydroxybutyrate)
TBM	Total biomass (dry weight)
YS	Yield space

Metabolites

3HA	3-hydroxyalkanoate

3PG	3-phosphoglycerate
αKG	Alpha-ketoglutarate
AcAcCoA	Acetoacetyl CoA
AcCoA	Acetyl CoA
ACE	Acetoacetate
ADP	Adenosine diphosphate
ATP	Adenosine triphosphate
AMC	Ammonium chloride
AMS	Ammonium sulfate
BIO	Non-P(3HB) biomass
CO_2	Carbon dioxide
E4P	Erythrose-4-phosphate
F16P	Fructose-1,6-Bisphosphate
F6P	Fructose-6-Phosphate
FAD	Flavin adenin dinucleotide, oxidized
FADH	Flavin adenin dinucleotide, reduced
Form	Formiate
FRU	Fructose
G3P	Glyceraldehyde-3-phosphate
G6P	Glucose-6-phosphate
GLC	Glucose
GLM	Glycolytic intermediates (pool)
GLUM	Glutamine
GLUT	Glutamate
GOX	Glyoxylate
ISC	Isocitrate
MAL	Malate
NAD	Nicotinamide adenine dinucleotide, oxidized
NADH	Nicotinamide adenine dinucleotide, reduced
NADP	Nicotinamide adenine dinucleotide phosphate, oxidized
NADPH	Nicotinamide adenine dinucleotide phosphate, reduced
NH_3	Ammonia

O_2	Oxygen
OXA	Oxaloacetate
PEP	Phosphoenol pyruvate
PYR	Pyruvate
R5P	Ribose-5-phosphate
Rl5P	Ribulose-5-phosphate
S7P	Sedoheptulose-7-phosphate
SUC	Succinate
SucCoA	Succinyl-CoA
SUCx	Succinate, external
X5P	Xylulose-5-phosphate

Nomenclature

b	fraction of catalytically active parts in biomass
c	biomass concentration
D	dilution rate
$\mathbf{e}$	vector of enzyme levels
$\mathbf{e}^{\max}$	vector of maximum enzyme levels
$\mathbf{e}^{\mathrm{rel}}$	vector of relative enzyme levels
$\mathbf{f_c}$	vector of uptaken carbon units
$\mathbf{h}$	weight vector for the modes of $\mathbf{Z_y}$
$\mathbf{k_e}$	vector of enzyme synthesis rate constants
$\mathbf{k_r}$	vector of rate constants
K_{AMC}	saturation constant for ammonium chloride
K_{FRU}	saturation constant for fructose
$K_{\mathrm{P(3HB)}}$	saturation constant for P(3HB)
$\mathbf{m}$	vector of specific internal concentrations
$\mathbf{m_f}$	vector of specific internal concentrations with fast dynamics
$\mathbf{m_s}$	vector of specific internal concentrations with slow dynamics
$m_{\mathrm{P(3HB)}}$	specific concentration of P(3HB)
OD_λ	Optical density at wave length λ

$\mathbf{p}$	vector of *returns on investment*
$\mathbf{r}$	vector of regulated fluxes
$\mathbf{r_M}$	vector of regulated fluxes through EMs
$\mathbf{r}_\mathbf{M}^{\text{kin}}$	purely kinetic part of $\mathbf{r_M}$
$\mathbf{r_{EM}}$	vector of regulated enzyme synthesis rates of EMs
$\mathbf{r}_\mathbf{EM}^{\text{kin}}$	purely kinetic part of $\mathbf{r_{EM}}$
$\mathbf{S_m}$	stoichiometry matrix of internal metabolites
$\mathbf{S_{m,f}}$	stoichiometry matrix of internal metabolites with fast dynamics
$\mathbf{S_{m,s}}$	stoichiometry matrix of internal metabolites with slow dynamics
$\mathbf{S_p}$	stoichiometry matrix of products
$\mathbf{S_s}$	stoichiometry matrix of substrates
$\mathbf{u}$	vector of cybernetic variables which control enzyme synthesis
$\mathbf{v}$	vector of cybernetic variables which control enzyme activity
$\mathbf{x}$	vector of external metabolite concentrations
$\mathbf{x_s}$	vector of substrate concentrations
$\mathbf{x_p}$	vector of product concentrations
x_{AMC}	concentration of ammonium chloride
x_{FRU}	concentration of fructose
$x_{\text{AMC}}^{\text{in}}$	concentration of ammonium chloride at inlet
$x_{\text{FRU}}^{\text{in}}$	concentration of fructose at inlet
$\mathbf{y}$	state vector of a metabolic system
$\mathbf{y_m}$	vector of measured yield data
$\mathbf{Z}$	EM matrix
$\mathbf{Z_y}$	normalized EM matrix
$\mathcal{M}-$	set of internal metabolite consuming EMs
$\mathcal{M}+$	set of internal metabolite producing EMs
$\boldsymbol{\alpha}$	vector of constitutive enzyme synthesis rates
$\boldsymbol{\beta}$	vector of enzyme consumption constants
ε_λ	attenuation coefficient
γ	feed composition
λ	wave length
μ	growth rate

1. Introduction

1.1. Motivation

Nowadays, one can hardly imagine a world without plastics. Plastics have changed our everyday life. It brings many technological, medical and societal advantages, since it is light weight, durable, strong, corrosion-resistant, has high thermal and electrical insulation properties and its production is very cheap. Due to this versatility a wide range of products (e. g. packaging, cases for electronical devices, medical implants, furniture) are made from various types of plastics featuring different properties. The use and therefore the production of plastics has strongly increased in the last decades (see Figure 1.1). In 2012 almost 300 million tonnes of synthetic plastics were produced world wide [57].

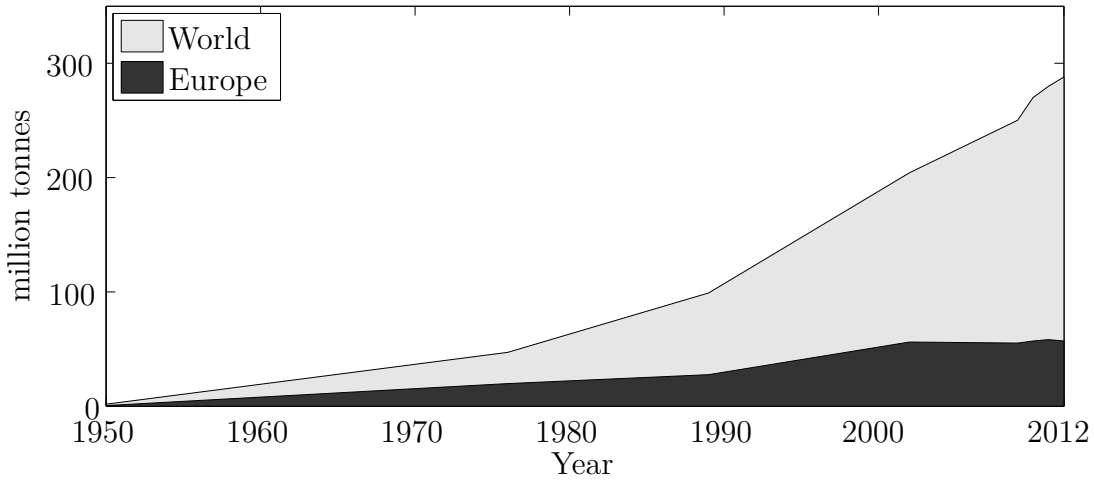

Figure 1.1.: Annual synthetic plastics production [57].

On the other hand, synthetic plastics hardly decompose and a large amount of these plastics have accumulated in landfills and natural environment. Today, 90%

of the rubbish in world's ocean is plastic [8, 22, 53] and it represents more than 10 percent of the municipal waste [3]. Over a third of plastic is used for packaging [81], which is usually only used once and then discarded. This is not sustainable at all, especially since 4 percent of the worlds oil production is used as feedstock for making plastic and yet another 4 percent is used as energy in the process [81, 82].

Plastics are not only harmful to natural environment, but also to human health. The versatility in thermal and mechanical properties is achieved by use of a wide range of chemicals, where some of them are known to be toxic or linked to reproductive problems or cancer. For example, polyethylene terephtalate (PET) releases endocrine disrupting chemicals like acetaldehyde, polyvinylchloride (PVC) leaches phthalates, carcinogens and dioxins, and polystyrene (PS) leaches very toxic brominated flame retardants over their entire life span.

In summary, plastics have a lot of advantages due to their versatility, but they also have some drawbacks, which can be classified into: environmental pollution, sustainability and human health issues.

To overcome these problems, different approaches are needed and some of them are already applied. Recycling of plastics, for instance, can reduce environmental pollution and safes oil and energy. Some countries (e.g. Bangladesh, Bhutan, France, Papua New Guinea, Rwanda, Tanzania) have even banned non-decomposable plastic bags to reduce pollution of the environment.

A different approach is the substitution of synthetic plastics with so called bioplastics [27]. These are polymers made from biomass (e.g. plants or microorganisms such as bacteria or fungi) and are usually biodegradable and even biocompatible. This has several advantages: production of biopolymers is independent from fossil resources, decomposition of bio-based plastics is usually much faster than decomposition of oil-based plastics [71, 73] and bio-based plastics are less or even not harmful to human health.

Several plants and microorganisms are able to synthesize these biopolymers as internal energy and carbon reserve material. For example, starch and cellulose are well known polymers, which can be synthesized by maize, wheat and sugar beet. Poly(lactic acid) is also a well known bioplastic, where only the monomer is synthesized by microorganisms via fermentation and later synthetically polymerized. Poly(hydroxyalkanoates) are also a major class of biopolymers, which are usually

synthesized by microorganisms, but also by transgenic plants [33, 61, 80].

Although there are a wide range of biopolymers known today, they only represent a very small fraction of the total amount of plastics. This has several reasons. For instance, production of bioplastics by plants (e.g. starch-based) may occupy fields for food production. Furthermore, industrial production of bio-based plastic is usually much more expensive than production of oil-based plastics, e.g. due to higher feedstock prices. Additionally, polymerization of biopolymers usually happens within the cells of microorganisms or plants. But cell internal processes are still not fully understood and are also very challenging to control in order to achieve desired polymer properties. But this is of course subject to current research activity, which aims at a better understanding of the underlying metabolic processes. This understanding is necessary to improve and optimize industrial production or to control and adjust certain polymer properties.

It is obvious, that the research field of biopolymers is huge and includes experimental as well as theoretical research. Experiments are usually the basis for theoretical studies, where experimental knowledge is translated into mathematical models. These models can help to analyze known behaviour and processes or to predict unknown behavior and unknown processes. For validation, extension or modification of these theoretical studies, new experiments are needed again. Interaction of theory and experiment is therefore very important.

The present thesis is contributing to this suspenseful research area. The focus is on poly(3-hydroxybutyrate), which belongs to the class of poly(hydroxyalkanoates) mentioned above. This bioplastic can be produced by several microorganisms and even plants. A well known poly(3-hydroxybutyrate) producing organism is the bacterium *R. eutropha* and this thesis will mainly focus on this organisms. Additionally, there are some new and very promising poly(3-hydroxybutyrate) producing organisms, e.g. the facultative photosynthetic bacterium *R. rubrum*, which is also subject of this thesis.

1.2. State of the Art and Objectives

As mentioned above, mathematical modeling is crucial to gain a better understanding of the underlying biochemical processes and for a systematical optimization of

industrial processes. Experiments build the basis of mathematical models and are very important to identify model parameter and to validate mathematical models.

As the importance of biopolymers increased over the last decades, as outlined above, extensive experimental and theoretical work already exists in literature. Among this work several researchers have modeled the production of the biopolymer poly(3-hydroxybutyrate) in *R. eutropha*, but no mathematical models, which describe poly(3-hydroxybutyrate) synthesis in *R. rubrum*, are published so far.

Mathematical models for poly(3-hydroxybutyrate) synthesis in microorganisms are derived from the knowledge, when and how poly(hydroxyalkanoates), in particular poly(3-hydroxybutyrate), are synthesized or even metabolized. Accumulation of poly(hydroxyalkanoates) is favored under excess of carbon source or unbalanced growth conditions, e.g. lack of essential nutrients such as nitrogen, phosphorus, etc., and can also be metabolized again if the limitation is removed. Therefore, the following three main processes have to be included into mathematical modeling:

- growth
- synthesis of poly(hydroxyalkanoates)
- metabolization of poly(hydroxyalkanoates).

It is convenient to divide the cell into two main compartments, namely internal storage material (e.g. poly(hydroxyalkanoates) (PHAs)) and residual biomass. These two compartments and three main processes are shown in Figure 1.2. The residual biomass contains all the proteins, lipids and DNA, and is therefore the catalytically active compartment.

Besides these three main processes, it is also crucial to include the ability of microorganisms to switch between these processes. Adaption of the microorganism to changing environmental condition and therefore switching between different cell internal processes is subject of cell internal regulation.

With increasing knowledge of cell internal processes and regulation, several models where already presented in literature. These models can be classified according to:

- unstructured models vs. structured models
- models which consider cell internal regulation vs. models which do not consider cell internal regulation

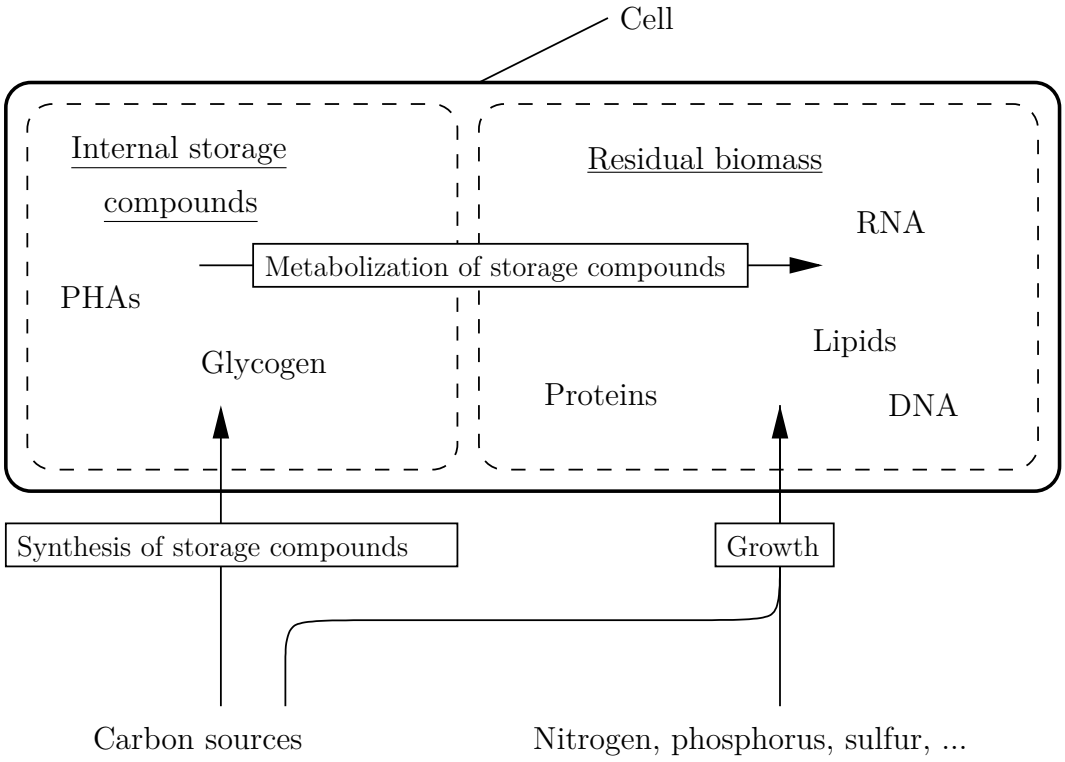

Figure 1.2.: Cell compartments and main processes.

- single cell models vs. models on population level

Early models were usually unstructured models, which do not explicitly address the underlying metabolic processes ([30, 54, 62, 78]). Process optimization [34, 35, 36] was often based on these unstructured and simple models. Since knowledge on cell internal structures increased, models arose, which addressed these structures [20, 60, 59]. Still, they are usually based on very simplified metabolic networks.

With increasing knowledge of metabolic structure, also cell internal regulation moved more and more into focus. However, cell internal regulation is very complex and still not fully understood, but can be included in a simplified way into metabolic modeling via the cybernetic modeling framework, [43, 63, 65].

Including regulatory features into modeling of biopolymer production is crucial. Depending on availability of cell external substrates and the state of cell internal metabolites, the organism regulates whether biopolymer is produced, metabolized or the organism grows without biopolymer synthesis. Cell internal regulation was therefore not only addressed in unstructured models for biopolymer synthesis in

R. eutropha [93], but also in structured models [20, 59, 60].

So far, all models usually neglect metabolization of biopolymer, which is obvious, if the focus is only on the synthesis of biopolymer. However, metabolization of biopolymer is an important metabolic process and can not be neglected if the model shall explain a wide range of metabolic behaviour. Metabolization of biopolymer in *R. eutropha* is included in the structure of some models [20, 59, 60], but parameters of these models were identified from experimental data which do not include biopolymer metabolization in reasonable amount.

An overview of these dynamic single cell models for biopolymer production in *R. eutropha* is given in Table 1.1. All of these models are non-segregated models, which are only able to predict average properties of the cells, but neglect cell to cell variance w.r.t. intracellular compounds. In contrast, heterogeneity can be described within the framework of population balance modeling. First attempts to describe poly(3-hydroxybutyrate) production in *R. eutropha* by a population balance model was recently published [66]. However, in this publication cell internal regulation is neglected and no comparison with experimental data is shown.

Focus of this thesis is to formulate a structured single cell model for the synthesis and metabolization of the biopolymer poly(3-hydroxybutyrate) in *R. eutropha*, which includes cell internal regulatory features within the framework of cybernetic modeling. To include metabolization of the biopolymer appropriate experiments where performed, which include a wide range of metabolic behaviour, including growth, synthesis and metabolization of poly(3-hydroxybutyrate). Multiple independent experiments were performed for parameter identification and validation of the model.

In a further step, based on the single cell model, different population balance models were formulated to describe the heterogeneity of the cells regarding their cell internal amount of poly(3-hydroxybutyrate). First, a two-dimensional population balance model is proposed, that considers the cell internal biopolymer and residual biomass as internal coordinates. However, concentration of internal biopolymer and amount of residual biomass are difficult to determine and usually include complex staining procedures, which are often very toxic for bacterial cells. Therefore afterwards a one-dimensional population balance model is discussed by means of correlating cell size with biopolymer concentration.

Table 1.1.: Theoretical studies for poly(3-hydroxybutyrate) synthesis in different strains of *R. eutropha* with different carbon sources. The column *exp.* indicates, if in the particular study also experiments were performed. Only a few of these studies use structured models (struct.) and consider cell internal regulation (regul.). Metabolization of poly(3-hydroxybutyrate) (P(3HB) met.) is also only considered in very few studies.

strain	carbon	exp.	struct.	regul.	P(3HB) met.	Ref.
ATCC 17697	fructose	✓				[34]
ATCC 17697	fructose	✓				[35]
ATCC 17697	fructose	✓				[36]
ATCC 17697	fructose	✓				[54]
ATCC 17697	fructose	✓				[62]
ATCC 17699	CO_2	✓				[30]
ATCC 17699	CO_2	✓				[78]
ATCC 17699	lactate					[83]
NCIMB 11599	glucose	✓		✓		[93]
NCIMB 11599	glucose		✓	✓	✓	[20]
NCIMB 11599	glucose		✓	✓	✓	[59]
NCIMB 11599	glucose		✓	✓	✓	[60]
NCIMB 11599	glucose	✓				[48]
NCIMB 11599	glucose	✓				[72]

For *R. rubrum* no dynamic models for poly(3-hydroxybutyrate) production exist so far in literature. However, *R. rubrum* is a new and promising candidate for poly(3-hydroxybutyrate) production. The findings for *R. eutropha* are therefore partially transferred to *R. rubrum* and discussed.

1.3. Structure of this Thesis

This thesis couples metabolic modeling of the poly(3-hydroxybutyrate) production in *R. eutropha* and *R. rubrum* with goal-oriented experiments needed for parameter identification and model validation. In the first part of this thesis general methods and basic principles are introduced, experimental methods in Chapter 2 and theoretical methods in Chapter 3.

The second part addresses the specific organism *R. eutropha*. Chapter 4 focuses on experiments with different substrates such as glucose, fructose and acetate.

Chapter 5 focuses on the modeling of the poly(3-hydroxybutyrate) synthesis and metabolization in *R. eutropha*.

The third part addresses the organism *R. rubrum*. In Chapter 6 the application of the developed methods for *R. eutropha* on *R. rubrum* are discussed.

The last part concludes and summarizes this thesis in Chapter 7.

1.4. Publications

A part of the work contained in this thesis has already been published in peer-reviewed literature and presented at conferences. Here is a list of those publications:

Journal paper

- André Franz, Hyun-Seob Song, Doraiswami Ramkrishna, Achim Kienle. Experimental and theoretical analysis of poly(β-hydroxybutyrate) formation and consumption in Ralstonia eutropha. *Biochemical Engineering Journal*, 55:49-58, 2011 (doi:10.1016/j.bej.2011.03.006)
- André Franz, Ruxandra Rehner, Achim Kienle, Hartmut Grammel. Rapid selection of glucose-utilizing variants of the polyhydroxyalkanoate producer Ralstonia eutropha H16 by incubation with high substrate levels. *Letters in Applied Microbiology*, 54:45-51, 2012 (doi:10.1111/j.1472-765X.2011.03171.x)

Papers in conference proceedings

- André Franz, Hyun-Seob Song, Doraiswami Ramkrishna, Achim Kienle. Hybrid Cybernetic Modeling of Poly-Beta-Hydroxybutyrate Synthesis and Degradation in Cupriavidus necator. *AIChE Annual Meeting, Conference Proceedings*, Nashville, TN, USA, 2009
- André Franz, Hartmut Grammel, Ruxandra Rehner, Achim Kienle. Nonlinear Dynamics of Poly(β-hydroxybutyrate) Production In Microorganisms. *AIChE Annual Meeting*, Minneapolis, MN, USA, 2011

- André Franz, Hartmut Grammel, Ruxandra Rehner, Philipp Paetzold, Achim Kienle. Multiscale modeling of bioploymer production in multicellular Systems. *Proceedings to the 7th Vienna International Conference on Mathematical Modeling - MATHMOD 2012*, 326-330, 2012 (doi:10.3182/20120215-3-AT-3016.00057)
- André Franz, Robert Dürr, Achim Kienle. Population balance modeling of biopolymer production in cellular systems. *Proceedings of the 19th IFAC World Congress*, 1705-1710, 2014 (doi:10.3182/20140824-6-ZA-1003.01504)

2. Experimental Methods

2.1. Organisms

2.1.1. *R. eutropha*

R. eutropha is a gram-negative bacterium, which was renamed several times in the past (e.g. *Hydrogenomonas eutropha*, *Alcaligenes eutrophus*, *Wautersia eutropha*) [7, 87, 92]. Recently, it has been classified as *Cupriavidus necator* [86]. However, in this study the name *R. eutropha* is used, since this name is still commonly used, even in recent literature. The genus was first described by N. S. Makkar and L. E. Casipa [49]. *R. eutropha* is rod shaped and peritrichous flagellated [2] and can have a diameter of 0.7 - 0.9 μm and a length of 0.9 - 1.3 μm.

Different strains of the genus *R. eutropha* are known. In this study, the wild-type strain H16 (DSM 428, ATCC 17699, NCIB 10442) is used. This strain was first isolated from soil by Wilde in 1962 [90].

The organism was obtained from DSMZ GmbH Braunschweig, Germany, as vacuum dried culture. In addition, NCCB, Utrecht, the Netherlands was chosen as a supplier of the same strain, as discussed in Chapter 4.3.

In this study, *R. eutropha* was cultivated under aerobic conditions in LB medium (see Table A.1) or mineral medium (see Table A.2). Fructose, glucose and acetate were applied as carbon sources with varying concentration in each particular experiment. The ammonia concentration was also varied in each particular experiment.

Permanent cultures were prepared in a mixture of glycerol and mineral medium (1:3) and stored at -80°C.

2.1.2. *R. rubrum*

R. rubrum is a gram-negative bacterium, which is facultative photosynthetic. Under anaerobic conditions *R. rubrum* satisfies its energy needs via photosynthesis, which leads to a purple color due to the production of carotenoids. Under aerobic conditions photosynthesis is suppressed and *R. rubrum* is colorless.

In this study, the strain *R. rubrum* S1 (DSM 467, ATCC 11170, NCIB 8255) is used and was obtained from DSMZ GmbH Braunschweig, Germany, as vacuum dried culture.

R. rubrum was cultivated under aerobic and dark conditions with LB medium (see Table A.1) or mineral medium (see Table A.4).

Permanent cultures were prepared in a mixture of glycerol and mineral medium (1:3) and stored at -80℃.

2.2. Poly(hydroxyalkanoates)

Poly(hydroxyalkanoates) are linear polyesters, which can be synthesized by many bacteria, e.g. *R. eutropha* and *R. rubrum*. These poly(hydroxyalkanoates) serve as cell internal carbon storage and energy reserve material [11]. Since these polyesters are not only biogen, but also biodegradable they are a promising alternative for oil-based plastics. Additionally, poly(hydroxyalkanoates) are biocompatible, which is in particular interesting for medical applications.

In this study the focus is on poly(3-hydroxyalkanoate), in particular, on poly(3-hydroxybutyrate).

In Figure 2.1 the chemical structure of the monomer 3-hydroxyalkanoate is shown [11]. Depending on the functional group (R in Figure 2.1) 3-hydroxyalkanoates can be classified. The classification is given in Table 2.1, e. g. for poly(3-hydroxybutyrate) R=CH_3 (methyl).

R. eutropha is able to synthesize 3-hydroxyalkanoates with a chain length of C3-C5 [13, 14, 11] and even copolymers, e.g. P(3HB-co-4HB) [12]. *R. rubrum* is able to synthesize 3-hydroxyalkanoates with a chain length of C4-C7 [6]. The chain lengths are given in Table 2.1.

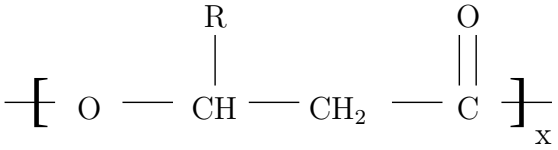

Figure 2.1.: Chemical structure of poly(3-hydroxyalkanoate). For classification, depending on the functional group R, see Table 2.1.

Table 2.1.: Classification of 3-hydroxyalkanoate units with different chain length.

R	Name	Chain length
hydrogen	3-hydroxypropionate (3HP)	C3
methyl	3-hydroxybutyrate (3HB)	C4
ethyl	3-hydroxyvalerate (3HV)	C5
propyl	3-hydroxycaproate (3HC)	C6
butyl	3-hydroxyheptanoate (3HH)	C7
pentyl	3-hydroxyoctanoate (3HO)	C8
hexyl	3-hydroxynonanoate (3HN)	C9
heptyl	3-hydroxydecanoate (3HD)	C10
octyl	3-hydroxyundecanoate (3HUD)	C11
nonyl	3-hydroxydodecanoate (3HDD)	C12

2.3. Cultivation

R. eutropha and *R. rubrum* were grown in a single biorector, a parallel bioreactor system or in shake flasks. In the following, the processes for each cultivation system are given. Potential modifications of these processes are given in the particular experimental section.

2.3.1. Bioreactor

The used bioreactor was a 7 liter fermenter (Biostat C, Sartorius, BBI Systems, Melsungen, Germany) with a 5 liter working volume (see Figure 2.2). The temperature in this bioreactor was kept constant at 30℃ and pH was automatically maintained at pH 6.8 by adding 2 mol/l NaOH as corrective agent. The culture broth was stirred at 400 rpm and dissolved oxygen was maintained above 70% air saturation with sterilized air at a constant flow rate of 1.5 ml/min. At higher biomass levels, the oxygen supply was changed to oxygen and nitrogen mixed with a gas mix station.

Figure 2.2.: Single bioreactor (left) with a 7 liter vessel and parallel bioreactor system (right) with up to 4 × 750 ml fermenters.

2.3.2. Parallel Bioreactor System

With the parallel bioreactor system (Dasgip, Jülich, Germany) (see Figure 2.2) up to four fermenters can be operated in parallel, but controlled individually. Fermenters with a volume of 750 ml or 400 ml were used. The temperature was kept constant at 30℃. The parallel bioreactor system allows control of various process parameters (e. g. pH value, oxygen saturation, ...). However, for this thesis the parallel bioreactor system was mainly used for cultivations with very low cell density, where control of these parameters are not crucial and consequently not applied.

2.3.3. Shake-Flask

Shake-flask cultivations of *R. eutropha* were carried out at 27℃ in a rack-shaker system at 150 rpm in baffled shake-flasks containing LB or mineral medium. Shake-flask cultivations of *R. rubrum* were carried out at 30℃.

2.4. Analytical Procedures

2.4.1. Optical Density and Biomass Concentration

For monitoring cell growth, the optical density of the cell suspension was measured with an Ultrospec 500 spectrophotometer (GE Healthcare, Buckinghamshire, UK) using a wavelength of 600 nm for *R. eutropha* and 660 nm for *R. rubrum*. Cell suspension was diluted with NaCl (0.98 % (w/v)) when necessary to ensure a measured optical density value within a linear range.

Total biomass concentration (g/l) was measured by determination of the cell dry weight. For that purpose, 10 ml of cell suspension were centrifuged in pre-weighed glass tubes at 3000 × g. The pellets were washed in NaCl (0.98% (w/v)) and subsequently dried in a freeze-dryer (Christ, Osterode am Harz, Germany). From the weight difference and the sample volume the biomass concentration was calculated. For each sample this procedure was done three times.

2.4.2. Poly(3-hydroxybutyrate)

Poly(3-hydroxybutyrate) content was measured as crotonic acid, formed by acid depolymerization of poly(3-hydroxybutyrate) [47]. Cell pellets, harvested by centrifugation, were dissolved in methylene chloride by rapid mixing and afterwards boiled for 10 min. After the samples were cooled down, they were centrifuged at 3000 × g for 15 min and the supernatants were carefully removed and collected in glass tubes. This procedure was repeated three times. The supernatants were then evaporated and the remaining poly(3-hydroxybutyrate)-containing samples were digested in 2 ml H_2SO_4 (96 %) at 100°C for 30 min and subsequently diluted with concentrated H_2SO_4. UV absorbance spectra were measured with an UV-vis spectrophotometer V-560 (Jasco, Gross-Umstadt, Germany). The concentration of crotonic acid was calculated from a set of reference standards.

2.4.3. Estimation of Poly(3-hydroxybutyrate) Concentration from Optical Density

Based on the Beer-Lambert law

$$\mathrm{OD}_\lambda = -\log\left(\frac{I}{I_0}\right) = \varepsilon_\lambda \, c \, l \quad , \tag{2.1}$$

biomass concentration c can be proportionally correlated to optical density OD_λ

$$c \sim \mathrm{OD}_\lambda \quad , \tag{2.2}$$

if attenuation coefficient ε_λ and the path length l are constant. Most spectrophotometers use a standardized path length of $l = 1$ cm. The attenuation coefficient ε_λ depends on wave length λ and specific properties of the cells, e. g. size, form, composition.

This correlation offers a very fast and simple method to analyse biomass concentration and is therefore commonly used in biology. However, this is only valid if the attenuation coefficient ε is constant, which is only true, if cells (e.g. in form or composition) do not change significantly.

In case of accumulation of poly(3-hydroxybutyrate), cells will change their composition and will additionally significantly grow in size. Therefore optical density cannot be used for direct estimation of the cell dry weight during poly(3-hydroxybutyrate) accumulation, but only for monitoring the growth process.

However, in this case, the biomass can be viewed as a combination of two compartments, namely the storage compound poly(3-hydroxybutyrate) and the residual biomass (BIO), which is the non-poly(3-hydroxybutyrate) biomass compartment. For these two compartments, it can be assumed, that their specific concentration will change, but not their composition. The optical density will obviously not only depend of the total biomass concentration but also on the particular concentration of poly(3-hydroxybutyrate) $c_{\mathrm{P(3HB)}}$ and residual biomass c_{BIO}

$$\mathrm{OD}_\lambda = l \, \varepsilon_{\lambda,\mathrm{P(3HB)}} \, c_{\mathrm{P(3HB)}} + l \, \varepsilon_{\lambda,\mathrm{BIO}} \, c_{\mathrm{BIO}} \quad , \tag{2.3}$$

where

$$c = c_{\mathrm{P(3HB)}} + c_{\mathrm{BIO}} \tag{2.4}$$

holds.

Once $l\,\varepsilon_{\lambda,\mathrm{P(3HB)}}$ and $l\,\varepsilon_{\lambda,\mathrm{BIO}}$ are known, the correlation in equation (2.3) can be used to calculate the poly(3-hydroxybutyrate) concentration of a sample, if optical density and concentration of residual biomass are known. This is very convenient, since direct measuring of poly(3-hydroxybutyrate) with the method described in section 2.4.2 is very complex and involves a lot of steps, and a relative huge amount of biomass is needed. In contrast, optical density is rather easy to determine even from small volumes.

However, to calculate the concentration of poly(3-hydroxybutyrate) from optical density, also knowledge about the concentration of the residual biomass (BIO) is needed, which is only synthesized if a nitrogen source (e.g. ammonium chloride) is available. It is therefore obvious to calculate the synthesized amount of the residual biomass from the amount of uptaken nitrogen source.

For *R. eutropha*, the amount of needed ammonium chloride (AMC) to synthesize 1 g BIO can be calculated from the metabolic network in Chapter 5.1 and the reaction equations in Appendix A.2 to

$$8.82\,\mathrm{mmol\ AMC} \rightarrow 1\,\mathrm{g\ BIO} \quad . \tag{2.5}$$

From the experimental data `Ralst01FruSingle` and `Ralst02FruSingle` in Chapter 4 the following correlation between optical density at 600 nm (OD_{600}) and biomass concentrations (c_{BIO} and $c_{\mathrm{P(3HB)}}$) is estimated to

$$\mathrm{OD}_{600} = 2.80\,c_{\mathrm{BIO}} + 4.76\,c_{\mathrm{P(3HB)}} \quad . \tag{2.6}$$

The experimental data from `Ralst03FruSingle` and `Ralst04FruSingle` are used to validate this correlation, which is shown in Figure 2.3. The figure shows the measured optical density in comparison with the estimated optical density. If the concentration of poly(3-hydroxybutyrate) is known (e.g. measured), then the concentration of residual biomass can be calculated from the concentration c of the cell dry weight, which is $c_{\mathrm{BIO}} = c - c_{\mathrm{P(3HB)}}$. If concentration of poly(3-hydroxybutyrate) is not known, then the concentration of residual biomass can be calculated from uptaken ammonium chloride according Equation (2.5). As seen in this figure, the correlation is in good agreement with the experimental data. The correlation can

therefore be used to estimate poly(3-hydroxybutyrate) concentration only from optical density and uptaken amount of nitrogen source. This is very useful if there are only small volumes available, e.g. from small fermenter or shake flasks. However, precise measurement of ammonium concentration is crucial, since only little ammonium is needed to synthesize biomass. For *R. eutropha* it is only 8.82 mmol NH_4 for 1 g of residual biomass.

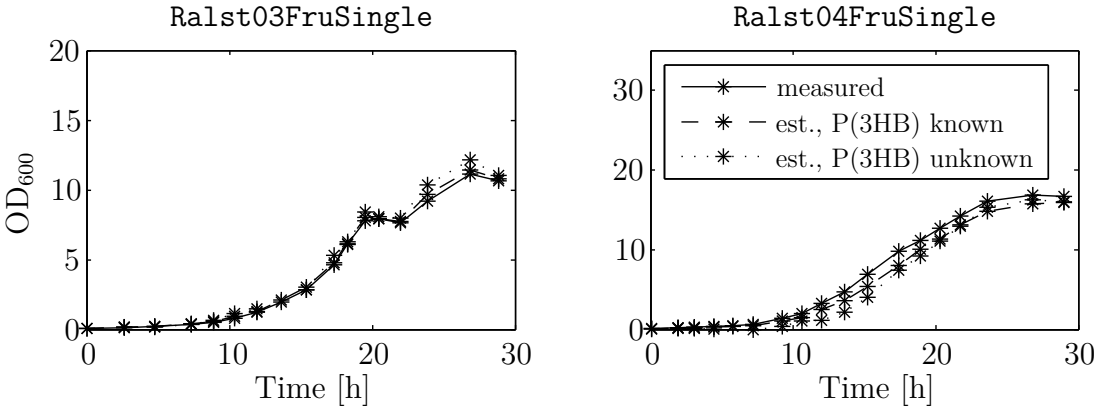

Figure 2.3.: Comparison of measured optical density (solid line) with estimated optical density. If P(3HB) concentration is known (dashed line), the amount of residual biomass can be calculated from cell dry weight. If P(3HB) concentration is unknown (dotted line), the amount of residual biomass can be calculated from the amount of uptaken nitrogen.

2.4.4. Carbon Sources

2.4.4.1. D-Glucose and D-Fructose

Concentrations of fructose and glucose in supernatants were determined with a D-Glucose/D-Fructose test kit from R-Biopharm (Darmstadt, Germany) according to the principle described by Schmidt [69]. Extinction was measured with a microplate spectrophotometer (Biotek PowerWave XS) at 340 nm after 3 seconds of rapid shaking (included within procedure).

The manufacturers recommended procedure was adjusted to microtiter plates. The test kit came with four bottles:

Bottle 1: 5g powder consisting of: triethanolamin buffer, NADP and ATP

Bottle 2: suspension consisting of hexokinase and G6P-dehydrogenase

Bottle 3: suspension of phosphoglucose-isomerase

Bottle 4: D-Glucose assay control solution

The content of bottle 1 was dissolved in 27 ml distilled water. A mastermix for (usually) 30 samples was prepared according to Table 2.2.

Table 2.2.: Mastermix for analysis of glucose and fructose.

	per sample	for 30 samples
H_2O	150 μl	4500 μl
solution from bottle 1	75 μl	2250 μl
suspension from bottle 2	1 μl	30 μl

The following steps were conducted:

1. 226 μl of the mastermix were pipetted into each well of the microtiter plates.
2. 7.5 μl sample, standard or H_2O (blank) were added into each particular well and slightly stirred with the pipette tip.
3. Extinction (E1) was measured.
4. 1.0 μl from bottle 3 was added into each particular well and slightly stirred with the pipette tip.
5. After 15 minutes extinction (E2) was measured.

From the extinction difference of the standards and blank a calibration curve was calculated. This calibration curve was then used to determine the glucose or fructose concentration from the extinction difference of the samples.

2.4.4.2. Acetate

Acetate concentration in supernatants was determined with reverse phase chromatography using a HP Agilent 1100 HPLC system (Agilent Technologies) with an Inertsil ODS-3 column (GL Science). Eluent flow rate was 1 ml/min and sample injection volume was 10 μl. As eluent 0.1 mol/l ammonium dihydrogen phosphate at pH 2.6 was used. Spectra were obtained with a diode array detector. The concentration of acetate was calculated from reference standards.

2.4.5. Ammonia

Ammonia concentration in culture supernatants broth was either measured by determining NH_3 concentration with a VITROS DT60 II Chemistry System and VITROS NH3 MicroSlide from Ortho-Clinical Diagnostics (Neckargemünd, Germany) using the manufacturers instructions or with an ammonia test kit from R-Biopharm (Darmstadt, Germany). Extinction was measured with a microplate spectrophotometer (Biotek PowerWave XS) at 340 nm after 3 seconds of rapid shaking (included within procedure).

For analysis of ammonia via the ammonia test kit from R-Biopharm the manufacturers recommended procedure was adjusted to microtiter plates as follows:

The ammonia test kit contains the following four bottles:

Bottle 1: 60 ml solution, consisting of: triethanolamine buffer (pH approx. 8.0), 2-oxoglutarate (150 mg)

Bottle 2: approx. 50 tablets, each tablet contains NADH (approx 0.4 mg)

Bottle 3: glutamate dehydrogenase solution

Bottle 4: ammonia assay control solution

Table 2.3.: Mastermix for analysis of ammonia.

	per sample	for 25 samples
H_2O	151 μl	3775 μl
NADH solution	80 μl	2000 μl

The following steps were conducted:

1. Preparation of NADH solution: 1 NADH tablet per 1 ml of solution from bottle 1
2. Preparation of mastermix (see Table 2.3)
3. 231 μl of the mastermix were pipetted into each well of the microtiter plate.
4. 8.0 μl sample, standard or H_2O (blank) were added into each particular well and slightly stirred with the pipette tip.
5. Incubation for 5 minutes in a thermomixer at 600 rpm and 25°C.

6. Extinction (E1) at 340 nm was measured.
7. 1.6 μl from bottle 3 was added into each particular well and slightly stirred with the pipette tip.
8. Incubation for 20 minutes in a thermomixer at 600 rpm and 25℃.
9. Extinction (E2) at 340 nm was measured.

From the extinction difference of the standards and blank a calibration curve was calculated. This calibration curve was then used to determine the ammonia concentration from the extinction difference of the samples.

2.4.6. Flow Cytometry

For flow cytometry a CyFlow Space (Partec GmbH, Münster, Germany) with forward scatter (FSC), sideward scatter (SSC) and the following detectors for fluorescence signals was used:

Detector	FL1	FL2	FL3	FL4
Wavelength	527 nm	590 nm	630 nm	455 nm

Samples were prepared and measured according the following steps:

1. Optical density of cell suspension was measured.
2. Sample volume was calculated (normalized w.r.t. optical density): $V_{\text{sample}} = 1\,\text{ml/OD}$.
3. Sample volume was centrifuged at 13000 rpm for 15 minutes.
4. Supernatant was removed carefully.
5. 39 μl PBS and 1 μl DAPI were added to the remaining cell pellet.
6. 5 μl of staining dye BODYPI ($\frac{3\,\text{mg}}{1\,\text{ml}}$, dissolved in ethanol) or Nile red ($\frac{0.1\,\text{g}}{1\,\text{ml}}$, dissolved in ethanol) were added to the cell pellet.
7. Incubation at 30℃ and 450 rpm for 15 minutes in a thermomixer.
8. 3 μl of the sample were added to a glass tube with 2 ml PBS and rapidly mixed.
9. Sample in glass tube was measured with flow cytometry.

3. Theoretical Methods

3.1. Metabolic Network Analysis

Bacteria are single-celled organisms and their cells contain metabolites which are transformed to other metabolites through a metabolic network of reactions catalyzed by enzymes. Reactions which transport metabolites across the cell border are called *exchange reactions*, while reactions which transform metabolites within the cell are called *internal reactions*. Metabolic reactions are either irreversible or reversible, depending on thermodynamic constraints. However, every reversible reaction can be splitted into two irreversible reactions.

Figure 3.1 shows a simple metabolic network ($\mathcal{N}_1$) of *R. eutropha* from Gadkar et. al [20]. This network aims to describe the synthesis and metabolization of poly(3-hydroxybutyrate) (P(3HB)), where the carbon source is glucose (GLC) and the nitrogen source is amonium sulfate (AMS). Non-P(3HB) biomass is denoted as BIO. Including this, the network has five external metabolites, eleven internal metabolites and fourteen metabolic reactions (see Table 3.1). Reaction r_5 is a reversible reaction and can be splitted into the two irreversible reactions r_{5_a} and r_{5_b}.

Such a metabolic system can be described by the state $\mathbf{y}$, which consist of the vector of external metabolite concentrations $\mathbf{x}$ (mmol/l), the vector of specific internal metabolite concentrations $\mathbf{m}$ (mmol/g) and the biomass concentration c (g/l)

$$\mathbf{y} = \begin{bmatrix} \mathbf{x} \\ \mathbf{m} \\ c \end{bmatrix} \quad . \tag{3.1}$$

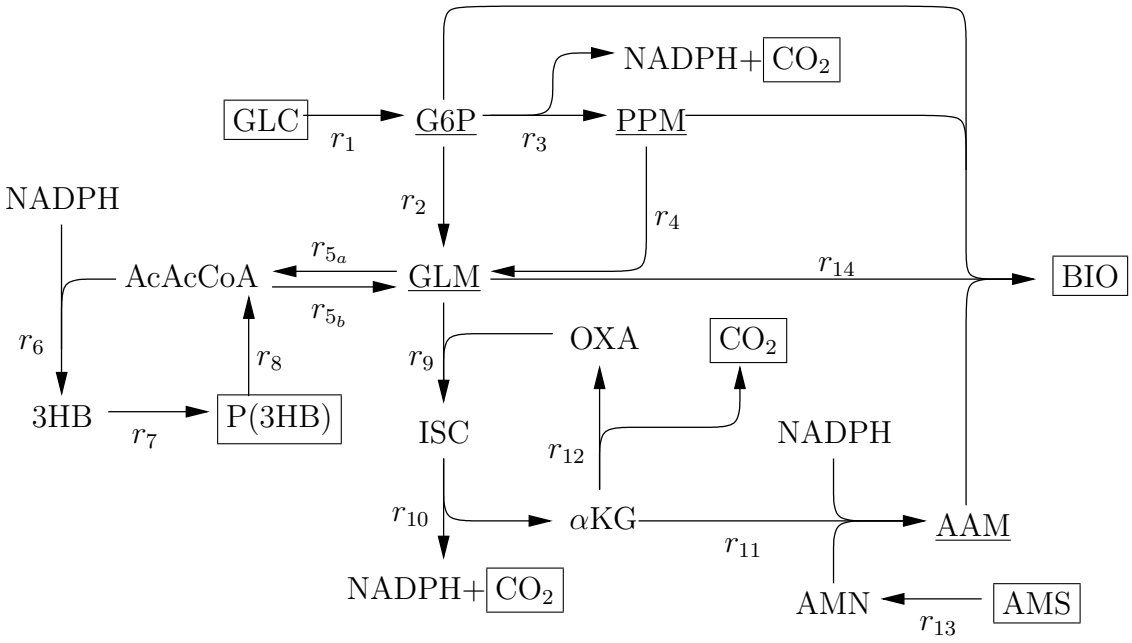

Figure 3.1.: Metabolic network $\mathcal{N}_1$ of *R. eutropha*. This network from Gadkar et al. [20] of *R. eutropha* has five external metabolites (boxed), eleven internal metabolites and fourteen metabolic reactions. Underlined metabolites are biomass precursors.

The equations for describing mass conversion of metabolites are defined as

$$\frac{1}{c}\frac{\mathrm{d}\mathbf{x}}{\mathrm{d}t} = \mathbf{S_x}\,\mathbf{r} \tag{3.2}$$

$$\frac{\mathrm{d}\mathbf{m}}{\mathrm{d}t} = \mathbf{S_m}\,\mathbf{r} - \mathbf{m}\,\mu \tag{3.3}$$

$$\frac{1}{c}\frac{\mathrm{d}c}{\mathrm{d}t} = \mu \quad , \tag{3.4}$$

where $\mathbf{r}$ (mmol/g/h) is the vector of n_r reaction rates, μ is the growth rate, $\mathbf{S_x}$ and $\mathbf{S_m}$ represent the $(n_\mathrm{x} \times n_\mathrm{r})$ and $(n_\mathrm{m} \times n_\mathrm{r})$ stoichiometric matrices, and n_x and n_m are the dimensions of the vectors $\mathbf{x}$ and $\mathbf{m}$, respectively.

In biological systems such as bacterial cells, dilution of internal metabolites due to growth is much slower than internal reaction rates and therefore usually considered to be negligible

$$\mathbf{m}\,\mu \approx 0 \quad . \tag{3.5}$$

Therefore, under quasi-steady state assumption of internal metabolites Equation

Table 3.1.: Metabolic reactions of the metabolic network $\mathcal{N}_1$ given in Figure 3.1. Stoichiometry coefficents of the metabolites are given in mmol, except the stoichiometry coefficents of the polymer P(3HB) and the stoichiometry of the non-P(3HB) biomass (BIO) are given in g.

no.	metabolic reaction	type
1	1 GLC $\rightarrow$ 1 G6P	exchange
2	1 G6P $\rightarrow$ 2 GLM	internal
3	1 G6P $\rightarrow$ 1 PPM + 2 NADPH + 1 CO_2	lumped
4	3 PPM $\rightarrow$ 5 GLM	internal
5	2 GLM $\leftrightarrow$ 1 AcAcCoA	internal
6	1 AcAcCoA + 1 NADPH $\rightarrow$ 1 3HB	internal
7	1 3HB $\rightarrow$ 0.086 P(3HB)	exchange
8	0.086 P(3HB) $\rightarrow$ 1 AcAcCoA	exchange
9	1 GLM + 1 OXA $\rightarrow$ 1 ISC	internal
10	1 ISC $\rightarrow$ 1 αKG + 1 NADPH + 1 CO_2	lumped
11	1 αKG + 1 AMN + 1 NADPH $\rightarrow$ 1 AAM	internal
12	1 αKG $\rightarrow$ 1 OXA + 1 CO_2	lumped
13	1 AMS $\rightarrow$ 2 AMN	exchange
14	0.3 G6P + 1.2 PPM + 10 GLM + 9 AAM $\rightarrow$ 1 BIO	exchange

(3.3) simplifies to

$$\mathbf{S_m}\,\mathbf{r} = 0 \quad . \tag{3.6}$$

Since every reversible reaction can be divided into two irreversible reactions, the vector of reaction rates can be constraint to

$$\mathbf{r} \geq \mathbf{0} \tag{3.7}$$

without loss of generality.

The stoichiometry matrix $\mathbf{S_m}$ is definded by the metabolic network and the flux distribution $\mathbf{r}$ needs to be computed. Equation (3.6) is typically an undetermined system, since usually $n_\mathrm{r} > n_\mathrm{m}$. Depending on the structure of $\mathbf{S_m}$, additional constraints and knowledge of (e.g. measured) rates, there are three main techniques to compute the internal fluxes: *metabolic flux analysis* (MFA), *flux balance analysis* (FBA) and *metabolic pathway analysis* (MPA) [84]. The term *flux* is usually used equivalently to the term *rate*. In particular, in metabolic network analysis *flux* is often used to indicate internal reaction rates under steady-state conditions.

3.2. Elementary Mode Analysis

Solutions of Equations (3.6) and (3.7) are steady-state flux (or rate) distributions and called *flux modes*. These solutions span an admissible flux space, which is a convex polyhedral cone. Application of a non-decomposability constraint to the flux space achieves a finite set of solutions, which are unique (up to a scaling factor) and consist of a minimal set of reactions. These flux modes are called *elementary (flux) modes*. An elementary mode can be viewed as a minimal functional sub unit (or sub network).

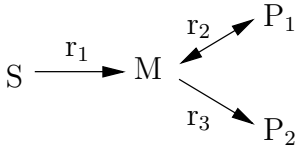

	EM_1	EM_2	EM_3
r_1	1	1	0
r_2	1	0	-1
r_3	0	1	1

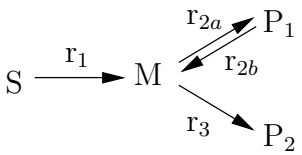

	EM_1	EM_2	EM_3
r_1	1	1	0
r_{2a}	1	0	0
r_{2b}	0	0	1
r_3	0	1	1

Figure 3.2.: Elementary modes (EM) in a network with reversible reaction vs. elementary modes in a network with only irreversible reactions (adapted from [40]).

The concept of elementary modes was first introduced in [70]. Calculation of elementary modes [21] can be done via available software tools such as Metatool [88] or CellNetAnalyzer [39]. Elementary modes are unique and non-decomposable steady-state flux distributions. They are genetically independent (e. g. each elementary mode contains a different set of genes) and even systematically independent, if there are only irreversible reaction in the metabolic network. Systematically independent means, that there exists no elementary mode which can be expressed by non-negative combination of other elementary modes. This is shown in Figure 3.2. These are two identical networks, except reaction r_2 is a reversible reaction in the upper subfigure and splitted into two irreversible reactions in the lower subfigure. Both networks have three elementary modes (EM). However, in the network with the reversible reactions elementary mode EM_2 can be obtained by a non-negative combination of EM_1 and EM_3, while in the network with only

irreversible reactions no elementary mode can be obtained by non-negative combinations of other elementary modes.

Typically every elementary mode includes one or more substrates and products. However, elementary modes exist, which are composed of only internal rates (e.g. internal cycles), but those modes are usually not considered, as they are thermodynamical infeasible.

Given the metabolic network $\mathcal{N}_1$ in Figure 3.1 six elementary modes can be calculated. As seen in Table 3.2, reactions r_{11}, r_{13} and r_{14} never occur in a steady state solution. These reactions are called *blocked reactions*. The metabolic network $\mathcal{N}_1$ is therefore not able to produce the metabolite BIO under steady state conditions. Even under non-steady state conditions BIO can only be produced, if there are already sufficient internal metabolites available at the beginning of the process (initial conditions). Furthermore, only the three modes EM_1, EM_2 and EM_4 have a net production of P(3HB) and the three remaining modes EM_3, EM_5 and EM_6 convert carbon source GLC and/or P(3HB) only into CO_2.

Table 3.2.: Elementary modes (EM) in flux space of the metabolic network $\mathcal{N}_1$.

	EM_1	EM_2	EM_3	EM_4	EM_5	EM_6
r_1	1.1	2.1	1.5	3.0	0	1.2
r_2	0.6	0	1.5	3.0	0	0
r_3	0.5	2.1	0	0	0	1.2
r_4	0.2	0.7	0	0	0	0.4
r_{5_a}	1.0	1.7	0	2.0	0	0
r_{5_b}	0	0	0	0	1.0	0
r_6	1.0	4.1	3.0	2.0	2.0	4.4
r_7	1.0	4.1	3.0	2.0	2.0	4.4
r_8	0	2.4	3.0	0	3.0	4.4
r_9	0	0	3.0	2.0	2.0	2.0
r_{10}	0	0	3.0	2.0	2.0	2.0
r_{11}	0	0	0	0	0	0
r_{12}	0	0	3.0	2.0	2.0	2.0
r_{13}	0	0	0	0	0	0
r_{14}	0	0	0	0	0	0

It is therefore obvious that certain reactions and/or metabolites in network $\mathcal{N}_1$ are missing, since there are three blocked reactions. Removing these blocked reactions would not change the steady state solution, but is not meaningful, since production

of biomass is obviously needed. Instead, missing reactions and metabolites have to be added to this metabolic network.

The network $\mathcal{N}_1$ can be extended with the additional reactions given in Table 3.3 to unblock reactions r_{11}, r_{13} and r_{14} and to allow production of biomass.

Table 3.3.: Additional reactions to extend the metabolic network $\mathcal{N}_1$ to unblock reactions r_{11}, r_{13} and r_{14} and to allow production of biomass.

no.	metabolic reaction	type
15	1 αKG $\rightarrow$ 1 SUC + 1 CO_2	lumped
16	1 SUC $\rightarrow$ 1 MAL	internal
17	1 MAL $\rightarrow$ 1 OXA	internal
18	1 ISC $\rightarrow$ 1 SUC + 1 GOX	internal
16	1 GLM + 1 GOX $\rightarrow$ 1 MAL	internal

The extended network $\mathcal{N}_2$ has then fourteen elementary modes, including the six modes from the network $\mathcal{N}_1$. The elementary modes of the extended network $\mathcal{N}_2$ are given in Table 3.4. In this network no reactions are blocked and biomass can be produced via elementary modes EM_7, EM_9, EM_{10} and EM_{14}, as can be seen in Table 3.5.

3.3. Metabolic Yield Analysis

In the hybrid cybernetic modeling approach (see section 3.4.3) *elementary mode analysis* is combined with the cybernetic modeling framework. Every elementary mode is assumed to be catalyzed by a particular key enzyme, which in turn is typically described by an ordinary differential equation. Larger metabolic networks are usually very complex and highly connected, which leads to exponential increase in the number of elementary modes and therefore system equations and parameters. However, usually a small subset of elementary modes is needed to describe the metabolic phenotype. This subset of elementary modes can be extracted from the whole set of elementary modes by *metabolic yield analysis* [75].

Elementary modes are usually viewed in flux space and are represented by a $(n_\mathrm{r} \times n_\mathrm{EMs})$ matrix $\mathbf{Z}$ (see Table 3.2 for an example), where n_EMs is the number of elementary modes. In *metabolic yield analysis* these vectors in flux space

Table 3.4.: Elementary modes (EM) in flux space of the extended network $\mathcal{N}_2$. EM_1 - EM_6 also occur in the network $\mathcal{N}_1$ (see Table 3.2) and therefore not included here.

	EM_7	EM_8	EM_9	EM_{10}	EM_{11}	EM_{12}	EM_{13}	EM_{14}
r_1	56.0	1.2	50	1.3	1.0	3.0	0	1.1
r_2	52.3	0	46.3	0	1.0	3.0	0	0
r_3	3.0	1.2	3.0	1.3	0	0	0	0.9
r_4	0	0.4	0	0.4	0	0	0	0
r_{5_a}	6.0	0	0	0	0	2.0	0	0
r_{5_b}	0	0	0	0	0	0	1.0	13.3
r_6	6.0	4.4	6.0	2.5	2.0	2.0	2.0	1.7
r_7	6.0	4.4	6.0	2.5	2.0	2.0	2.0	1.7
r_8	0	4.4	6.0	2.5	2.0	0	3.0	15.1
r_9	45.0	2.0	45.0	1.0	2.0	2.0	2.0	13.0
r_{10}	22.5	2.0	22.5	0.5	2.0	2.0	2.0	6.5
r_{11}	22.5	0	22.5	0.5	0	0	0	6.5
r_{12}	0	0	0	0	0	0	0	0
r_{13}	11.3	0	11.3	0.2	0	0	0	3.2
r_{14}	2.5	0	2.5	0.1	0	0	0	0.7
r_{15}	0	2.0	0	0	2.0	2.0	2.0	0
r_{16}	22.5	2.0	22.5	0.5	2.0	2.0	2.0	6.5
r_{17}	45.0	2.0	45.0	1.0	2.0	2.0	2.0	13.0
r_{18}	22.5	0	22.5	0.5	0	0	0	6.5
r_{19}	22.5	0	22.5	0.5	0	0	0	6.5

are converted into vectors in yield space. Elementary modes in yield space are represented by the stoichiometry of the net reactions $\mathbf{S_x Z}$, where $\mathbf{S_x}$ is the $(n_x \times n_r)$ stoichiometry matrix for n_x external metabolites. Usually there are less external metabolites than metabolic reactions ($n_\mathrm{x} < n_\mathrm{r}$), thus the dimension of elementary mode matrix $\mathbf{S_x Z}$ is smaller then the dimension of the elementary mode matrix in flux space $\mathbf{Z}$. Elementary modes in yield space are therefore typically not systematically independent and can even have identical stoichiometric coefficients. Table 3.5 lists the net reactions of the elementary modes from network $\mathcal{N}_2$. It can be seen, that some elementary modes have the same stoichiometry (e.g. EM_3 and EM_{11}) in yield space and are not distinguishable from each other anymore, although the underlying *full* elementary modes in flux space are systematically independent.

In *metabolic yield analysis* the elementary modes in yield space are usually nor-

Table 3.5.: Net reactions of the elementary modes of the extended sample network above. Stoichiometry coefficents of the metabolites are given in mmol, except the stoichiometry coefficents of the polymer P(3HB) and the stoichiometry of the non-P(3HB) biomass (BIO) are given in g.

EM	net reaction
EM_1	1.1 GLC $\rightarrow$ 0.5 CO_2 + 0.086 P(3HB)
EM_2	2.1 GLC $\rightarrow$ 2.1 CO_2 + 0.146 P(3HB)
EM_3	1.0 GLC $\rightarrow$ 4.0 CO_2
EM_4	3.0 GLC $\rightarrow$ 4.0 CO_2 + 0.172 P(3HB)
EM_5	0.086 P(3HB) $\rightarrow$ 4.0 CO_2
EM_6	1.2 GLC $\rightarrow$ 5.2 CO_2
EM_7	56.0 GLC + 11.3 AMS $\rightarrow$ 25.5 CO_2 + 0.516 P(3HB) + 2.5 BIO
EM_8	1.2 GLC $\rightarrow$ 5.2 CO_2
EM_9	50.0 GLC + 11.3 AMS $\rightarrow$ 25.5 CO_2 + 2.5 BIO
EM_{10}	1.3 GLC + 0.2 AMS $\rightarrow$ 1.8 CO_2 + 0.1 BIO
EM_{11}	1.0 GLC $\rightarrow$ 4.0 CO_2
EM_{12}	3.0 GLC $\rightarrow$ 4.0 CO_2 + 0.172 P(3HB)
EM_{13}	0.086 P(3HB) $\rightarrow$ 4.0 CO_2
EM_{14}	1.1 GLC + 3.2 AMS + 1.144 P(3HB) $\rightarrow$ 7.4 CO_2 + 0.7 BIO

malized w.r.t. a reference substrate. If there is more than one substrate, the yield space can be decomposed into disjoint sub spaces for each single substrate and mixed substrate uptake. The network $\mathcal{N}_2$ has glucose as carbon substrate and P(3HB) can act as carbon substrate as well as product. It is therefore convenient to normalize the elementary modes in yield space of this network w.r.t. the number of net uptaken carbon units from glucose and P(3HB). Since glucose has six carbon units and the monomer 3HB has four carbon units, the net uptake of carbon units of, for example EM_1, is $6 \cdot 1.1 - 4 \cdot 86/M_{3HB}$, since glucose is metabolized and P(3HB) is produced in this elementary modes. M_{3HB} is the molecular weight of the monomer 3HB.

The yields w.r.t. to carbon units of all elementary modes of the network $\mathcal{N}_2$ are given in Table 3.6. Additionally, the yield of BIO w.r.t. to the substrate ammonium sulfate AMS is given and it can be seen, that production of BIO is linear correlated to the uptake of AMS, which reduces the dimension of the yield space.

For describing metabolic phenotype, it is sufficient to extract the systematically independent elementary modes in yield space. These modes are called *generating*

Table 3.6.: Selected yields of the elementary modes of the extended sample network.

EM	$Y_{CO_2/C}$	$Y_{BIO/C}$	$Y_{BIO/AMS}$
EM_1	0.2000	0	–
EM_2	0.6667	0	–
EM_3	0.0817	0.0080	0.2222
EM_4	0.7222	0	–
EM_5	0.3750	0	–
EM_6	0.0850	0.0083	0.2222
EM_7	0.2278	0.0070	0.2222
EM_8	0.4000	0	–
EM_9	0.6667	0	–
EM_{11}	0.4000	0	–
EM_{12}	1.0000	0	–
EM_{13}	1.0000	0	–
EM_{14}	0.1229	0.0120	0.2222
EM_{15}	0.7222	0	–

modes and are the vertices of the convex hull of the yield space. In Figure 3.3 the fourteen elementary modes of the extended sample network are displayed in a two-dimensional yield space. The hull of this yield space has only four generating modes. These four modes are sufficient to represent any point within the convex hull by non-negative combinations.

Examination of elementary modes in yield space has also the advantage that the elementary modes can be compared easily with experimental data. If experimental data are outside the convex hull of the yield space, then it is not possible to find any non-negative combination of elementary modes which can represent these data. In this case crucial reactions might be missing in the metabolic network or the experimentalists have done some mistakes and experiments have to be repeated. However, one can always find a non-negative combination of elementary modes which minimize the distance of the convex hull to the experimental data outside the hull. This can be done by solving the following least-square problem

$$\min_{\mathbf{h}} \frac{1}{2} \|\mathbf{Z_y}\, \mathbf{h} - \mathbf{y_m}\|_2^2 \tag{3.8}$$

such that

$$\mathbf{h} \geq \mathbf{0}, \quad \|\mathbf{h}\| = \mathbf{1} \tag{3.9}$$

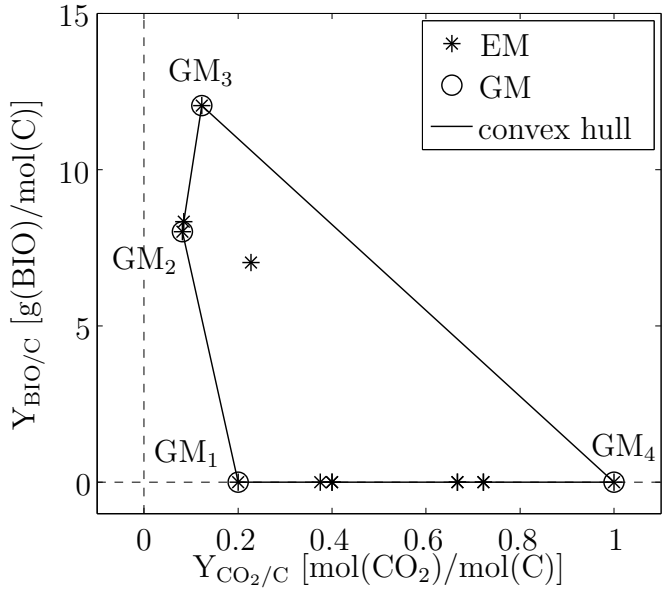

Figure 3.3.: Yield space of the network $\mathcal{N}_2$. Any elementary mode EM within the convex hull of the yield space can be represented by non-negative combination of the generating modes GM, which are the vertices of the convex hull.

where $\mathbf{Z_y}$ is a $n_\mathrm{x} \times n_\mathrm{GM}$ matrix, which contains the yields of the generating modes ($\mathbf{Z_y} \subset \mathbf{S_x Z}$), $\mathbf{y_m}$ is the vector with experimental yield data and $\mathbf{h}$ is the vector of non-zero weights among generating modes. This subset of generating modes is called *active modes*, since these modes have to be at least active to minimize the distance or even represent the experimental data exactly. As seen in Figure 3.4 a), two active modes can be found to minimize the distance to the experimental data outside the convex hull.

In the case of experimental data within the convex hull, a set of a minimal number of elementary modes can be found, whose non-negative combinations can exactly represent these data. However, this set is usually not unique. In case of the two-dimensional yield space in Figure 3.4 b) at least three generating modes (GM) are necessary to represent the experimental data. This can be either the set GM_1-GM_2-GM_4 or GM_1-GM_3-GM_4. In *metabolic yield analysis* it is suggested to select such a particular set by minimizing the sum of squared weights:

$$\min_{\mathbf{h}} \frac{1}{2}\|\mathbf{h}\|_2^2 \tag{3.10}$$

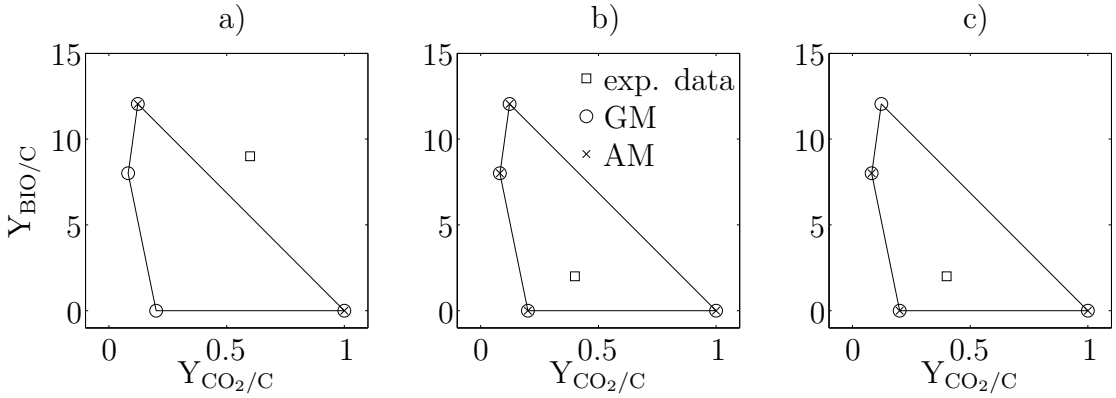

Figure 3.4.: Generating modes (GM) and active modes (AM) for network $\mathcal{N}_2$ and some artificial experimental data.

such that

$$\mathbf{Z_y}\,\mathbf{h} - \mathbf{y_m} = \mathbf{0}, \quad \mathbf{h} \geq \mathbf{0}, \quad \|\mathbf{h}\| = \mathbf{1} \tag{3.11}$$

However, this will distribute the non-zero weights among as many generating modes as possible and this is obviously not a minimal set. In this case it is therefore necessary to exclude a priori generating modes or to impose additional constraints.

To circumvent this, the least-square problem used for data outside the convex hull can also be solved for experimental data within the hull. This will result in a minimal, but not unique set of active modes whose non-negative combination can exactly represent the experimental data. This is seen in Figure 3.4 c).

3.4. Cybernetic Modeling

Microorganisms are usually highly regulated and can adapt to changes in environmental conditions very quickly. However, in many applications these regulations are often neglected. Nevertheless, there are cases where considering cell internal regulation is crucial. This applies to the synthesis of poly(3-hydroxybutyrate) in microorganisms, where the organisms can switch between cell growth, synthesis of poly(3-hydroxybutyrate) and metabolization of poly(3-hydroxybutyrate), depending on environmental and cell internal conditions.

Unfortunately, cell internal microbial regulation can be very complex and is often not fully understood. In cases where knowledge of the underlying metabolic regulation is limited, but has to be included into dynamic modeling, the cybernetic modeling framework offers a convenient method with moderate complexity. The cybernetic modeling framework was introduced three decades ago by Ramkrishna and co-worker [9, 42, 43, 63, 65] and since then improved significantly and successfully applied to a multitude of microorganisms [15, 19, 20, 28, 31, 38, 41, 55, 74, 93].

The concept of the cybernetic modeling approach is based on the assumption, that microorganisms are *optimally* regulated in view of available resources due to evolutionary processes. From this *optimality* criteria, cybernetic control variables are derived and included into the mass balance equations.

3.4.1. First Cybernetic Models

The first cybernetic models were formulated to describe diauxic growth [43]. This is a consecutive growth on two different substrates S_1 and S_2 into biomass B, e.g.

$$S_1 + B \longrightarrow (1 + Y_1)\, B \tag{3.12}$$

$$S_2 + B \longrightarrow (1 + Y_2)\, B \quad . \tag{3.13}$$

The substrates are not metabolized simultaneously, but in a sequential pattern, which results in two separate growth phases. That means, a dynamic model has to include a regulatory feature which can represent this behaviour.

In a purely kinetic model the reaction rates are only defined by a kinetic part r^{kin}, e.g. mass action, Monod [52], or other. In case of Monod, the reaction rates are

$$r_1 := r_1^{\text{kin}} = k_{r,1}\, \frac{x_{S_1}}{K_1 + x_{S_1}} \tag{3.14}$$

$$r_2 := r_1^{\text{kin}} = k_{r,2}\, \frac{x_{S_2}}{K_2 + x_{S_2}} \quad . \tag{3.15}$$

The balance equations for this simple example are then

$$\frac{\mathrm{d}x_{S_1}}{\mathrm{d}t} = -\frac{1}{Y_1} r_1 \, c \tag{3.16}$$

$$\frac{\mathrm{d}x_{S_2}}{\mathrm{d}t} = -\frac{1}{Y_2} r_2 \, c \tag{3.17}$$

$$\frac{\mathrm{d}c}{\mathrm{d}t} = \mu \, c \quad , \tag{3.18}$$

where Y_i are the yield coefficients, x_i are the substrate concentrations in mmol/l, c is the biomass concentration in g/l, $k_{r,i}$ are the maximum specific growth rates, K_i are the so called Monod-constants or half-velocity-constants and μ is the growth rate with $\mu = r_1 + r_2$ in this case.

Figure 3.5 (left subfigure) shows the simulation of this pure kinetic model with Monod kinetics. With this approach both substrates are metabolized simultaneously, which is not a diauxic growth behavior observed experimentally. To achieve such a behaviour, reaction rates could be modified and for example extended with inhibition terms. Another approach is the cybernetic modeling approach, which is discussed in the following.

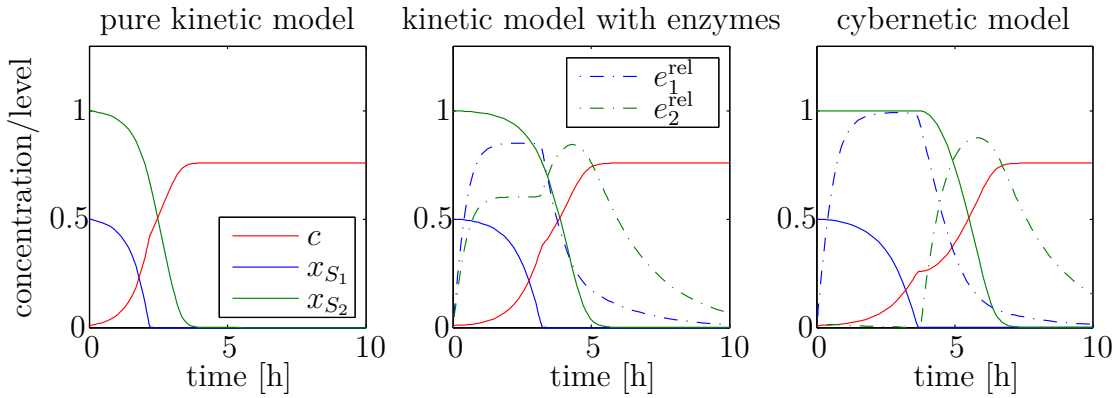

Figure 3.5.: Simulation and comparison of diauxic growth with different modeling approaches. Left subfigure: pure kinetic model (Monod), middle subfigure: Monod kinetic with additional enzyme dynamics, right subfigure: cybernetic model. Initial conditions are: $c_0 = 0.01$ g/l, $x_{S_1,0} = 0.5$ g/l, , $x_{S_2,0} = 1.0$ g/l, $e^{\mathrm{rel}}_{1,0} = 0.001$, $e^{\mathrm{rel}}_{2,0} = 0.001$. Model parameters are given in Table 3.7.

First, an intermediate step is discussed, where enzymes are integrated into the

Table 3.7.: Model parameters for diauxic growth model.

parameter	$k_{r,1}$	$k_{r,1}$	K_1	K_2	$k_{e,1}$	$k_{e,2}$	β_1	β_2	Y_1	Y_2
value	1.08	0.82	0.01	0.20	0.1	0.1	0.5	0.5	0.5	0.5

model, since metabolic reactions are usually catalyzed by enzymes (E)

$$S_1 + B \xrightarrow{E_1} (1 + Y_1)\, B \tag{3.19}$$

$$S_2 + B \xrightarrow{E_2} (1 + Y_2)\, B \quad . \tag{3.20}$$

The specific enzyme concentrations e_i are then included into the rate equations, e.g. for Monod

$$r_1 := e_1^{\mathrm{rel}} \overbrace{k_{r,1} \frac{x_{S_1}}{K_1 + x_{S_1}}}^{r_1^{\mathrm{kin}}} \tag{3.21}$$

$$r_2 := e_2^{\mathrm{rel}} \underbrace{k_{r,2} \frac{x_{S_2}}{K_2 + x_{S_2}}}_{r_2^{\mathrm{kin}}} \quad , \tag{3.22}$$

with the relative enzyme level

$$e_i^{\mathrm{rel}} = \frac{e_i}{e_i^{\max}}, \quad i = 1, 2 \quad . \tag{3.23}$$

Furthermore, balance equations for the enzyme levels are needed, which are

$$\frac{\mathrm{d}e_i}{\mathrm{d}t} = \alpha_i + r_{\mathrm{E},i} - \beta_i\, e_i - e_i\, \mu, \quad i = 1, 2 \quad , \tag{3.24}$$

where α_i is a constitutive enzyme synthesis rate [85], β_i is a enzyme degradation constant and $e_i\, \mu$ represents the "dilution" of enzyme due to growth. The enzyme synthesis rate $r_{\mathrm{E},i}$ is also often represented by a Monod type of kinetics, e.g.

$$r_{\mathrm{E},i} = k_{\mathrm{e},i} \frac{x_{S_i}}{K_{\mathrm{e},i} + x_{S_i}} \quad . \tag{3.25}$$

By setting the initial conditions for the enzyme levels appropriately (e.g. high value for the prefered substrate and low value for the unfavored substrate), one might achieve a slightly better diauxic behavior than without enzyme catalyzed

reaction rates. In Figure 3.5 middle subfigure both initial enzyme levels are set to very low values for comparison with the cybernetic model. Enzymes have to be synthesized to catalyze the reactions. Since there is no regulation incorporated into this model, both enzymes are synthesized simultaneously and therefore both substrates are metabolized simultaneously.

To account for regulatory features, the cybernetic modeling approach introduces two so called cybernetic control variables u and v, which regulate enzyme synthesis and enzyme activity and are included into r_{E} and r, respectively

$$r_i := v_i \, e_i^{\mathrm{rel}} \, r_i^{\mathrm{kin}}, \quad i = 1, 2 \tag{3.26}$$

$$r_{\mathrm{E},i} := u_i \, r_{\mathrm{E},i}^{\mathrm{kin}}, \quad i = 1, 2 \quad . \tag{3.27}$$

Based on the assumption that microorganisms are optimally regulated, they will distribute available resources in an optimal manner such that a certain objective is maximized (e.g. cell growth). From this assumption the cybernetic control laws can be derived. This was first done by Dhurjati [9] and Kompala [43] and results in the following heuristic control laws:

$$\mathbf{u} = \frac{\mathrm{diag}(\mathbf{e}) \, \mathbf{r}^{\mathrm{kin}}}{||\mathrm{diag}(\mathbf{e}) \, \mathbf{r}^{\mathrm{kin}}||_1}, \quad \mathbf{v} = \frac{\mathrm{diag}(\mathbf{e}) \, \mathbf{r}^{\mathrm{kin}}}{||\mathrm{diag}(\mathbf{e}) \, \mathbf{r}^{\mathrm{kin}}||_\infty} \quad . \tag{3.28}$$

As seen in Figure 3.5 (right subfigure) the cybernetic modeling approach successfully describes the diauxic growth behaviour. Although both initial enzyme levels have the same low value, the enzyme for metabolizing the preferred substrate is synthesized first. Only after depletion of the preferred substrate the enzyme for metabolization of the unfavored substrate is synthesized. Furthermore, a main advantage of the cybernetic modeling approach is, that no additional parameters are needed for the cybernetic control laws. However, for each metabolic reaction a so called key enzyme is needed and therefore n_r balance equations for the according enzyme levels.

Optimality of the cybernetic control laws in (3.28) was later proven by Young [96] using linear optimal control theory and generalized to the form

$$\mathbf{u} = \frac{\mathbf{p_u}}{||\mathbf{p_u}||_1}, \quad \mathbf{v} = \frac{\mathbf{p_v}}{||\mathbf{p_v}||_\infty} \quad , \tag{3.29}$$

where $\mathbf{p_u}$ and $\mathbf{p_v}$ are the so called *returns on investment*. There are two main policies to compute these *returns on investment* from a metabolic objective function ϕ (see Table 3.8): the *temperate* and the *greedy* policy. In the temperate policy knowledge about the time span Δt is necessary. This is the time span for which the organism optimizes the allocation of available resources. Since these time span is usually not known it is set to zero in the greedy policy (e.g. $\Delta t = 0$).

Table 3.8.: Policies for computing the *return on investment*.

	temperate		greedy	
	unweighted	weighted	unweighted	weighted
$\mathbf{p_u}$	$\mathbf{B_u^T e^{A^T \Delta t} q}$	$\mathbf{R^{-1} B_u^T e^{A^T \Delta t} q}$	$\mathbf{B_u^T q}$	$\mathbf{R^{-1} B_u^T q}$
$\mathbf{p_v}$	$\mathbf{B_v^T e^{A^T \Delta t} q}$	$\mathbf{B_v^T e^{A^T \Delta t} q}$	$\mathbf{B_v^T q}$	$\mathbf{B_v^T q}$

Both policies (temperate and greedy) can be formulated as weighted or unweighted policies. The weighting matrix $\mathbf{R}$ in the weighted policies has the following form

$$\mathbf{R} = \begin{bmatrix} \frac{e_1^\circ}{e_1} & 0 & \dots & 0 \\ 0 & \ddots & & \vdots \\ \vdots & & \ddots & 0 \\ 0 & \dots & 0 & \frac{e_{n_r}^\circ}{e_{n_r}} \end{bmatrix} \quad , \tag{3.30}$$

where e° is a reference enzyme level, which corresponds to the steady state level of the fully induced enzyme under current conditions [96]. By using the weighted forms, investment of resources into rates with high enzyme levels is favored.

Matrices $\mathbf{B_u}$, $\mathbf{B_v}$ and $\mathbf{A}$ are calculated from the linearized systems equations $\mathbf{f} = \frac{\mathrm{d}\mathbf{y}}{\mathrm{d}t}$

$$\mathbf{B_u} = \frac{\partial \mathbf{f}}{\partial \mathbf{u}}(\mathbf{y}(t), \mathbf{u}^\circ, \mathbf{v}^\circ) \tag{3.31}$$

$$\mathbf{B_v} = \frac{\partial \mathbf{f}}{\partial \mathbf{v}}(\mathbf{y}(t), \mathbf{u}^\circ, \mathbf{v}^\circ) \tag{3.32}$$

$$\mathbf{A} = \frac{\partial \mathbf{f}}{\partial \mathbf{y}}(\mathbf{y}(t), \mathbf{u}^\circ, \mathbf{v}^\circ) \quad , \tag{3.33}$$

where $\mathbf{u}^\circ$ and $\mathbf{v}^\circ$ are reference control inputs.

The vector $\mathbf{q}$ is computed from the metabolic objective function ϕ

$$\mathbf{q} = \frac{\partial \phi(\mathbf{y})}{\partial \mathbf{y}} \quad . \tag{3.34}$$

For the given example of diauxic growth a reasonable metabolic objective function would be to maximize biomass

$$\phi(\mathbf{y}) = c \quad . \tag{3.35}$$

It can then be shown [96] that the generalized control laws in Equation (3.29) will have the same form as the classic control laws in equation (3.28) for the diauxic growth.

However, one advantage of the generalized form of the cybernetic control laws is, that now any metabolic objective function $\phi(\mathbf{y})$ can be specified and the cybernetic approach is no longer limited to the cases where only biomass is maximized. Another reasonable metabolic objective is for instance maximizing substrate uptake.

3.4.2. Structured Cybernetic Modeling

Early cybernetic models were unstructured models. That means, that only metabolic net conversions from substrate to biomass and/or products were considered, but cell internal dynamics were neglected.

To account for cell internal dynamics, structured cybernetic models were introduced [79]. In this formulation, every metabolic network, regardless of complexity, consists of a multitude of four basic cybernetic units (see Figure 3.6):

- linear processes
- diverging processes
- converging processes
- cyclic processes

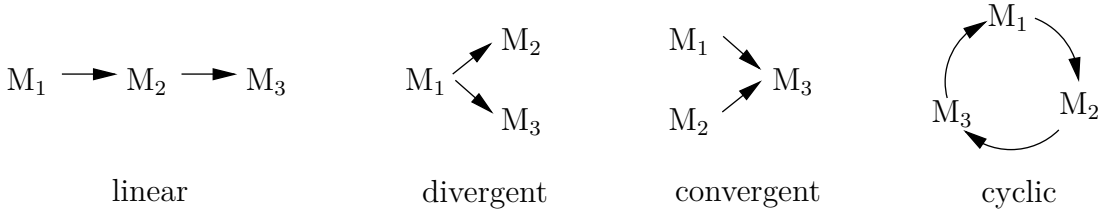

Figure 3.6.: Basic cybernetic units of the structured cybernetic modeling approach.

In contrast to that, elementary modes can also be viewed as subnetworks [95].

In a first step, *local* cybernetic control laws are defined for each basic unit or elementary mode separately, since it is assumed, that for each basic unit a certain pool of resources has to be allocated to the individual reactions of this unit.

In a second step, *global* cybernetic control laws are formulated which allocate resources between the basic subunits or elementary modes, respectively.

Local and global control variables are then finally combined.

3.4.3. Hybrid Cybernetic Modeling

The hybrid cybernetic modeling approach combines the cybernetic modeling framework with *elementary mode analysis*. It was first suggested by Kim et al. [38] and more elaborated by Song and Ramkrishna [75] and Song et al. [74].

In this approach not every single reaction is catalyzed by a key enzyme, but every relevant elementary mode. The vector of reactions rates $\mathbf{r}$ can then be expressed by the elementary mode decomposition and the vector of reaction rates (or fluxes) $\mathbf{r_M}$ through the elementary modes

$$\mathbf{Z}\,\mathbf{r_M} = \mathbf{r} \tag{3.36}$$

Balance equations can then be rewritten to

$$\frac{1}{c}\frac{\mathrm{d}\mathbf{x}}{\mathrm{d}t} = \mathbf{S_x Z}\,\mathbf{r_M} \tag{3.37}$$

$$\frac{\mathrm{d}\mathbf{e}}{\mathrm{d}t} = \boldsymbol{\alpha} + \mathbf{r_{EM}} - \mathrm{diag}(\boldsymbol{\beta})\,\mathbf{e} - \mathbf{e}\,\mu \tag{3.38}$$

$$\frac{1}{c}\frac{\mathrm{d}c}{\mathrm{d}t} = \mu \quad , \tag{3.39}$$

where $\mathbf{r_M}$ and $\mathbf{r_{EM}}$ are regulated rates

$$\mathbf{r_M} = \mathrm{diag}(\mathbf{v})\,\mathrm{diag}(\mathbf{e}^{\mathrm{rel}})\,\mathbf{r}_{\mathbf{M}}^{\mathrm{kin}} \tag{3.40}$$

$$\mathbf{r_{EM}} = \mathrm{diag}(\mathbf{u})\,\mathbf{r}_{\mathbf{EM}}^{\mathrm{kin}} \quad . \tag{3.41}$$

The vector $\mathbf{e}$ now represents the specific enzyme concentrations of the key enzymes

for the elementary modes and $\mathbf{r_{EM}}$ the synthesis rates of these key enzymes.

One of the main advantages of the hybrid cybernetic approach in comparison to the cybernetic modeling approach by Young et al. [96] is, that the use of local cybernetic variables is circumvented, since the quasi-steady state approximation for intracellular components allows the calculation of internal fluxes relative to uptake rates through exploitation of the stoichiometric coupling. Especially the application to large networks is much less computationally demanding by using HCM instead of the cybernetic model formulation by Young et al. [94]. However, this advantage has to be paid for by the quasi-steady state assumption for all internal metabolites.

4. Experiments with *R. eutropha*

R. eutropha can utilize various carbohydrates and organic acids, e.g. fructose, gluconic acid, lactate, acetate, etc. In this chapter all experiments, which were performed with various carbon sources are described. Experiments are mainly used for parameter estimation and model validation in Chapter 5.

In the following the experiments are named with a unique ID:
`OrganismNumberCarbonsubstrateDevice`. `Organism` can be `Ralst` for *R. eutropha* or `Rhod` for *R. rubrum*.`Carbonsubstrate` can be `Fru` for fructose, `Ace` for acetate or `Glc` for glucose as single carbon source. `Device` indicates in which device or system the experiment was performed. The single bioreactor is indicated by `Single`, the parallel fermenting system is indicated by `Parallel` and shake flasks are indicated by `Flask`.

4.1. *R. eutropha* Growing on Fructose

4.1.1. Ralst01FruSingle

As described above, most models in literature neglect poly(3-hydroxybutyrate) metabolization and therefore there are usually no experimental data available which show poly(3-hydroxybutyrate) metabolization. There are even no experimental data available which show growth, poly(3-hydroxybutyrate) synthesis and poly(3-hydroxybutyrate) metabolization in one single process. Therefore, this experiment was performed to study the different processes: growth, P(3HB) synthesis and P(3HB) metabolization as shown in Figure 1.2.

Initial substrate conditions are 20.0 g/l fructose and 1.5 g/l amonium chloride. This experiment can be divided into four stages (see Figure 4.1):

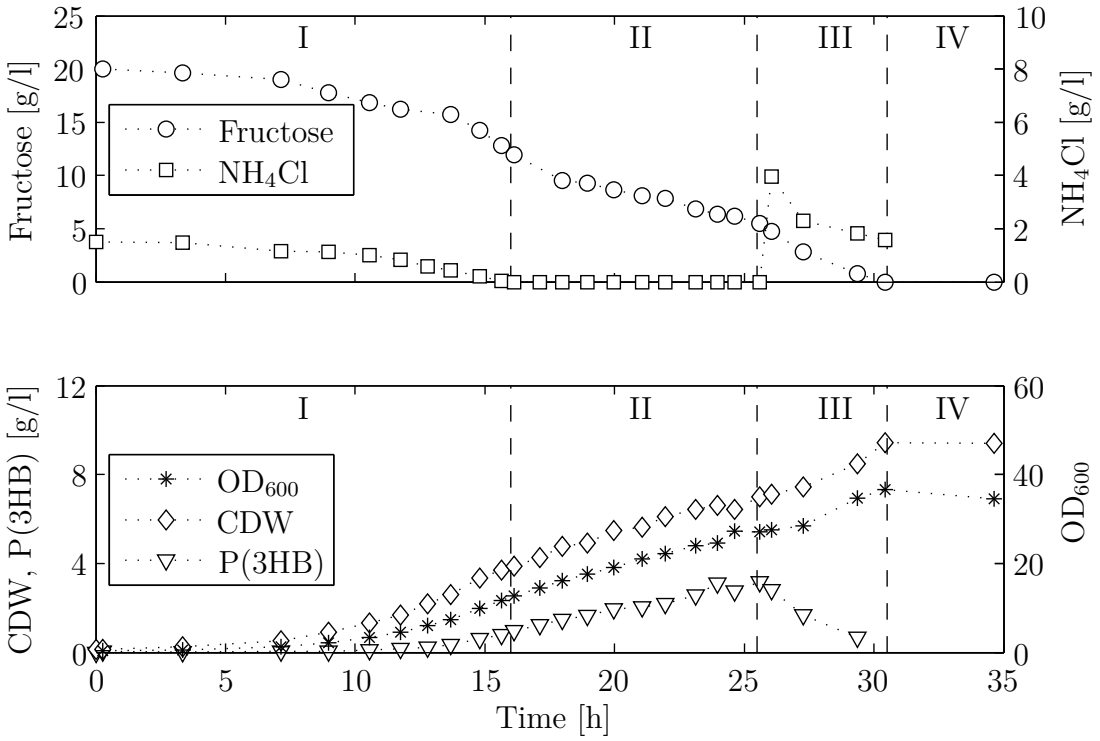

Figure 4.1.: Time course of experiment `Ralst01FruSingle`.

- Stage I: growth
- Stage II: P(3HB) synthesis
- Stage III: P(3HB) metabolization
- Stage IV: maintenance

In the beginning of the experiment sufficient carbon- and nitrogen source is available and total biomass is increasing exponentially (growth phase). After approximately 16 hours the nitrogen source is depleted, but there is still carbon source available. The organism is now storing external carbon source into internal P(3HB), stage II (P(3HB) synthesis). Since nitrogen source is depleted, which is necessary for growth of non-P(3HB) biomass, and no cell internal nitrogen storages are considered, the increase in cell dry weight (CDW) is only due to increase of P(3HB). In this case, one would expect a parallel increase of CDW and P(3HB) in Figure 4.1, which is not the case. Instead of that, CDW and P(3HB) are slightly diverging for higher P(3HB) values. This might be due to cell internal nitrogen storage materials, but which is not considered in this thesis. Furthermore, there

might be a small systematical error in the measurement of P(3HB). The concentration of P(3HB) is calculated from an UV absorbtion spectrum and a set of reference standards (see Chapter 2.4.2). However, P(3HB) from reference standards was already available in a pure form, while P(3HB) from the samples has to be first extracted from the cells. Although extraction was done three times for each sample, the extracted amount of P(3HB) might be lower than the actual amount of P(3HB).

Nevertheless, if no cell internal nitrogen storage is considered, the amount of non-P(3HB) biomass remains constant during this phase. Since this is the catalytically active compartment, the increase of P(3HB) and therefore total biomass and the decrease of fructose is linear, which can be clearly observed during this phase. It is also seen in the experiment that P(3HB) synthesis already starts shortly before all nitrogen source is depleted when only little nitrogen is available (end of stage I). After 26 hours new nitrogen (NH_4Cl) was injected into the bioreactor. At this time point stage III starts. Since there is nitrogen available the organism can metabolize internal P(3HB) and also external carbon source. After approximately 30.5 hours all P(3HB) and external carbon source is depleted and the organism stops growing (stage VI).

4.1.2. Ralst02FruSingle

This experiment is done to repeat the results from experiment `Ralst01FruSingle` (Figure 4.1), with different initial substrate conditions: 21.0 g/l fructose and 0.6 g/l ammonium chloride. In this experiment five stages can be observed (see Figure 4.2):

- Stage I: growth
- Stage II: P(3HB) synthesis
- Stage III: P(3HB) metabolization
- Stage IV: P(3HB) synthesis
- Stage V: maintenance

In the beginning there are sufficient carbon and nitrogen source available and growth is exponential (stage I). After approximately 11 hours nitrogen source is

depleted and remaining carbon source is stored into cell internal storage material P(3HB), stage II. Ammonium chloride is added at t=35 h and the organisms starts to metabolize internal P(3HB), stage III. Growth is now again exponentially. The added nitrogen is again depleted at t=40.5 h and external carbon source is again accumulated into internal P(3HB) until external carbon is fully consumed (stage IV). After approximately 45 hours all substrates are depleted and the organisms stop growing. (stage V)

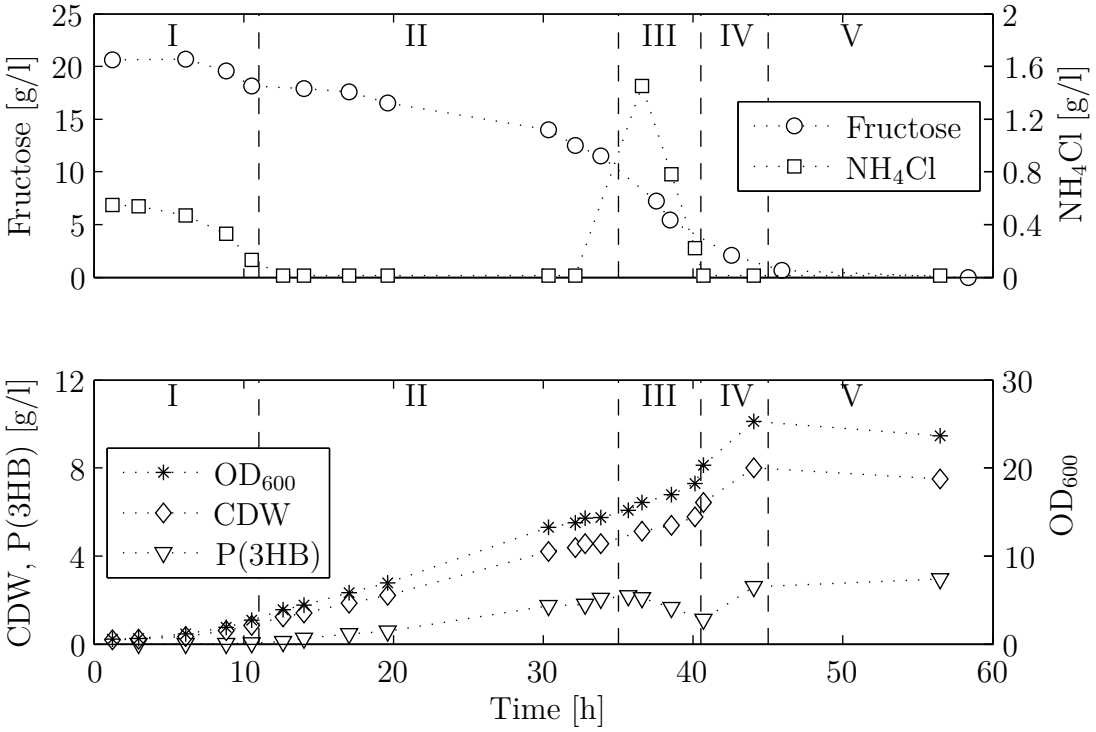

Figure 4.2.: Time course of experiment `Ralst02FruSingle`.

4.1.3. Ralst03FruSingle

In the experiments `Ralst01FruSingle` and `Ralst02FruSingle` the nitrogen source was limited to stimulate P(3HB) synthesis and afterwards added again to study P(3HB) metabolization. The following experiment is therefore performed to study the influence of a fructose pulse instead of an ammonium pulse. Initial substrate conditions are 5.0 g/l fructose and 1.0 g/l amonium chloride. The experiment can be divided into four stages (see Figure 4.3):

- Stage I: growth
- Stage II: maintenance
- Stage III: P(3HB) synthesis
- Stage IV: maintenance

In the first 19 hours total biomass is increasing while fructose and ammonium chloride are decreasing (stage I). After that, both substrates are depleted and the organisms can not grow (stage II). At t = 22 h fructose is added. Since nitrogen source is not available the organisms store the external fructose into internal P(3HB), stage III. Fructose is again depleted after 27 hours and the organisms stop growing (stage IV):

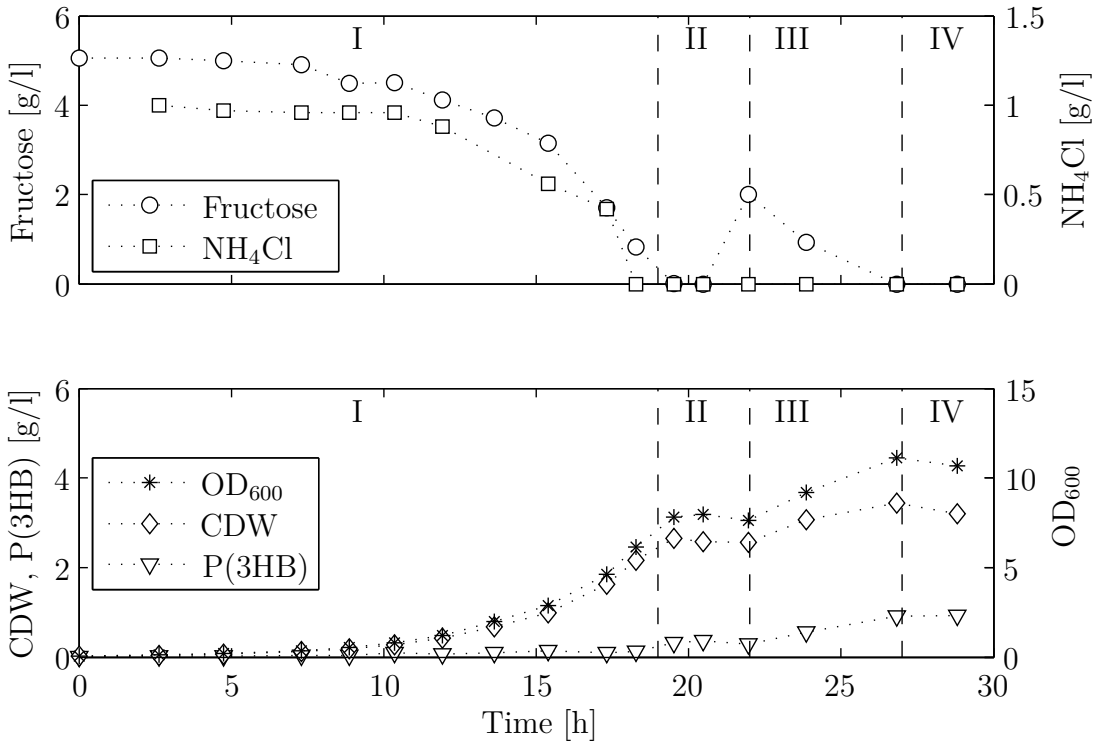

Figure 4.3.: Time course of experiment `Ralst03FruSingle`.

4.1.4. Ralst04FruSingle

In this experiment no substrate was added after depletion and initial substrate conditions are 9.6 g/l fructose and 1.0 g/l amonium chloride. However, there can

be still three stages observed (see Figure 4.4):

- Stage I: growth
- Stage II: P(3HB) synthesis
- Stage III: maintenance

Both substrates are available from the beginning and the organisms are growing. Nitrogen is depleted after approximately 15 hours. Remaining external fructose is stored into internal P(3HB). Growth is now linear since catalytical active biomass remains constant. After approximately 24.5 hours fructose is also depleted and growth stops.

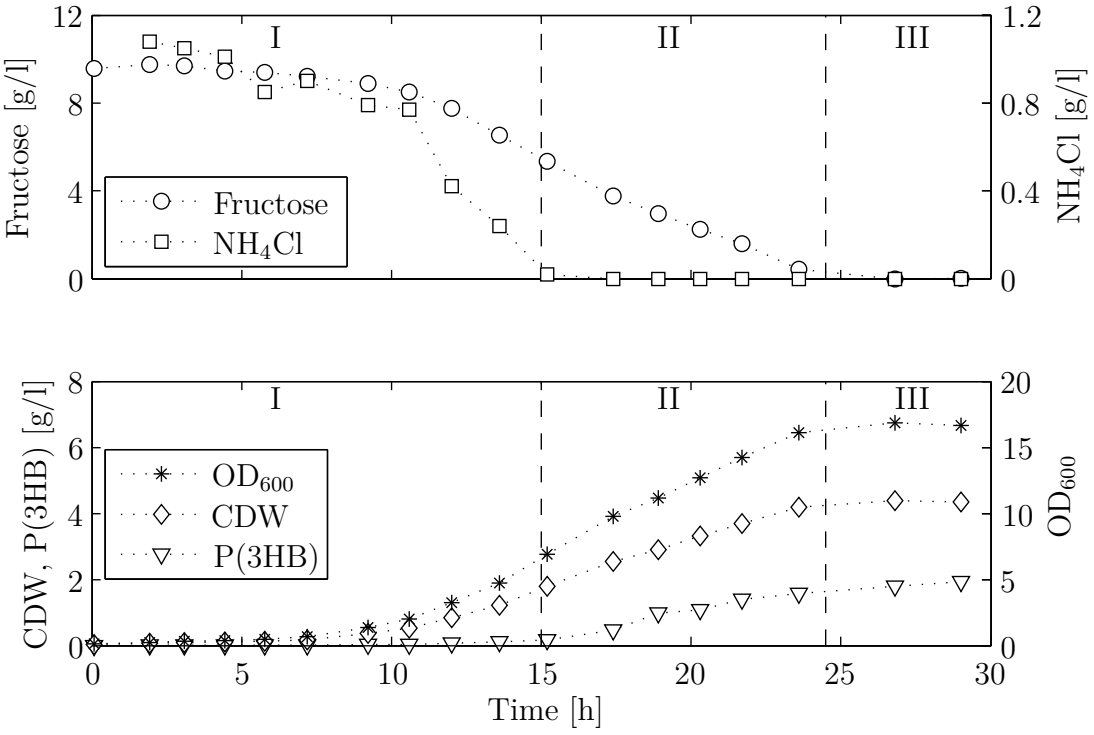

Figure 4.4.: Time course of experiment `Ralst04FruSingle`.

4.1.5. Ralst05FruParallel

This experiment was performed in the parallel fermenting system with four fermenter and an initial volume of 400 ml each. Two fermenter contain fructose as

single carbon source (which are presented in this subsection) and two fermenter contain acetate as single carbon source (which is described in section 4.2).

Due to the small volume only optical density, ammonium chloride concentration and fructose concentration was measured. For measuring cell dry weight and P(3HB) concentration large volumes are necessary. However, P(3HB) concentration and concentration of non-P(3HB) biomass (BIO) can be estimated from optical density and uptaken ammonium chloride as described in section 2.4.3.

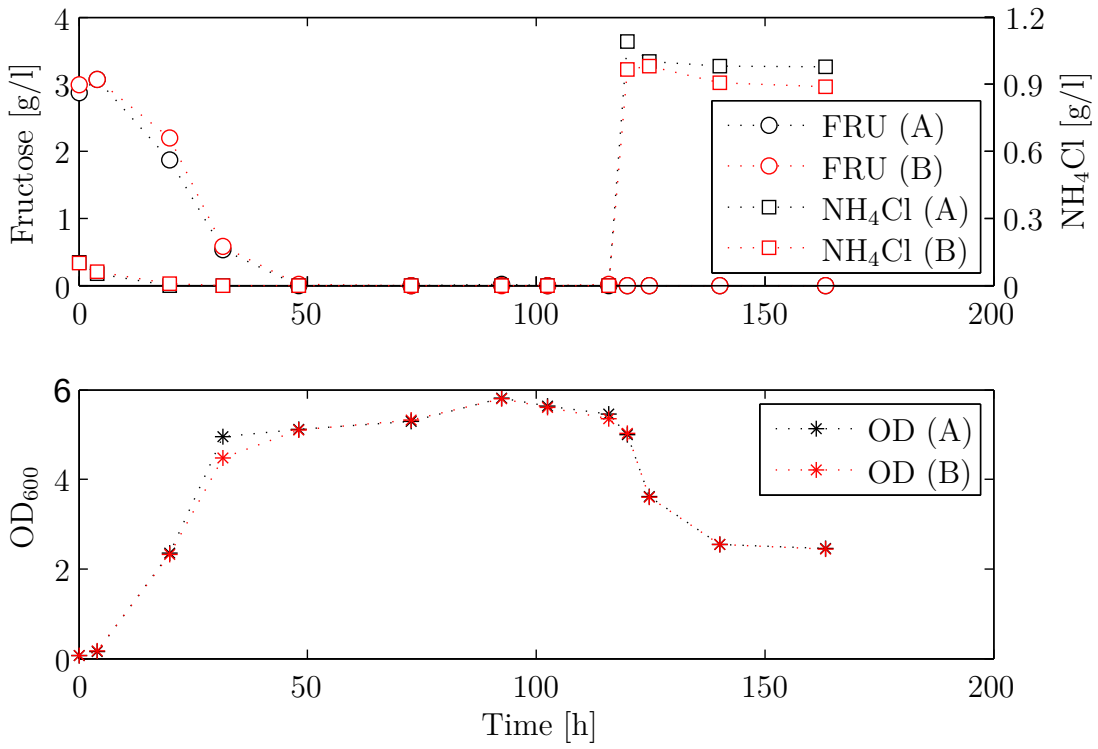

Figure 4.5.: Time course of experiment `Ralst05FruParallel`.

Figure 4.5 shows the time course of the experiments for both parallel fermenter (A) and (B). The experiments starts with a very low ammonium chloride concentration to induce a very early synthesis of P(3HB). Ammonium chloride is depleted after a few hours and external fructose is then stored into P(3HB). Fructose is also depleted after 50 hours. Between 50 and 116 hours neither a carbon nor a nitrogen source is available to the organisms. Usually one would expect that cells die and optical density will decrease. However, OD_{600} remains constant and even increases slightly. It is interesting, that after depletion of all substrates the organisms seem to maintain themselves over such a long time period. This was

also already observed in the experiments above. At time point t=116 h 5 ml of an ammonium stock solution (40 g/l) were added to each of the fermenter. Due to availebility of ammonium chloride, P(3HB) is metabolized and non-P(3HB) biomass is synthesized.

Growth was monitored by measuring optical density and it is first surprising that optical density decreases after adding of ammonium chloride. With available nitrogen source the organisms are able to grow and divide and one would therefore expect an increase in optical density. However, as described in section 2.4.3, P(3HB) and non-P(3HB) biomass have different influence on the optical density, which explains this decrease.

With the correlation given in section 2.4.3 the concentration of P(3HB) and non-P(3HB) biomass and therefore cell dry weight can be estimated from optical density and uptaken ammonium chloride. As seen in Figure 4.6 the concentrations of P(3HB) and CDW are increasing, since ammonium chloride and fructose are available. After a few hours ammonium chloride is depleted and external fructose is stored into cell internal P(3HB), which leads to an increase in CDW. At t = 116 h the organisms start to metabolize P(3HB) and to synthesize non-P(3HB) biomass, because ammonium chloride is now available. Since P(3HB) has a higher influence on the optical density than non-P(3HB) biomass, the optical density is now decreasing, although cells are growing and dividing. Furthermore, there is no external carbon source available and therefore the internal carbon source P(3HB) is metabolized for cell growth. Since even bacterial cells do not have a degree of efficiency of 100%, the cell dry weight will be obviously lower, after metabolization of P(3HB).

The cell internal storage material P(3HB) is fully metabolized, since there is sufficient nitrogen source in the medium. After depletion of P(3HB) the organisms stop growing, and again optical density remains almost constant over a long time period.

P(3HB) can be stained within the cells with different fluorescence dyes. Here, boron-dipyrromethene (BODIPY) was used. Stained cells can be analyzed with flow cytometry which measures the fluorescence intensity of each single cell. This allows to analyze cell to cell heterogeneity. The fluorescence intensity of the dye is correlated with the amount of P(3HB) within the cells. The higher the amount

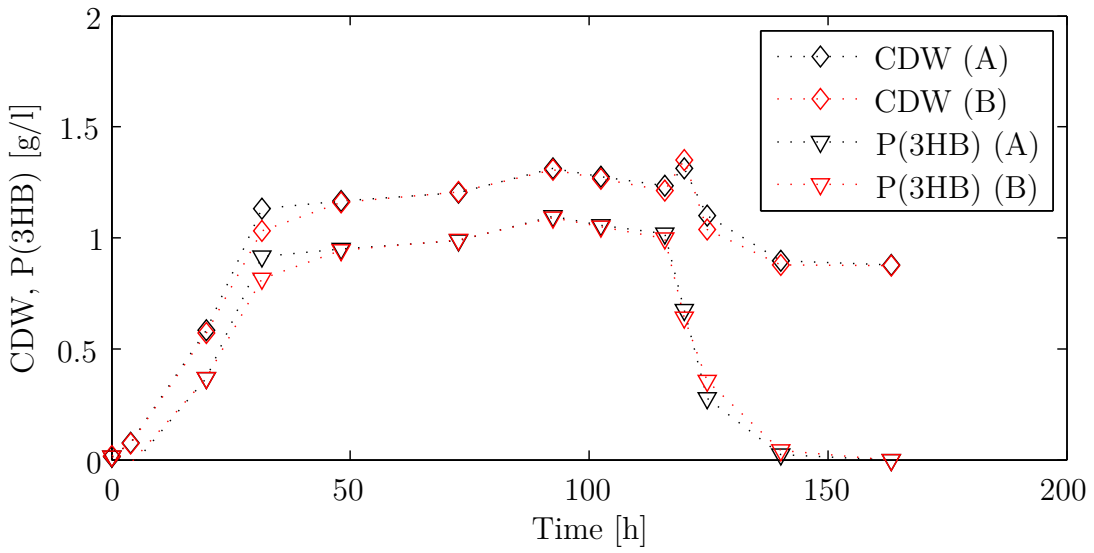

Figure 4.6.: Time course of experiment `Ralst05FruParallel`. P(3HB) and CDW were estimated from optical density and uptaken ammonium chloride.

of P(3HB), the higher the intensity. This is shown in Figure 4.7. In the beginning of the experiment P(3HB) concentration is low and therefore also fluorescence intensity. Within the first 30 hours P(3HB) is increasing, as can be also seen in Figure 4.6 and fluorescence intensity is therefore shifted to higher values and stays there until t=116 h when ammonium chloride is added to the fermenter. P(3HB) concentration is decreasing and fluorescence intensity is therefore shifted back to lower values.

As argued in Chapter 2.4.3 P(3HB) concentration has a significant influence on optical density. This is (also) because, P(3HB) accumulating cells will grow in size, but do not divide under lack of nitrogen. Cells with accumulated P(3HB) are therefore usually bigger than cells without internal P(3HB). With flow cytometry the forward scatter can be measured which is correlated to cell size.

The forward scatter is shown in Figure 4.8. Again, it can be seen, that in the beginning of the experiment cells are rather small, since they do not have accumulated much P(3HB) so far. With increasing P(3HB) concentration the forward scatter is shifted to higher values within the first 30 hours and stays there until ammonium chloride is added. P(3HB) concentration is then decreasing and the forward scatter is shifted backward to lower values.

The advantage of the forward scatter is, that cells do not need to be stained, which is usually a complex procedure. However, in this experiment the parameter for the forward scatter were not well chosen and the resolution is therefore poor. But still, the shifting of the forward scatter peak can be observed.

Fluorescence intensity and forward scatter show mono-modal distributions. Multi-modal distributions would give a hint on potentially multi-stationarity. This seems to be not the case, which is in agreement with the findings to be discussed in Chapter 5.2.3.

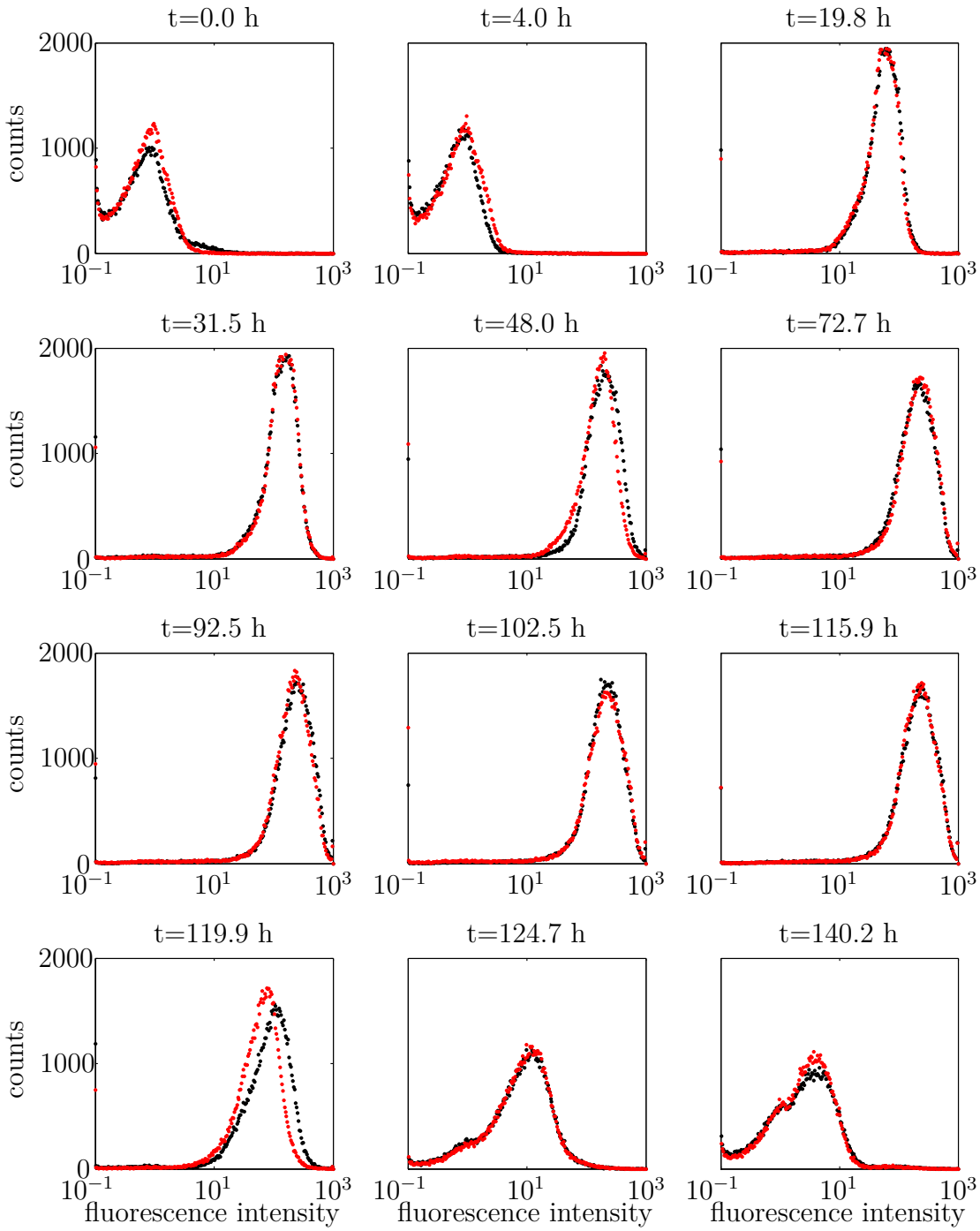

Figure 4.7.: Flow cytometry measurement of experiment `Ralst05FruParallel`, fluorescence intensity. Parallel fermenting system with two fermenter, A: black, B: red.

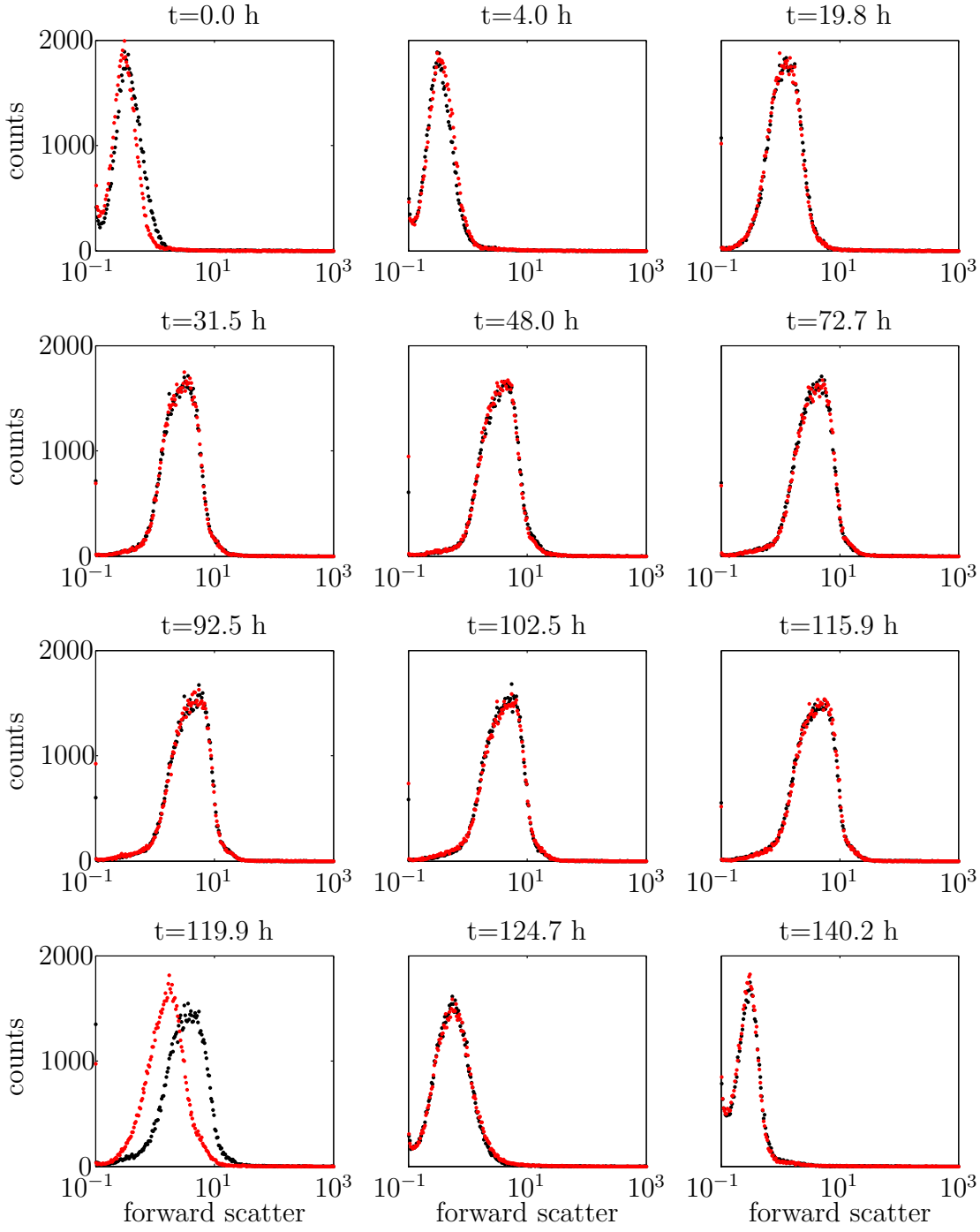

Figure 4.8.: Flow cytometry measurement of experiment `Ralst05FruParallel`, forward scatter. Parallel fermenting system with two fermenter, A: black, B: red.

4.2. *R. eutropha* Growing on Acetate

4.2.1. Ralst06AceParallel

This experiment is similar to experiment `Ralst05FruParallel`, except fructose was substituted with sodium acetate as single carbon source. Both substrates (carbon and nitrogen) are fully depleted after 50 hours (see Figure 4.9). In contrast to experiment `Ralst05FruParallel` the optical density is decreasing after depletion of the substrates. This is quite interesting, since it means, that the organisms grown on fructose can maintain themselves longer, than organisms grown an acetate as single carbon source. Even after adding ammonium chloride at t=116 h the optical density does not increase.

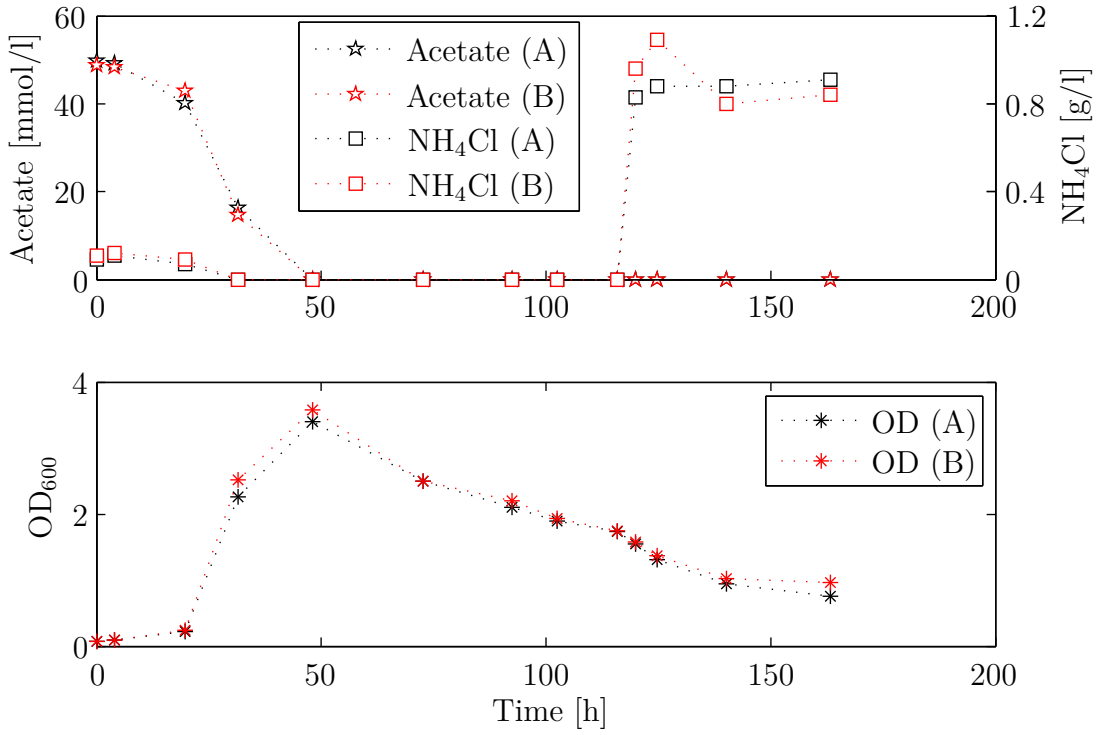

Figure 4.9.: Time course of experiment `Rals06AceParallel`.

Cells were stained with BODYPI and fluorescence intensity measured by flow cytometry is correlated to the amount of cell internal P(3HB). As seen in Figure 4.10 fluorescence intensity is increasing until t=31.5 h. From this time point until t=116 h the peak does not shift significantly, but the shape gets broader and less

high. Since there is no ammonium chloride in the medium cell will not divide at this stage. However, optical density is decreasing (see Figure 4.9). An explanation might be, that some cells die and lyse. *R. eutropha* is known to be able to utilize other organisms. Released nitrogen of lysed cells can be uptaken by healthy cells, which might then be able to divide. Even released carbon source might be uptaken to synthesize further P(3HB) and even new non-P(3HB) biomass. New cells are formed with lower P(3HB) concentration which could explain the broadening of the fluorescence intensity distribution and the decrease in optical density. After adding new ammonium chloride at t=116 h the fluorescence intensity is shifted backwards again to lower values, which means, that P(3HB) is metabolized.

Additionally to the fluorescence intensity the forward scatter was measured with flow cytometry (Figure 4.11). The forward scatter peak also shifts to higher values due to increasing P(3HB) concentration and shifts back after adding ammonium chloride.

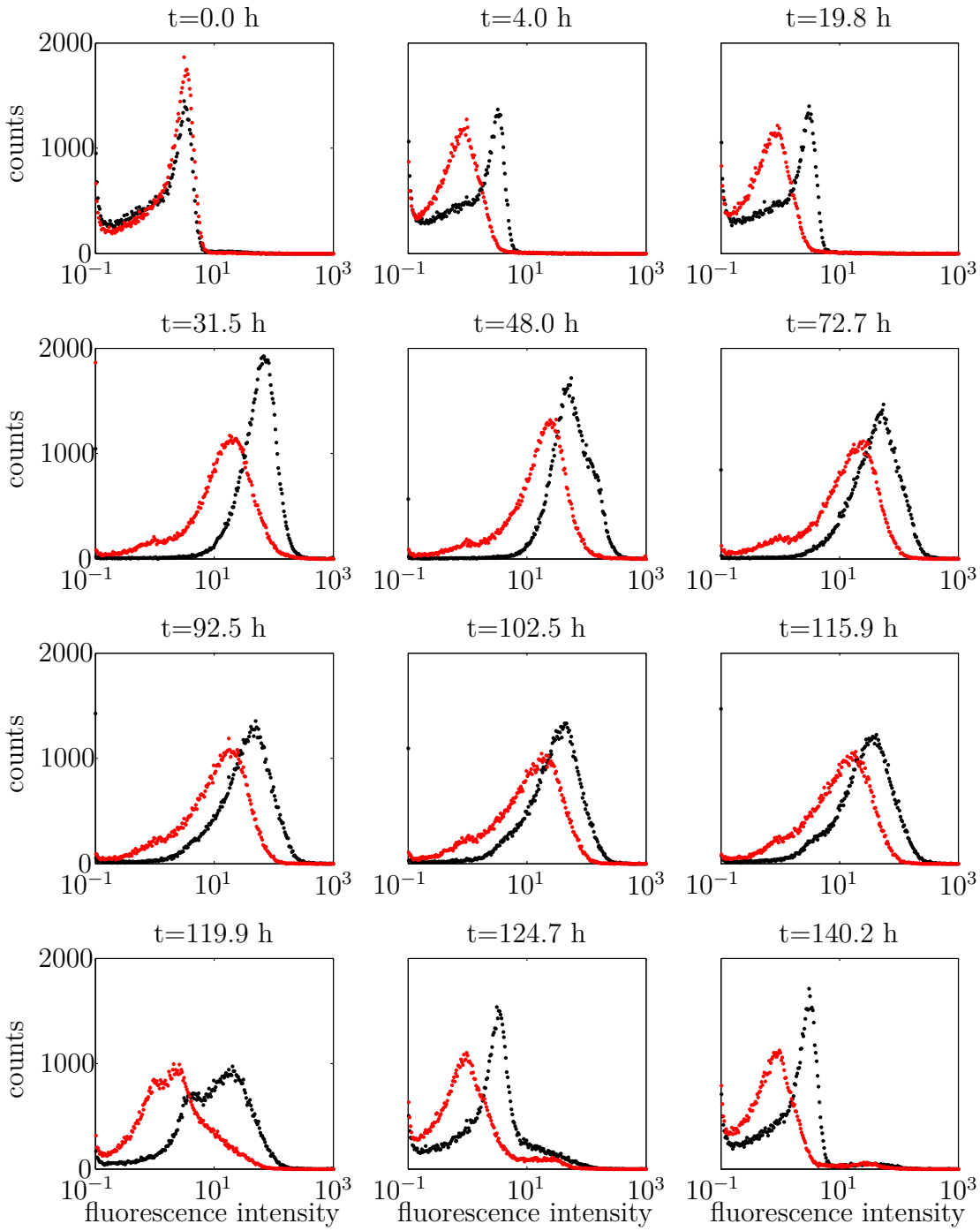

Figure 4.10.: Flow cytometry measurement of experiment `Ralst06AceParallel`, fluorescence intensity. Fermenter (A): black dots, fermenter (B): red dots.

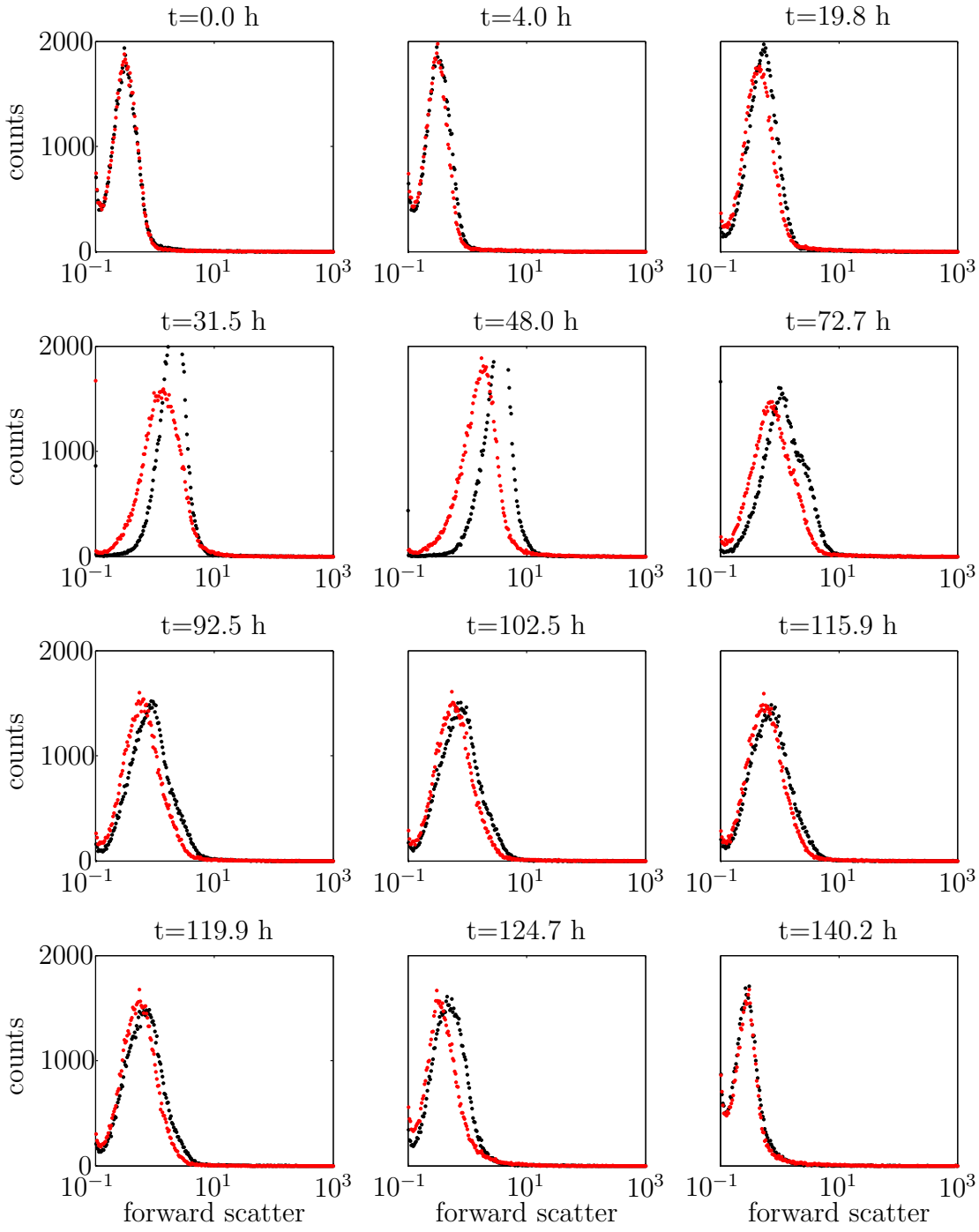

Figure 4.11.: Flow cytometry measurement of experiment `Ralst06AceParallel`, forward scatter. Fermenter (A): black dots, fermenter (B): red dots.

4.3. *R. eutropha* Growing on Glucose

According to literature *R. eutropha* wild-type H16 is not able to grow on glucose as single carbon source [26, 44]. However, glucose-utilizing mutant strains of *R. eutropha* are in principal not unusual. Besides mutagenic approaches, it was also observed that spontaneous glucose mutants appeared in a chemostat with fructose as carbon source after cultivation for several weeks [44]. Kim et al. [37] applied UV mutagenesis to H16 and selected glucose mutants after incubation with very high glucose concentration (60 g/l glucose) for 5-6 days.

In this section experiments are shown, which surprisingly show growth of *R. eutropha* wild-type H16 on glucose as single carbon source.

4.3.1. Ralst07GlcSingle

Similar to experiment `Ralst01FruSingle` an experiment was performed, where fructose was substituted with glucose as single carbon source. As seen in Figure 4.12 *R. eutropha* wild-type H16 is growing on glucose, which is in contradiction to literature. Even the growth behavior is very similar to experiment `Ralst01FruSingle`: P(3HB) concentration is significantly increasing after ammonium source is depleted and decreases again after adding ammonium to the fermenter.

It was therefore a surprise that the wild-type *R. eutropha* H16 in a minimal medium (see table A.2) containing 20 g/l glucose started to grow spontaneously after passing a lag period of 70 h. This observation could be reproduced with three independent *R. eutropha* H16 strains delivered by two different stock culture collections (DSM and NCCB).

4.3.2. Ralst08GlcFlask

For a closer examination a shake flask experiment was performed, where the initial glucose concentration was varied and *R. eutropha* H16 was incubated with 20, 15, 10, 5 and 2 g/l, respectively. The inoculum for all cultivations was derived from H16 stock cultures grown with fructose- and glucose-free LB medium. As

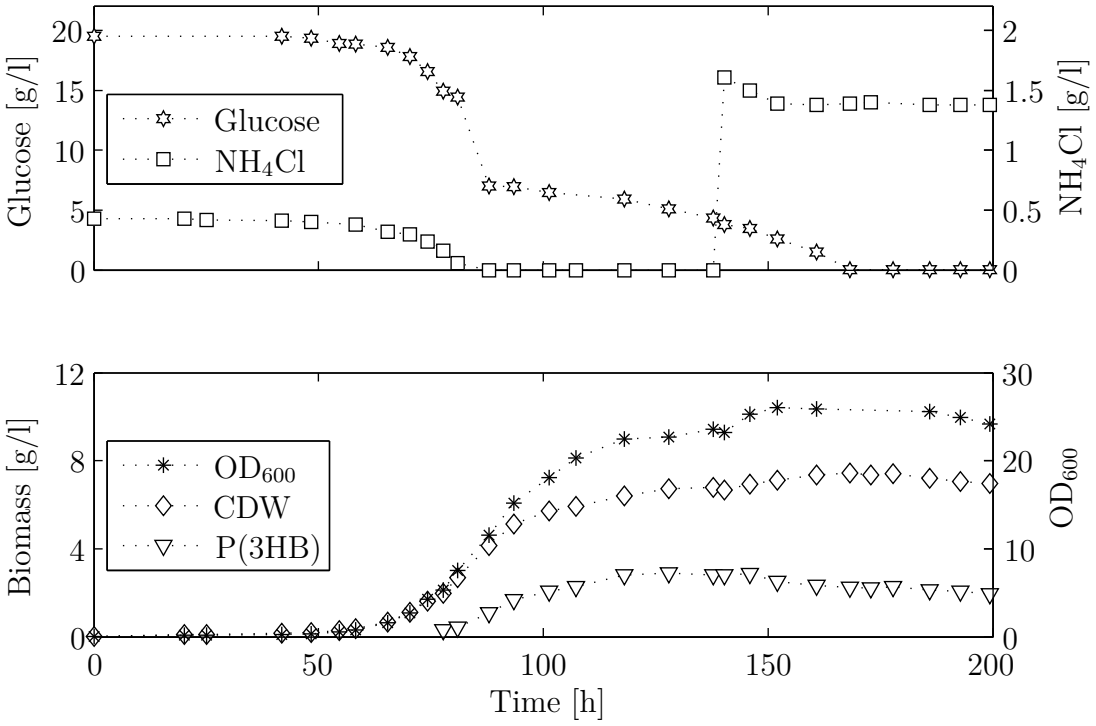

Figure 4.12.: Time course of experiment `Ralst07GlcSingle`.

illustrated in figure 4.13, all applied glucose concentrations resulted in cell growth after prolonged incubation. The time period until the onset of growth was clearly correlated with the initial glucose concentration. With 10-20 g/l glucose, the lag phase lasted about 70 h. When 5 g/l was applied, growth was significantly delayed for 120 h. Even with the lowest concentration of 2 g/l , cell growth occurred after incubation for ca 170 h.

The identical final optical densities in the growth curves are a result of the termination of growth by a severe drop in pH values caused by the consumption of ammonia from the growth medium, since pH value was not controlled in shake flask experiments. With the higher initial concentrations (5-20 g/l), glucose was still present in the culture supernatant in substantial amounts (between 14 and 17 g/l) at the end of the cultivation. Only with 2 g/l glucose, the growth phase was limited by complete consumption of the carbon source. A plot of the observed adaptation time against the initial glucose concentrations for the growth curves of Figure 4.13 reveals an exponential decay function (see insert) thus illustrating an inverse correlation of the initial glucose concentration and the time span upon

which growth occurred. The higher the initial glucose concentration, the earlier was the onset of growth with a saturation at 10-20 g/l. Accordingly, the minimal incubation time for inducing glucose-utilizing mutants was about 70 h.

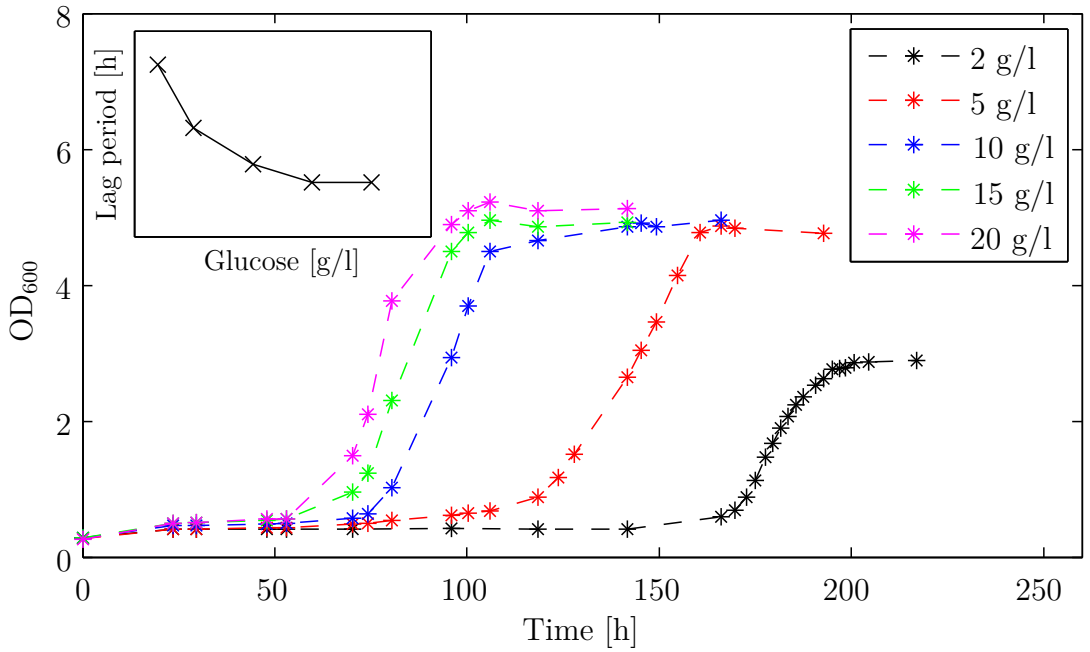

Figure 4.13.: Time course of experiment `Ralst08GlcFlask`. Insert shows the exponential decay of the lag period with increasing glucose concentration.

4.3.3. Ralst09GlcFlask

In contrast to the cultivations in the experiments above, in this experiment cells were taken from adapted 20 g/l glucose cultures and then inoculated into the low-glucose (2 g/l) medium, the long lag phase of Figure 4.13 was gone, and instant growth now occurred without the long delay of non-adapted cultures in the same glucose concentration. Figure 4.14 shows cell growth and substrate consumption of two comparative cultivations, using 2 g/l fructose and 2 g/l glucose as growth substrates, respectively. Fructose cultures grew rapidly and within 12 h reached their maximal cell density. In comparison, high-glucose-adapted cells, now cultivated with low-glucose medium, grew slightly slower.

Since all these experimental observations are in contradiction with literature and rather surprising, further studies were performed in a joint work with Hartmut

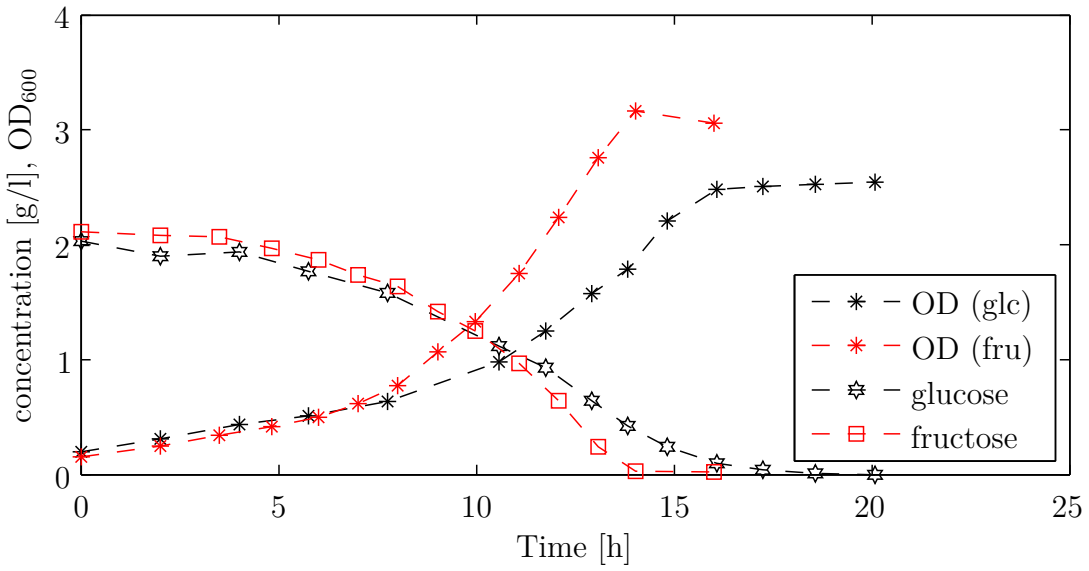

Figure 4.14.: Comparison of growth and substrate consumption of wild type *R. eutropha* H16 cultivated with 2 g/l fructose vs. high-glucose-adapted *R. eutropha* H16 cultivated with 2 g/l glucose.

Grammel and Ruxandra Rehner and recently published [18].

4.4. Conclusion and Summary

In this chapter different experiments with different carbon sources were performed. Fructose is a very common carbon source for *R. eutropha*. These experiments are therefore used in the next chapter to estimate model parameters and to validate the model. Flow cytometry reveals that P(3HB) is unimodal distributed among all cells.

External acetate is directly uptaken into internal acetyl-CoA, which is a direct precursor of P(3HB). Acetate is therefore an interesting carbon source to study synthesis of P(3HB). Cells which were grown on acetate as single carbon source seem to die and lyse faster than cells grown on fructose as single carbon source. Fructose grown cells are able to maintain even a few days.

According to literature, the used strain *R. eutropha* H16 can not grow on glucose, although several glucose-utilizing mutants of *R. eutropha* exist. It was shown that H16 is able to grow on glucose after a prolonged lag phase.

5. Modeling the Production of Poly(3-hydroxybutyrate) in *R. eutropha*

Focus in this chapter is on mathematical modeling of poly(3-hydroxybutyrate) production in *R. eutropha*. For estimation of model parameters and model validation the experiments in Chapter 4 are used. Fructose is used as carbon substrate. As pointed out above, cellular regulation is an essential feature of this process. Since a detailed description of the regulatory processes is complex, a cybernetic approach is applied. In particular, the hybrid cybernetic modeling approach as described in Chapter 3.4.3 is used and extended to internal metabolites with slow dynamics. The hybrid cybernetic model is based on a detailed description of the metabolic processes to be discussed in Chapter 5.1. Although the formulated model is of moderate complexity, it is still computationally challenging when translated into a population balance model. Therefore reductions of this model are discussed. To account for heterogeneity and cell to cell variability, which is a characteristic feature of large scale bioprocesses, finally in Chapter 5.4 a population balance approach is applied and combined here for the first time with the cybernetic approach to describe the kinetics of the metabolic process.

5.1. Metabolic Network

A metabolic network for the production of poly(3-hydroxybutyrate) should at least include metabolic reactions which describe poly(3-hydroxybutyrate) synthesis and metabolization, certain essential building blocks such as TCA-cycle and glycolysis and of course uptake and excretion reactions.

The network $\mathcal{N}_1$ in Figure 3.1 of Chapter 3.1 has these features, although very simplified. TCA cycle is lumped into three reactions r_9, r_{10} and r_{12}; glycolysis is lumped into reaction r_2; penthose-phosphate pathway is lumped into reactions r_3 and r_4; poly(3-hydroxybutyrate) cycle is lumped into reactions r_6, r_7 and r_8; and amino acid synthesis is lumped into reaction r_{11}. Amino acid synthesis is crucial for modeling poly(3-hydroxybutyrate) synthesis, since if essential nutrients for amino acid synthesis are missing, the organism can not grow and stores external carbon source into internal poly(3-hydroxybutyrate).

However, as described in Chapter 3.2 this metabolic network has some drawbacks, since it can not produce biomass under steady state conditions. This can be revised by introducing missing reactions as also described in Chapter 3.2.

The revised metabolic network $\mathcal{N}_2$ has a moderate complexity, but includes all necessary features, as mentioned above. However, this network uses glucose as main carbon source instead of fructose. 1 mol external glucose is transferred to 1 mol internal glucose-6-phosphate (G6P), which then enters the glycolysis. Since this network is rather simplified and many reactions are lumped together, the glucose uptake can be substituted with a fructose uptake, where 1 mol external fructose will also be converted into 1 mol G6P. This is usually done via F16P and F6P, but can also be lumped together.

The network $\mathcal{N}_2$ is a possible candidate for further dynamic modeling. However, the last step is to evaluate if this metabolic network can predict experimental data. This is done via metabolic yield analysis as described in Chapter 3.3. Figure 5.1 shows a section of the two dimensional yield space $Y_{\mathrm{P(3HB)/FRU}}$ vs. $Y_{\mathrm{BIO/FRU}}$ and the yield date from experiment `Ralst01FruSingle`. Unfortunately experimental data are outside the yield space and can not be represented by the metabolic network. Any dynamic model based on this network will therefore fail to predict these data.

If experimental data are outside the yield space, this can have different reasons: either the experimental data are wrong or the network is oversimplified and essential reactions are missing. Since several experimental data were outside the yield space, it is concluded that the given metabolic network is too simple and a more detailed network is needed.

There are several metabolic networks for *R. eutropha* available in literature, which

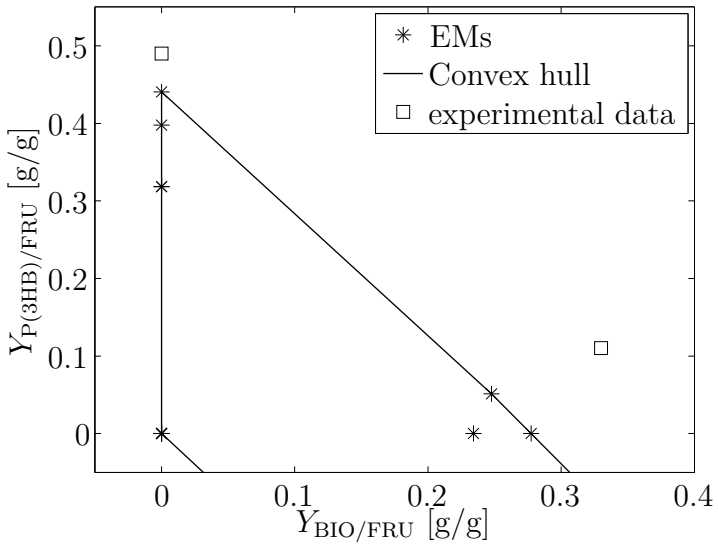

Figure 5.1.: Two dimensional yield space of the extended network from Chapter 3.2. All experimental data are outside the convex hull. This network is therefore not suitable to represent experimental data.

are usually constructed for certain needs. From these, the metabolic network for *R. eutropha* from Katoh [32] is chosen, since it is not that simple than the previous network from Gadkar [20] and it contains most of the essential parts needed for dynamic modeling of poly(3-hydroxybutyrate) synthesis, this are: poly(3-hydroxybutyrate) synthesis rate and essential cell internal building blocks, such as glycolysis, penthose phosphate pathway and TCA cycle.

However, the network by Katoh lacks an uptake rate for fructose. Therefore this was added to the network. Additionally, the network by Katoh only produces poly(3-hydroxybutyrate), but is not able to metabolize it. The poly(3-hydroxybutyrate) cycle is therefore extended. Furthermore the penthose-phosphate pathway is formulated in a more detailed way. The resulting network is shown in Figure 5.2 and all reaction equations are given in Appendix A.2.

5.1.1. Metabolic yield analysis

The metabolic network in Figure 5.2 has 36 reactions, some of them are reversible. From this network 122 elementary modes are calculated by using Metatool [84]. However, it is not necessary to use all elementary modes for dynamic model-

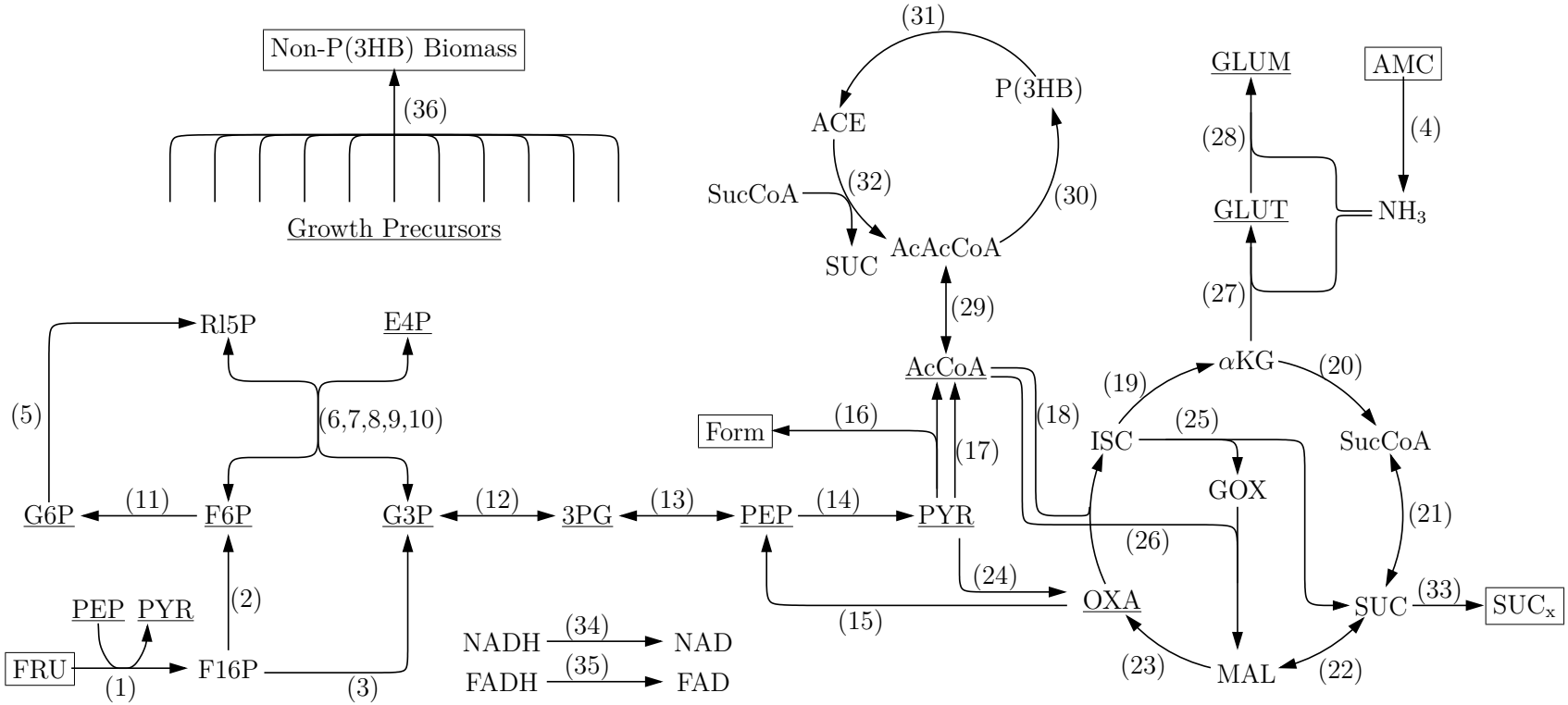

Figure 5.2.: Metabolic network of *R. eutropha* for synthesis and metabolization of poly(3-hydroxybutyrate). External metabolites are boxed. Growth precursors are underlined.

ing, but a smaller subset which is essential for describing and predicting observed metabolic behavior. For reducing the full set of elementary modes to a smaller subset *metabolic yield analysis* is used as described in Chapter 3.3.

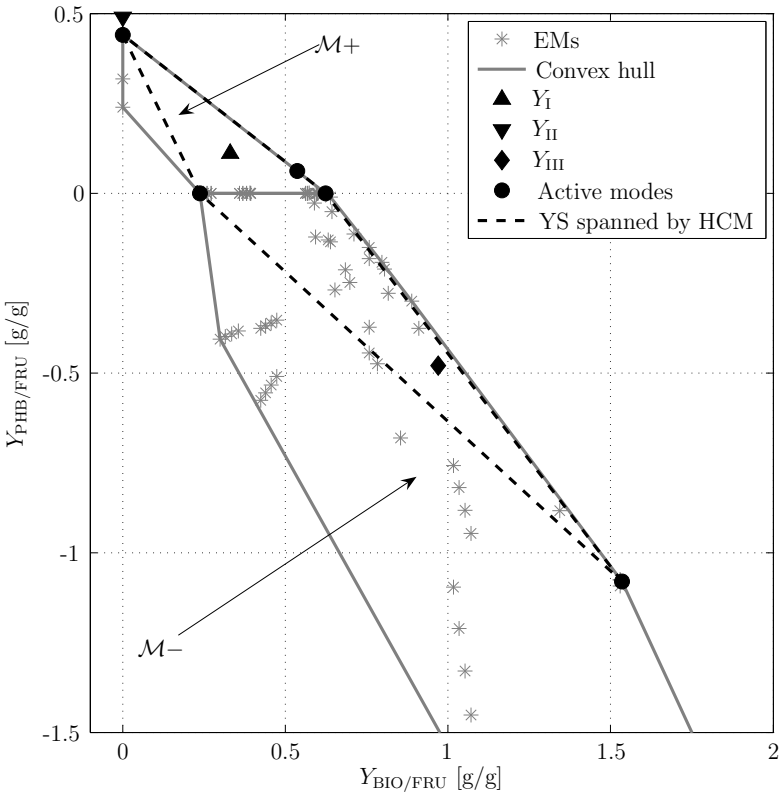

Figure 5.3.: Yield space of sets $\mathcal{M}-$ and $\mathcal{M}+$ with experimental yield data ($\blacktriangle, \blacktriangledown, \blacklozenge$) from experiment `Ralst01FruSingle` and active modes ($\bullet$) for the hybrid cybernetic model.

This is done by dividing all elementary modes into subgroups. Group $\mathcal{M}-$ contains the elementary modes where the internal metabolite poly(3-hydroxybutyrate) does not act as product and group $\mathcal{M}+$ contains the elementary modes where poly(3-hydroxybutyrate) does not act as substrate. These subgroups are convex in yield space and both groups include the elementary modes which do not produce or metabolize poly(3-hydroxybutyrate). Since internal metabolites with slow dynamics can act as source and sinks (e.g. substrates and products), it is not guaranteed that the full yield space is convex. It is therefore necessary to group the elementary modes into convex subgroups.

It is convenient to normalize all elementary modes to a certain metabolite, since this will reduce the dimension of the yield space. Usually elementary modes are

normalized with respect to a preferred substrate. In the following fructose is chosen as preferred substrate and all elementary modes are normalized with respect to fructose. Hence, the yield space becomes three dimensional ($Y_{\mathrm{P(3HB)/FRU}}$, $Y_{\mathrm{BIO/FRU}}$, $Y_{\mathrm{AMC/FRU}}$).

However, due to the stoichiometry of the network, the concentration of the non-P(3HB) biomass compartment BIO is linearly correlated with the uptaken nitrogen source ammonium chloride (AMC). Therefore the yield space reduces to only two dimensions ($Y_{\mathrm{P(3HB)/FRU}}$, $Y_{\mathrm{BIO/FRU}}$).

For each convex group ($\mathcal{M}-$ and $\mathcal{M}+$) the metabolic yield analysis is performed separately (see Figure 5.3). At first so called generating modes are chosen from both groups. These are the vertices of the convex hull of the yield space. Group $\mathcal{M}+$ has five generating modes and group $\mathcal{M}-$ has eight generating modes. Since experimental data are available the number of generating modes is further reduced to so called active modes.

In Table 5.1 the stoichiometry of the generating and active modes are presented. Additionally Table 5.2 lists the active modes with their corresponding reactions. These active modes span a subspace of the yield space which is necessary to represent the experimental yield data from experiment `Ralst01FruSingle`. These five active modes are later used for the hybrid cybernetic model in Chapter 5.2.

Table 5.1.: Stoichiometry of generating modes (GMs) and computed subgroup of active modes (AMs), which are necessary to reproduce experimental data and hence are used for the hybrid cybernetic model.

	Stoichiometry of GMs					
GM	Y_{AMC}	Y_{BIO}	Y_{FRU}	$Y_{\mathrm{P(3HB)}}$	Group	AM
1	0.00	0.00	-1.00	0.24	$\mathcal{M}+$	–
2	0.00	0.00	-1.00	0.44	$\mathcal{M}+$	1
3	-0.25	0.54	-1.00	0.06	$\mathcal{M}+$	2
4	-2.62	5.55	-1.00	-8.91	$\mathcal{M}-$	–
5	-0.14	0.30	-1.00	-0.41	$\mathcal{M}-$	–
6	-0.30	0.64	-1.00	-0.01	$\mathcal{M}-$	–
7	-0.38	0.80	-1.00	-0.19	$\mathcal{M}-$	–
8	-0.42	0.89	-1.00	-0.30	$\mathcal{M}-$	–
9	-0.72	1.53	-1.00	-1.08	$\mathcal{M}-$	5
10	-0.29	0.62	-1.00	0.00	$\mathcal{M}+$, $\mathcal{M}-$	4
11	-0.11	0.24	-1.00	0.00	$\mathcal{M}+$, $\mathcal{M}-$	3

Table 5.2.: Chosen active modes with their corresponding metabolic reactions and the synthesized/consumed biomass compartments.

AM	Corresponding reactions	BIO	P(3HB)
1	1-3, 5-15, 17, 24, 29, 30, 34	–	synthesized
2	1-14, 16, 18, 19, 24, 27-30, 34, 36	synthesized	synthesized
3	1-4, 6-15, 17-21, 24, 27-28, 33, 34, 36	synthesized	–
4	1-15, 17-19, 24, 27-28, 34, 36	synthesized	–
5	1, 2, 4-13, 15, 18-29, 31-32, 34-36	synthesized	consumed

5.2. Hybrid Cybernetic Model

In the original formulation of the hybrid cybernetic modeling (HCM) approach (see Chapter 3.4.3) it is assumed that all internal metabolites are quasi-static, which allows the calculation of internal fluxes relative to uptake rates through exploitation of the stoichiometric coupling. This is based on the assumption, that internal rates are very fast in comparison to exchange rates. However, for some internal metabolites this assumption may not hold, e.g. membranes or internal storage materials like poly(3-hydroxybutyrate).

For these cases, the hybrid cybernetic modeling approach is extended to include internal metabolites with slow dynamics. To do so, the vector of internal metabolite concentrations $\mathbf{m}$ is splitted into the vector of internal metabolite concentrations with fast dynamics $\mathbf{m_f}$ and the vector of internal metabolite concentrations with slow dynamics $\mathbf{m_s}$. Similarly, the matrix $\mathbf{S_m}$ is splitted into $\mathbf{S_{m,f}}$ and $\mathbf{S_{m,s}}$. Equation (3.3) is rewritten to

$$\frac{\mathrm{d}}{\mathrm{d}t}\begin{bmatrix}\mathbf{m_s}\\ \mathbf{m_f}\end{bmatrix} = \begin{bmatrix}\mathbf{S_{m,s}}\\ \mathbf{S_{m,f}}\end{bmatrix}\mathbf{r} - \begin{bmatrix}\mathbf{m_s}\\ \mathbf{m_f}\end{bmatrix}\mu \tag{5.1}$$

where only for metabolites with fast dynamics the quasi-steady state assumption holds:

$$\frac{\mathrm{d}\mathbf{m_f}}{\mathrm{d}t} = 0 \tag{5.2}$$

Elementary modes are then calculated from Equation (5.2).

However, these metabolites still contribute to biomass concentration c. Conversion from substrates into biomass is usually an auto-catalytic process, where the biomass is the catalytical component and growth rate and uptake rates are there-

fore proportional to biomass concentration. It is obvious that not all biomass compartments are catalytical active, but as long as biomass composition does not change significantly, the fraction of the catalytical biomass compartments will stay constant and is then included into the rate constants. By doing so, it can be assumed that growth and uptake rates are proportional to total biomass concentration instead of a certain catalytical active compartment.

However, this can not be applied, if biomass composition changes significantly, because fraction of catalytical active compartment may also change significantly. In the case of internal metabolites with slow dynamics, biomass composition will change. And it is obvious that for instance membranes and internal storage compounds are usually no catalytical active components. Therefore, the fraction of catalytical active components has to be considered in this case.

In the cybernetic modeling approach reaction rates are catalyzed by key enzymes. The fraction b of catalytical active biomass is therefore included into enzyme synthesis:

$$\frac{\mathrm{d}\mathbf{e}}{\mathrm{d}t} = \boldsymbol{\alpha} + \mathbf{r_{EM}}\, b - \mathrm{diag}(\boldsymbol{\beta})\, \mathbf{e} - \mu\, \mathbf{e} \tag{5.3}$$

with

$$0 \leq b \leq 1 \tag{5.4}$$

In the standard approach, where biomass composition does not change (e.g. total biomass is the catalytical active component) $b = 1$. In all other cases b has to be calculated from knowledge about metabolites with slow dynamics. In the case, where all metabolites with slow dynamics are not catalytical active, b is simply calculated by:

$$b = 1 - ||\mathbf{m_s}||_1 \tag{5.5}$$

Even if this fraction still contains non catalytical active components, the same assumption as for total biomass as catalytical active component holds.

The formulated approach allows to include internal metabolites for which the quasi-steady state assumption does not hold, but still gets along with only global control. It is obvious that this approach lies between the formulation of Young et al. [96] and the original HCM [38], but combines the advantages from both formulations.

In the present case, P(3HB) is considered as the only internal metabolite with slow dynamics.

The balance equations for the hybrid cybernetic model in *R. eutropha* are therefore given as follows

$$\frac{\mathrm{d}}{\mathrm{d}t}\begin{bmatrix} x_{\mathrm{FRU}} \\ x_{\mathrm{AMC}} \end{bmatrix} = \mathbf{S_s Z}\,\mathbf{r_M}\,c \tag{5.6}$$

$$\frac{\mathrm{d}}{\mathrm{d}t} m_{\mathrm{P(3HB)}} = \mathbf{S_{m,s} Z}\,\mathbf{r_M} - \mu\, m_{\mathrm{P(3HB)}} \tag{5.7}$$

$$\frac{\mathrm{d}\mathbf{e}}{\mathrm{d}t} = \boldsymbol{\alpha} + \mathbf{r_{EM}}\, b - \mathrm{diag}(\boldsymbol{\beta})\,\mathbf{e} - \mu\,\mathbf{e} \tag{5.8}$$

$$\frac{\mathrm{d}c}{\mathrm{d}t} = \mu\, c \tag{5.9}$$

where $b = 1 - m_{\mathrm{P(3HB)}}$ and $\mu = \mathbf{S}_\mu \mathbf{Z}\,\mathbf{r_M}$.

The stoichiometric matrices $\mathbf{S_s Z}$, $\mathbf{S_{m,s} Z}$ and $\mathbf{S}_\mu \mathbf{Z}$ are given due to the metabolic yield analysis:

$$\mathbf{S_s Z} = \begin{bmatrix} -1.00 & -1.00 & -1.00 & -1.00 & -1.00 \\ 0.00 & -0.25 & -0.11 & -0.29 & -0.72 \end{bmatrix} \tag{5.10}$$

$$\mathbf{S_{m,s} Z} = \begin{bmatrix} 0.44 & 0.06 & 0.00 & 0.00 & -1.08 \end{bmatrix} \tag{5.11}$$

$$\mathbf{S}_\mu \mathbf{Z} = \begin{bmatrix} 0.44 & 0.60 & 0.24 & 0.62 & 0.45 \end{bmatrix} \tag{5.12}$$

The reaction rates $\mathbf{r_M}$ are controlled by the cybernetic control variable $\mathbf{v}$ and catalyzed by key enzymes $\mathbf{e}$:

$$\mathbf{r_M} = \mathrm{diag}(\mathbf{v})\,\mathrm{diag}(\mathbf{e}^{\mathrm{rel}})\,\mathbf{r}_\mathbf{M}^{\mathrm{kin}} \tag{5.13}$$

The kinetic parts $\mathbf{r}_\mathbf{M}^{\mathrm{kin}}$ of the reaction rates are modeled with Monod type kinetics:

$$r_{\mathrm{M},1}^{\mathrm{kin}} = k_{r,1}\,\frac{x_{\mathrm{FRU}}}{K_{\mathrm{FRU}} + x_{\mathrm{FRU}}} \tag{5.14}$$

$$r_{\mathrm{M},i}^{\mathrm{kin}} = k_{r,i}\,\frac{x_{\mathrm{FRU}}}{K_{\mathrm{FRU}} + x_{\mathrm{FRU}}}\,\frac{x_{\mathrm{AMC}}}{K_{\mathrm{AMC}} + x_{\mathrm{AMC}}}, \quad i = 2,3,4 \tag{5.15}$$

$$r_{\mathrm{M},5}^{\mathrm{kin}} = k_{r,5}\,\frac{x_{\mathrm{FRU}}}{K_{\mathrm{FRU}} + x_{\mathrm{FRU}}}\,\frac{x_{\mathrm{AMC}}}{K_{\mathrm{AMC}} + x_{\mathrm{AMC}}}\,\frac{m_{\mathrm{P(3HB)}}}{K_{\mathrm{P(3HB)}} + x_{\mathrm{P(3HB)}}} \tag{5.16}$$

The enzyme synthesis rates $\mathbf{r_{EM}}$ are controlled by the cybernetic control variable $\mathbf{u}$:

$$\mathbf{r_{EM}} = \mathrm{diag}(\mathbf{u})\, \mathbf{r}^{\mathrm{kin}}_{\mathbf{EM}} \tag{5.17}$$

where the kinetic part $\mathbf{r}^{\mathrm{kin}}_{\mathbf{EM}}$ is also modelled with Monod type kinetics:

$$r^{\mathrm{kin}}_{\mathrm{EM},1} = k_{e,1} \frac{x_{\mathrm{FRU}}}{K_{\mathrm{FRU}} + x_{\mathrm{FRU}}} \tag{5.18}$$

$$r^{\mathrm{kin}}_{\mathrm{EM},i} = k_{e,i} \frac{x_{\mathrm{FRU}}}{K_{\mathrm{FRU}} + x_{\mathrm{FRU}}} \frac{x_{\mathrm{AMC}}}{K_{\mathrm{AMC}} + x_{\mathrm{AMC}}}, \quad i = 2,3,4 \tag{5.19}$$

$$r^{\mathrm{kin}}_{\mathrm{EM},5} = k_{e,5} \frac{x_{\mathrm{FRU}}}{K_{\mathrm{FRU}} + x_{\mathrm{FRU}}} \frac{x_{\mathrm{AMC}}}{K_{\mathrm{AMC}} + x_{\mathrm{AMC}}} \frac{m_{\mathrm{P(3HB)}}}{K_{\mathrm{P(3HB)}} + x_{\mathrm{P(3HB)}}} \tag{5.20}$$

5.2.1. Cybernetic Control Laws and Metabolic Objective Function

For computing the cybernetic control laws, one has to chose a policy for computing the return on investment (see Table 3.8) and a metabolic objective function $\phi(\mathbf{y})$. Since the time span Δt for which organisms optimize the allocation of their limited resources is usually unknown, the *Greedy* policy is chosen. An often used objective function is maximizing biomass, e.g. $\phi(\mathbf{y}) = c$. P(3HB) is an integral part of the biomass, and maximizing biomass as metabolic objective function will obviously try to increase P(3HB) as well as non-P(3HB) biomass. This is in fact a favourable behaviour. On the other hand, if there is sufficient internal carbon source in terms of P(3HB) available, but no external carbon source, then, this metabolic objective function will lead to a behaviour were no P(3HB) is metabolized to synthesize more non-P(3HB) biomass. That means, that no cell division will occur. This is in fact in contradiction to what is observed. Maximizing biomass is therefore not the best choice.

An other often used alternative as metabolic objective function is maximizing substrate uptake. It is reasonable to maximize a carbon source substrate, e.g. fructose. The metabolic objective function can then be formulated as:

$$\phi(\mathbf{y}) = -x_{\mathrm{FRU}} \tag{5.21}$$

This would lead to minimize external fructose and therefore to maximize the fruc-

tose uptake. However, fructose is not the only carbon source in this system. PHB also acts as carbon source in EM_5, where P(3HB) is metabolized. If only fructose update is maximized, this would lead to the same problems as described for maximizing biomass. The metabolic objective function should therefore maximize any carbon uptake, e.g.

$$\phi(\mathbf{y}) = -x_{\mathrm{FRU}} - x_{\mathrm{P(3HB)}} \tag{5.22}$$

where $x_{\mathrm{P(3HB)}} = m_{\mathrm{P(3HB)}}\, c$. It it reasonable to use $x_{\mathrm{P(3HB)}}$ instead of $m_{\mathrm{P(3HB)}}$, since it has the same dimension as x_{FRU}.

However, fructose and the monomer 3HB have different number of carbon units and obviously different molar masses. It is therefore reasonable to include this into the metabolic objective function, e.g.:

$$\phi(\mathbf{y}) = -\left(\frac{6}{M_{\mathrm{FRU}}}\, x_{\mathrm{FRU}} + \frac{4}{M_{\mathrm{3HB}}}\, x_{\mathrm{P(3HB)}}\right) \frac{M_{\mathrm{FRU}}}{6} \tag{5.23}$$

where M_{FRU}=180 g/mol is the molar mass of fructose and M_{3HB}=86 g/mol is the molar mass of monomer 3HB. Fructose has 6 carbon units and 3HB has 4. The metabolic objective function is additionally scaled with $\frac{M_{\mathrm{FRU}}}{6}$. This has no effect, but emphasizes that fructose is the preferred carbon substrate.

From the metabolic objective function the vector $\mathbf{q}$ is calculated:

$$\mathbf{q} = \frac{\partial \phi(\mathbf{y})}{\partial \mathbf{y}} = \begin{bmatrix} -1 & 0 & -1.4 & 0 & 0 & 0 & 0 & 0 & 0 \end{bmatrix}^{\mathrm{T}} \tag{5.24}$$

where

$$\mathbf{y} = \begin{bmatrix} x_{\mathrm{FRU}} & x_{\mathrm{AMC}} & x_{\mathrm{P(3HB)}} & e_1 & e_2 & e_3 & e_4 & e_5 & c \end{bmatrix}^{\mathrm{T}} \tag{5.25}$$

Since most of the entries in $\mathbf{q}$ are zero, it is only necessary to compute the first

and the third row of the matrices $\mathbf{B_v}$ and $\mathbf{B_u}$:

$$\mathbf{B_v^T} = \begin{bmatrix} -1\, e_1^{\mathrm{rel}}\, r_1^{\mathrm{kin}}\, c & * & 0.44\, e_1^{\mathrm{rel}}\, r_1^{\mathrm{kin}}\, c & * & * & * & * & * & * \\ -1\, e_2^{\mathrm{rel}}\, r_2^{\mathrm{kin}}\, c & * & 0.06\, e_2^{\mathrm{rel}}\, r_2^{\mathrm{kin}}\, c & * & * & * & * & * & * \\ -1\, e_3^{\mathrm{rel}}\, r_3^{\mathrm{kin}}\, c & * & 0 & * & * & * & * & * & * \\ -1\, e_4^{\mathrm{rel}}\, r_4^{\mathrm{kin}}\, c & * & 0 & * & * & * & * & * & * \\ -1\, e_5^{\mathrm{rel}}\, r_5^{\mathrm{kin}}\, c & * & -1.08\, e_5^{\mathrm{rel}}\, r_5^{\mathrm{kin}}\, c & * & * & * & * & * & * \end{bmatrix} \tag{5.26}$$

$$\mathbf{B_u^T} = \begin{bmatrix} 0 & * & 0 & * & * & * & * & * & * \\ 0 & * & 0 & * & * & * & * & * & * \\ 0 & * & 0 & * & * & * & * & * & * \\ 0 & * & 0 & * & * & * & * & * & * \\ 0 & * & 0 & * & * & * & * & * & * \end{bmatrix} \tag{5.27}$$

Unfortunately all necessary entries in $\mathbf{B_u}$ in Equation (5.27) are zero, which would lead to $\mathbf{p_u} = \mathbf{0}$. This is a drawback of the *Greedy* policy, due to $\Delta t = 0$. This was already described in [96] and suggested to evaluate $\mathbf{B_u}$ at quasi steady state for enzyme levels. To do so, the enzyme levels in the reaction rate $\mathbf{r_M}$ are set to:

$$e_i := e_i^{\mathrm{qss}} = \frac{\alpha_i}{\beta_i + \mu} + \underbrace{\left(\frac{r_{\mathrm{E},i}\, b}{\beta_i + \mu}\right)}_{e_i^\circ} u_i \tag{5.28}$$

and $\mathbf{B_u}$ now computes to:

$$\mathbf{B_u^T} = \begin{bmatrix} -1\, v_1^\circ\, e_1^\circ / e_1^{\max}\, r_1^{\mathrm{kin}}\, c & * & 0.44\, v_1^\circ\, e_1^\circ / e_1^{\max}\, r_1^{\mathrm{kin}}\, c & * & * & * & * & * & * \\ -1\, v_2^\circ\, e_2^\circ / e_2^{\max}\, r_2^{\mathrm{kin}}\, c & * & 0.06\, v_2^\circ\, e_2^\circ / e_2^{\max}\, r_2^{\mathrm{kin}}\, c & * & * & * & * & * & * \\ -1\, v_3^\circ\, e_3^\circ / e_3^{\max}\, r_3^{\mathrm{kin}}\, c & * & 0 & * & * & * & * & * & * \\ -1\, v_4^\circ\, e_4^\circ / e_4^{\max}\, r_4^{\mathrm{kin}}\, c & * & 0 & * & * & * & * & * & * \\ -1\, v_5^\circ\, e_5^\circ / e_5^{\max}\, r_5^{\mathrm{kin}}\, c & * & -1.08\, v_5^\circ\, e_5^\circ / e_5^{\max}\, r_5^{\mathrm{kin}}\, c & * & * & * & * & * & * \end{bmatrix} \tag{5.29}$$

As mentioned above, the metabolic objective function is maximizing carbon uptake. This corresponds to negative values in the $\mathbf{B_v}$ and $\mathbf{B_u}$ matrices. Fructose is an external carbon source and only uptaken, e.g. all values in the first row in $\mathbf{B_v}$ and $\mathbf{B_u}$ are negative. However, PHB is an internal carbon storage material and sometimes synthesized and sometimes metabolized (= uptaken). It is therefore necessary to consider only the entries which corresponds to carbon source uptake,

e.g. only the negative values in $\mathbf{B_v}$ and $\mathbf{B_u}$. This is done by defining new matrices $(\mathbf{B_v})_-$ and $(\mathbf{B_u})_-$ where the positive values of $\mathbf{B_v}$ and $\mathbf{B_u}$ are set to zero, e.g.

$$(\mathbf{B_v^T})_- = \begin{bmatrix} -1\, e_1^{\text{rel}}\, r_1^{\text{kin}}\, c & * & 0 & * & * & * & * & * & * \\ -1\, e_2^{\text{rel}}\, r_2^{\text{kin}}\, c & * & 0 & * & * & * & * & * & * \\ -1\, e_3^{\text{rel}}\, r_3^{\text{kin}}\, c & * & 0 & * & * & * & * & * & * \\ -1\, e_4^{\text{rel}}\, r_4^{\text{kin}}\, c & * & 0 & * & * & * & * & * & * \\ -1\, e_5^{\text{rel}}\, r_5^{\text{kin}}\, c & * & -1.08\, e_5^{\text{rel}}\, r_5^{\text{kin}}\, c & * & * & * & * & * & * \end{bmatrix} \tag{5.30}$$

$$(\mathbf{B_u^T})_- = \begin{bmatrix} -1\, v_1^\circ\, e_1^\circ / e_1^{\max}\, r_1^{\text{kin}}\, c & * & 0 & * & * & * & * & * & * \\ -1\, v_2^\circ\, e_2^\circ / e_2^{\max}\, r_2^{\text{kin}}\, c & * & 0 & * & * & * & * & * & * \\ -1\, v_3^\circ\, e_3^\circ / e_3^{\max}\, r_3^{\text{kin}}\, c & * & 0 & * & * & * & * & * & * \\ -1\, v_4^\circ\, e_4^\circ / e_4^{\max}\, r_4^{\text{kin}}\, c & * & 0 & * & * & * & * & * & * \\ -1\, v_5^\circ\, e_5^\circ / e_5^{\max}\, r_5^{\text{kin}}\, c & * & -1.08\, v_5^\circ\, e_5^\circ / e_5^{\max}\, r_5^{\text{kin}}\, c & * & * & * & * & * & * \end{bmatrix} \tag{5.31}$$

In [96] it is assumed that the reference control inputs v_i° correspond to the unregulated network state, e.g. $v_i^\circ = 1\ \forall i$.

The return on investment (ROI) are now calculated with the *weighted Greedy* policy

$$\mathbf{p_v} = \mathbf{R}^{-1}\,(\mathbf{B_u^T})_-\,\mathbf{q} = \text{diag}(\mathbf{f_c})\,\text{diag}(\mathbf{e}^{\text{rel}})\,\mathbf{r_M}\,c \tag{5.32}$$

$$\mathbf{p_u} = (\mathbf{B_v^T})_-\,\mathbf{q} = \text{diag}(\mathbf{f_c})\,\text{diag}(\mathbf{e}^{\text{rel}})\,\mathbf{r_M}\,c \tag{5.33}$$

with

$$\mathbf{f_c} = \begin{bmatrix} 1 & 1 & 1 & 1 & 2.51 \end{bmatrix}^{\text{T}} \tag{5.34}$$

Since c will appear in the nominator and denominator in Equation (3.29) and therefore canceled out, the ROIs can be simplified to:

$$\mathbf{p_v} = \text{diag}(\mathbf{f_c})\,\text{diag}(\mathbf{e}^{\text{rel}})\,\mathbf{r_M} \tag{5.35}$$

$$\mathbf{p_u} = \text{diag}(\mathbf{f_c})\,\text{diag}(\mathbf{e}^{\text{rel}})\,\mathbf{r_M} \tag{5.36}$$

This corresponds to the cybernetic control laws in Equation (3.28), except that

the ROIs are weighted with a vector $\mathbf{f_c}$, which contains a normalized number of uptaken carbon units.

5.2.2. Parameter Estimation and Model Validation

The formulated model has 31 unknown parameters. These are: $k_{r,i}$, $k_{e,i}$, α_i, β_i and $e_i^{\max}$ with $i \in \{1,2,3,4,5\}$ and K_j and $K_{e,j}$ with $j \in \{\mathrm{FRU}, \mathrm{AMC}, \mathrm{P(3HB)}\}$.

The maximal enzyme level $e_i^{\max}$ is usually not known, especially since the key enzymes in HCM are pools of lumped enzymes which are needed to catalyze all reactions, which belong to the ith elementary mode. However $e_i^{\max}$ can be estimated from the systems equations. It is obvious that for $e_i = e_i^{\max}$ the following condition holds:

$$\left.\frac{\mathrm{d}e_i}{\mathrm{d}t}\right|_{e_i=e_i^{\max}} = \alpha_i + u_i\, r_{ME,i}^{\mathrm{kin}}\, b - \beta_i\, e_i^{\max} - e_i^{\max}\,\mu \stackrel{!}{=} 0 \tag{5.37}$$

which leads to

$$e_i^{\max} = \frac{\alpha_i + u_i\, r_{\mathrm{ME},i}\, b}{\beta_i + \mu} \quad . \tag{5.38}$$

It is obvious that the maximal enzyme level is only achieved, if all resources are allocated to the synthesis of this enzyme, e.g. $u_i = 1$ and $r_{\mathrm{ME},i} = k_{e,i}$ and non-catalytic active biomass is minimal, e.g. $b = 1$. Under this conditions growth of biomass only occurs via the ith elementary mode, e.g. $\mu = \mu_i = (\mathbf{S}_\mu \mathbf{Z})_i\, k_{r,i}$.

The ith maximum enzyme level $e_i^{\max}$ is therefore not an independent parameter, but depends on other parameters:

$$e_i^{\max} = \frac{\alpha_i + k_{e,i}}{\beta_i + (\mathbf{S}_\mu \mathbf{Z})_i\, k_{r,i}} \tag{5.39}$$

The constitutive enzyme synthesis α_i is very small compared to the inducible enzyme synthesis $r_{EM,i}$, e.g. $\alpha_i << k_{e,i}$ [85]. Very often, constitutive enzyme synthesis is even neglected, e.g. $\alpha_i = 0$. For the hybrid cybernetic model of *R. eutropha* α_i is set to 1 percent of $k_{e,i}$, e.g. $\alpha_i := 0.01\, k_{e,i}$. For simplicity, it is assumed that all rate constants $k_{e,i}$ and all degradation constants β_i are identical, e.g.: $k_e := k_{e,1} = k_{e,2} = k_{e,3} = k_{e,4} = k_{e,5}$ and $\beta := \beta_1 = \beta_2 = \beta_3 = \beta_4 = \beta_5$.

Since the inducible synthesis of the key enzyme for a certain elementary mode depends on the availability of the metabolizable substrates of this elementary mode, it is reasonable to use the same Monod constants in the kinetic part of the enzyme synthesis rate as in the kinetic part of the corresponding reaction rate: $K_{e,j} := K_j$ with $j \in \{\text{FRU}, \text{AMC}, \text{P(3HB)}\}$.

The parameter space is therefore reduced to 10 parameters, where $\mathbf{k_r}$ appeared to be the most sensitive parameters [5] and were estimated by fitting the model to the experimental data of experiment `Ralst01FruSingle`. All other parameter values were fixed. Saturation constant for fructose K_{FRU} was taken from literature [45]. The used parameter values are listed in Table 5.3.

Table 5.3.: Model parameters for the hybrid cybernetic model of *R. eutropha*.

Parameter	Value
$\mathbf{k_r}$	$[0.21\ \ 0.82\ \ 0.84\ \ 0.73\ \ 0.52]^{\text{T}}$ [1/h]
$\mathbf{k_e}$	$[0.10\ \ 0.10\ \ 0.10\ \ 0.10\ \ 0.10]^{\text{T}}$ [1/h]
$\boldsymbol{\alpha}$	$0.01\,\mathbf{k_e}$ [1/h]
$\boldsymbol{\beta}$	$[5.0\ \ 5.0\ \ 5.0\ \ 5.0\ \ 5.0]^{\text{T}}$ [1/h]
K_{AMC}	0.01 [g/l]
K_{FRU}	0.06 [g/l] [45]
$K_{\text{P(3HB)}}$	0.05 [$g_{\text{P(3HB)}}/g_{\text{DW}}$]

For model validation the experiments `Ralst02FruSingle`, `Ralst03FruSingle` and `Ralst04FruSingle` with different initial conditions and different substrate pulses were performed. These are shown in Figures 5.4.

All experiments show very good agreement with the hybrid cybernetic model. In addition, the prediction of the washout point in the simulation of the continuous process in Figure 5.5 is very accurate. At washout point the dilution rate D equals the maximal growth rate $\mu^{\max}$, which is $\mu^{\max} = 0.31\ \text{h}^{-1}$[45] for *R. eutropha* growing on fructose.

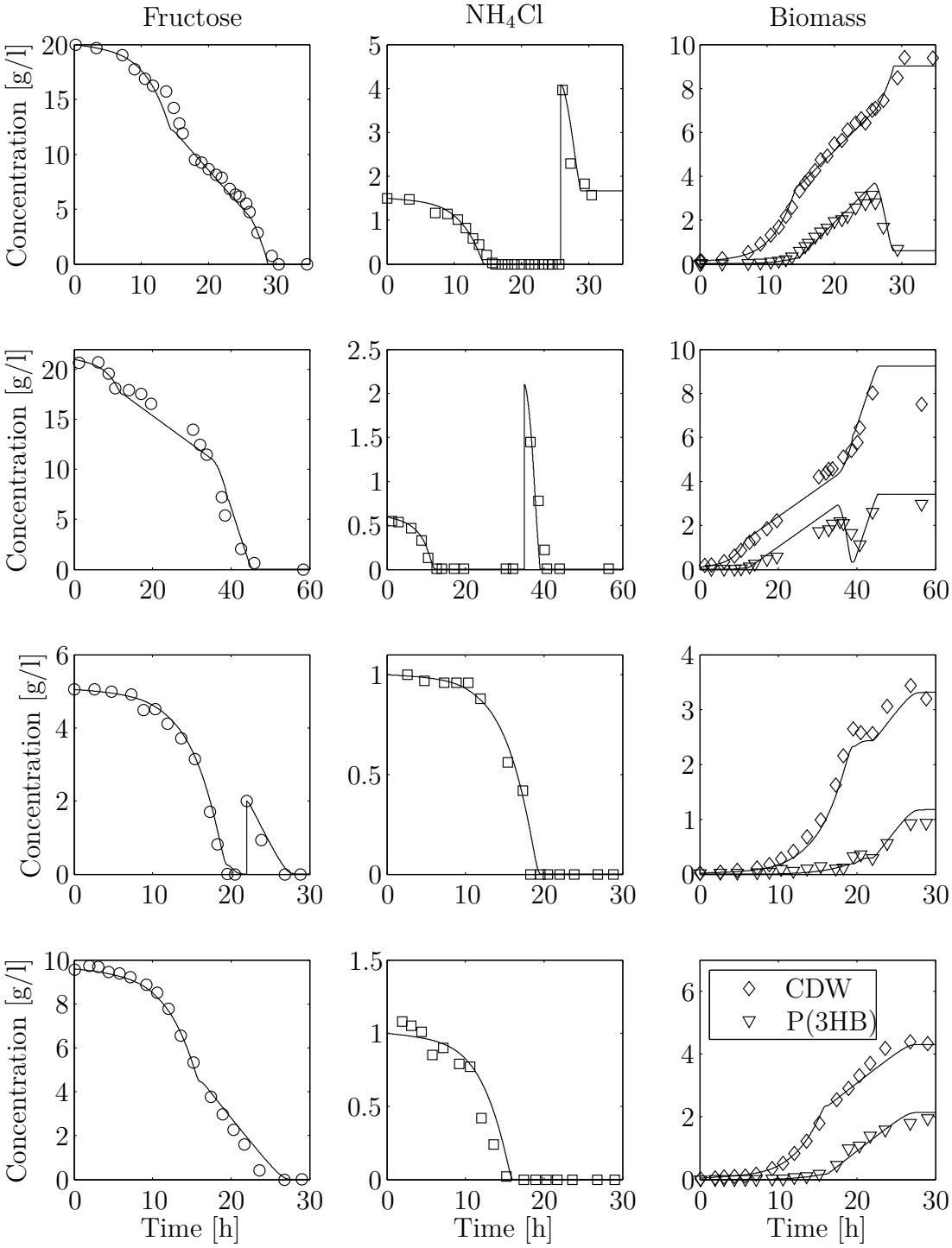

Figure 5.4.: Comparison of the hybrid cybernetic model (solid line) with experimental data. Experiment `Ralst01FruSingle` (1st row) was used for parameter estimation. Experiments `Ralst02FruSingle`, `Ralst03FruSingle` and `Ralst04FruSingle` (2nd, 3rd and 4th row) were used for model validation.

5.2.3. Nonlinear Analysis

Continuous processes have the advantage of longer periods of operating time, which can reduce production costs. Because the production of P(3HB) is still much more expensive then of conventional plastics, it is not surprising that there are already experimental studies available in literature which deal with continuous P(3HB) production [97, 91, 36]. However, in continuous cultures nonlinear phenomena such as oscillation [89, 31] and multiple steady states [10, 46, 55] can occur. Therefore, following the idea of Pinto and Immanuel [60] the model is used to investigate the possibility of multiple steady states in a continuous bio reactor.

The hybrid cybernetic model is therefore extended to continuous processes:

$$\frac{\mathrm{d}}{\mathrm{d}t}\begin{bmatrix} x_{\mathrm{FRU}} \\ x_{\mathrm{AMC}} \end{bmatrix} = D\left(\begin{bmatrix} x^{\mathrm{in}}_{\mathrm{FRU}} \\ x^{\mathrm{in}}_{\mathrm{AMC}} \end{bmatrix} - \begin{bmatrix} x_{\mathrm{FRU}} \\ x_{\mathrm{AMC}} \end{bmatrix}\right) + \mathbf{S_s Z}\,\mathbf{r_M}\,c \tag{5.40}$$

$$\frac{\mathrm{d}}{\mathrm{d}t} m_{\mathrm{P(3HB)}} = \mathbf{S_{m,s}Z}\,\mathbf{r_M} - \mu\, m_{\mathrm{P(3HB)}} \tag{5.41}$$

$$\frac{\mathrm{d}\mathbf{e}}{\mathrm{d}t} = \boldsymbol{\alpha} + \mathbf{r_{EM}}\, b - \mathrm{diag}(\boldsymbol{\beta})\,\mathbf{e} - \mu\,\mathbf{e} \tag{5.42}$$

$$\frac{\mathrm{d}c}{\mathrm{d}t} = (\mu - D)\, c \tag{5.43}$$

where D is the dilution rate and $x^{\mathrm{in}}_{\mathrm{FRU}}$ and $x^{\mathrm{in}}_{\mathrm{AMC}}$ are the inlet concentrations of fructose and ammonium chloride.

The parameter dependent steady state behavior is studied by numerical continuation methods provided in Diva [50]. Principal bifurcation parameters are the dilution rate D and the feed ratio $\gamma = \frac{x^{\mathrm{in}}_{\mathrm{AMC}}}{x^{\mathrm{in}}_{\mathrm{FRU}}}$. The fructose feed concentration $x^{\mathrm{in}}_{\mathrm{FRU}}$ was fixed at 20g/l. It is worth noting, that the cybernetic model is not differentiable at points where the return on investment of different elementary modes coincide due to the non differentiability of the control variables $\mathbf{v}$ according to Equation (3.29). Such points are called *catch up points* and will show up as sharp corners in the solution diagram. For a proper resolution of these corners the step size of the continuation is adjusted accordingly.

Two bifurcation points (A) and (B) and one catch up point (C) were detected, see Figure 5.5. Although batch data were used for parameter identification, the washout point (A) equals the maximal growth rate as reported in literature [45].

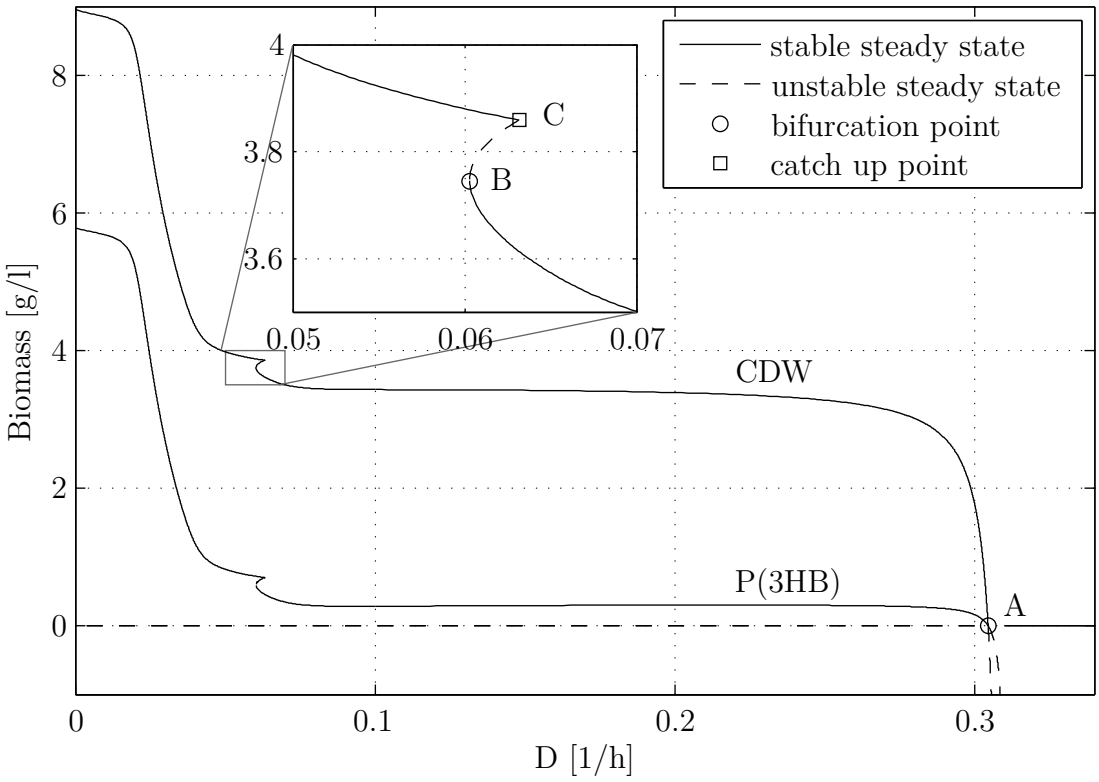

Figure 5.5.: Bifurcation diagram of cell dry weight (CDW) and P(3HB) concentration w.r.t. dilution rate D for $x^{\text{in}}_{\text{FRU}}$=20.0 g/l, $x^{\text{in}}_{\text{AMC}}$=1.5 g/l ($\gamma = 0.075$). Two bifurcation points were detected: washout point (A) and turning point (B), and a catch up point (C).

A small hysteresis is detected over $0.060 \leq D \leq 0.063$. The hysteresis is bordered by the points (B) and (C). A two parameter continuation of these points with respect to the substrate composition at the inlet of the reactor $\gamma = \frac{x^{\text{in}}_{\text{AMC}}}{x^{\text{in}}_{\text{FRU}}}$ and dilution rate D shows that the hysteresis unfolds from $\gamma = 0$ and vanishes for $\gamma > 0.17$, see Figure 5.6.

Such kind of hysteresis is usually observed if there are two or more substitutable substrates available as shown by Namjoshi and Ramkrishna [56] and by Kumar et al. [46]. However in this study there are only two complementary substrates (FRU and AMC), but no substitutable. But as mentioned before, due to the introduction of internal metabolites and their dynamics into the model, new products and substrates are added. The internal metabolite P(3HB) can be viewed as an additional carbon source besides fructose. But still fructose and P(3HB) are not substitutable in the strict sense, since P(3HB) is formed from fructose. However,

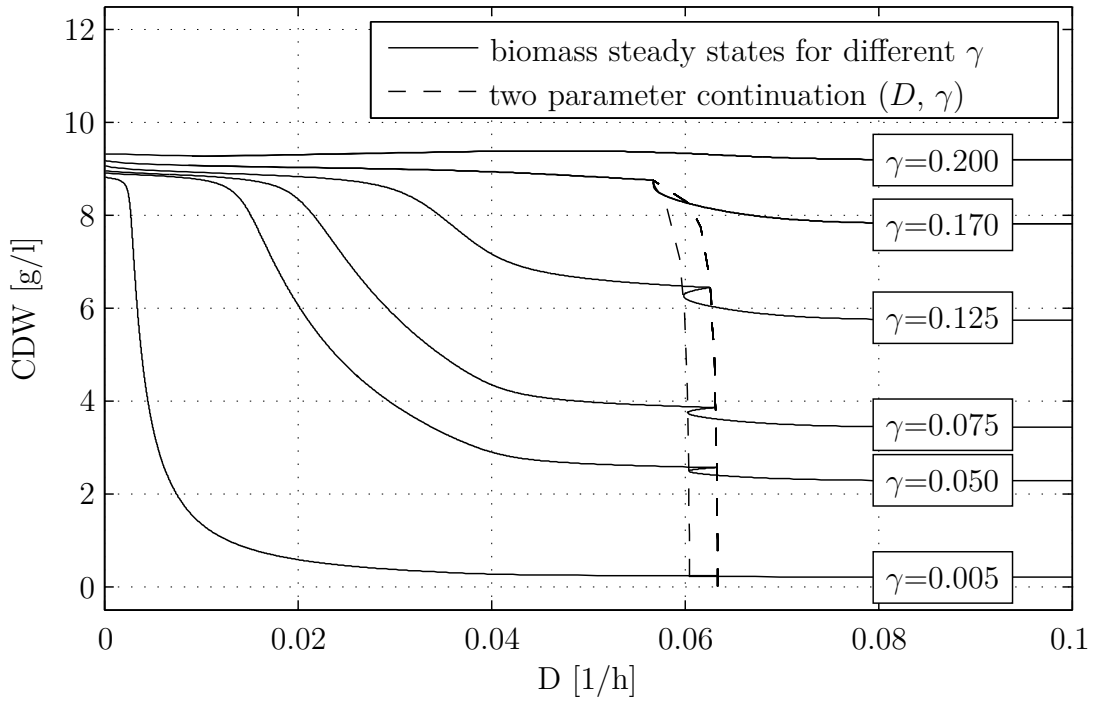

Figure 5.6.: Two parameter continuation with respect to dilution rate D and feed composition γ.

once P(3HB) is synthesized the organism can choose between fructose or P(3HB) as growth substrate.

Fig. (5.7) illustrates the effect of P(3HB) consumption on biomass in a continuous bio reactor. If P(3HB) consumption is neglected, then the concentrations of total biomass and P(3HB) (not shown) are significantly higher at low dilution rates ($D \leq 0.1$ h^{-1}) and the hysteresis disappears. As mentioned before, this kind of hysteresis is observed if there are two or more substitutable substrate. If P(3HB) consumption is neglected, then there is only one carbon substrate, namely fructose, and therefore the hysteresis disappears. Furthermore, at low dilution rates and $\gamma < 0.17$ AMC is growth limiting and therefore there is excess of fructose. Due to the chosen metabolic objective function of maximizing substrate uptake, P(3HB) concentration and therefore concentration of total biomass are higher if P(3HB) consumption is not considered in the model. At high dilution rates ($D > 0.1$ h^{-1}) the consumption of P(3HB) has no significant effect.

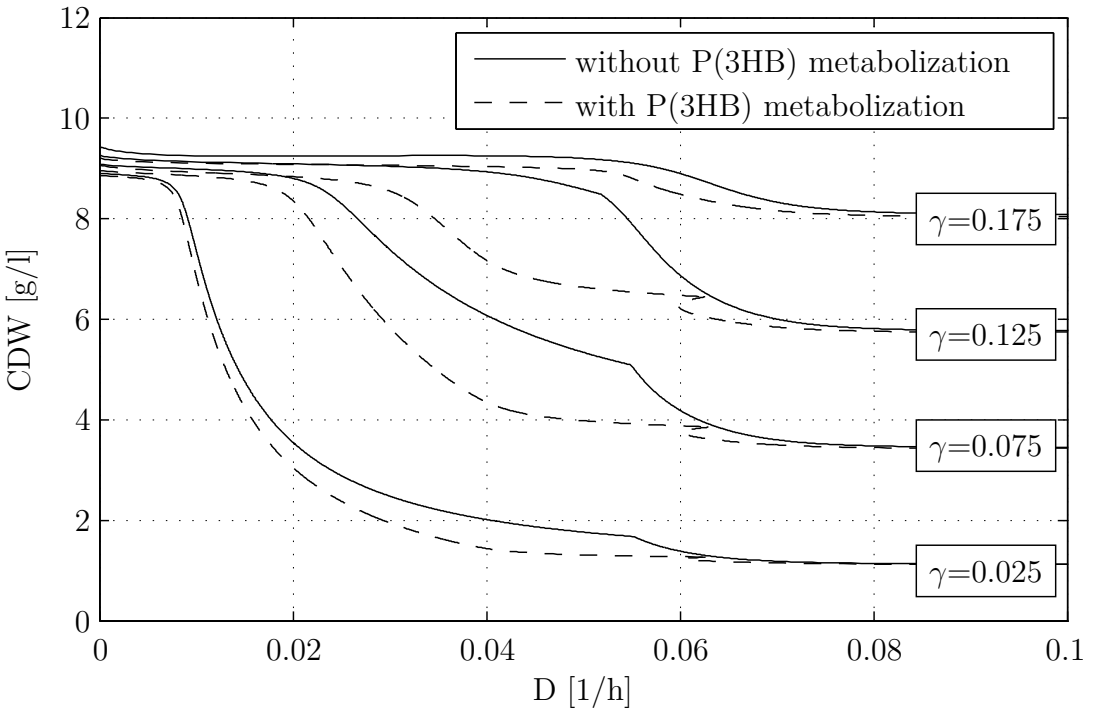

Figure 5.7.: Comparison of biomass steady states (CDW) with and without metabolization of P(3HB) at different feed compositions γ.

5.3. Reduction of the Hybrid Cybernetic Model

The developed hybrid cybernetic model consists of nine ODEs: five ODEs for the key enzymes of the five (active) elementary modes, two ODEs for the cell external substrate concentrations of fructose and ammonium chloride, one ODE for the internal metabolite concentration of poly(3-hydroxybutyrate) and one ODE for the biomass concentration.

Although this is a model with moderate complexity, for some applications a model reduction is necessary. For example, in the later formulated population balance model, the seven states of this model would translate into seven internal coordinates of the population balance equations (PBE), which is computationally challenging.

There are two reasonable options to reduce this model. The first option is to lump some of the used active elementary modes (AMs). Lumping of active modes would reduce the number of parameters, but more important also the number of key enzymes. Since each enzyme level in the hybrid cybernetic model will translate into an internal coordinate in the population balance equation, this would be a favourable reduction.

A second option is a general reduction of the enzyme levels. Since key enzymes play an important role in the cybernetic modeling framework, the enzyme levels can not be fully omitted. Nevertheless, key enzymes are also internal metabolites and their dynamics are usually much faster than dynamics of exchange rates. Therefore, quasi stationarity for enzyme levels can be assumed. This can be done in two ways: a) formulation of a DAE system, where the former ODEs for the enzyme levels are then algebraic constraints, or b) omitting ODEs for enzyme levels, but finding a suitable representation of the enzyme levels, which are still needed in the rate equations.

5.3.1. Lumping of Active Modes

In Chapter 5.1.1 five active modes were chosen from the 122 elementary modes of the metabolic network. These five modes are necessary to represent the yields of experimental data and span a reasonable large yield space to allow for metabolic

flexibility. Any further reduction or lumping of modes will decrease this yield space.

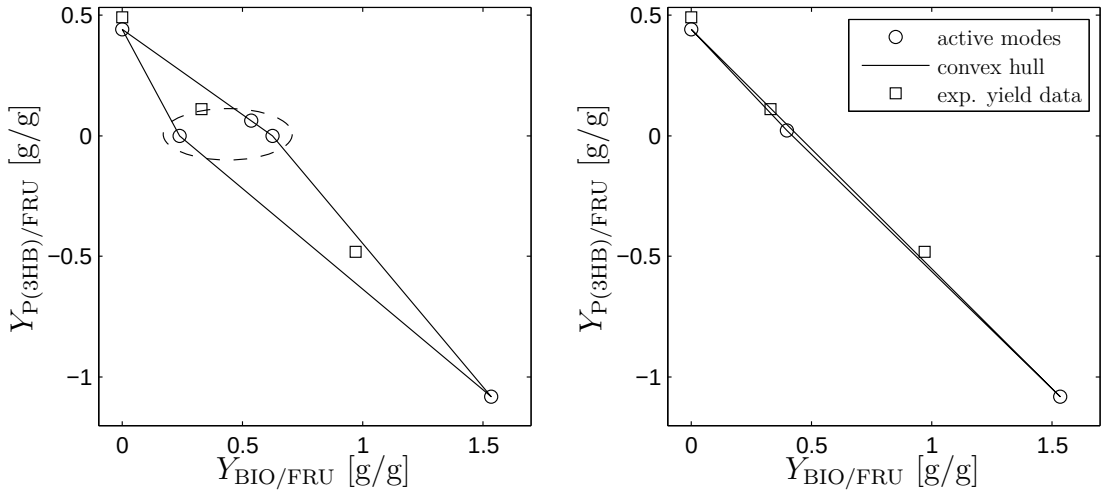

Figure 5.8.: Yield spaces of the full hybrid cybernetic model (left) and the lumped hybrid cybernetic model (right). The three active modes of the full hybrid cybernetic model within the dashed ellipse are lumped to one single mode. The new yield space is much smaller, but experimental yield data are still within or very close to the convex hull.

Figure 5.8 (left) shows the yield space of the full hybrid cybernetic model. It is reasonable to lump the three active modes which are annotated with a red dashed ellipse in 5.8 (left) into one single active mode. This will reduce the yield space significantly (5.8 (right)), but experimental yield data are still within or at least very close to the convex hull.

A systematic way of lumping elementary modes is described in [76, 77], especially if there are some internal fluxes known. Since this is not the case here, it is sufficient to find a non negative combination of the three modes annotated with the red dashed ellipse in Figure 5.8 (left), which represent the experimental yield data best.

These three modes are lumped by multiplying with a weighting vector $\mathbf{w}$:

$$\begin{bmatrix} -1.00 & -1.00 & -1.00 \\ -0.25 & -0.11 & -0.29 \\ 0.06 & 0.00 & 0.00 \\ 0.60 & 0.24 & 0.62 \end{bmatrix} \underbrace{\begin{bmatrix} 0.34 \\ 0.51 \\ 0.15 \end{bmatrix}}_{\mathbf{w}} = \begin{bmatrix} -1.00 \\ -0.19 \\ 0.02 \\ 0.42 \end{bmatrix} \tag{5.44}$$

where $||\mathbf{w}||_1 = 1$, resulting in the new lumped active modes given in Table 5.4.

Table 5.4.: Stoichiometry of lumped active modes (lAMs).

lAM	Y_{FRU}	Y_{AMC}	$Y_{\mathrm{P(3HB)}}$	Y_{TBM}
lAM_1	-1.00	0.00	0.44	0.44
lAM_2	-1.00	-0.19	0.02	0.42
lAM_3	-1.00	-0.72	-1.08	0.45

The full hybrid cybernetic model is reduced to the lumped hybrid cybernetic model with:

$$\frac{\mathrm{d}}{\mathrm{d}t}\begin{bmatrix} x_{\mathrm{FRU}} \\ x_{\mathrm{AMC}} \end{bmatrix} = \mathbf{S_s Z}\,\mathbf{r_M}\,c \tag{5.45}$$

$$\frac{\mathrm{d}}{\mathrm{d}t} m_{\mathrm{PHB}} = \mathbf{S_{m,s} Z}\,\mathbf{r_M} - \mu\, m_{\mathrm{PHB}} \tag{5.46}$$

$$\frac{\mathrm{d}\mathbf{e}}{\mathrm{d}t} = \boldsymbol{\alpha} + \mathbf{r_{EM}}\, b - \mathrm{diag}(\boldsymbol{\beta})\,\mathbf{e} - \mu\,\mathbf{e} \tag{5.47}$$

$$\frac{\mathrm{d}c}{\mathrm{d}t} = \mu\, c \tag{5.48}$$

where the matrices $\mathbf{S_s Z}$ and $\mathbf{S_{m,s} Z}$ include the lumped active modes and the rates $\mathbf{r_M}$ are given by:

$$r^{\mathrm{kin}}_{\mathrm{M},1} = k_{r,1}\,\frac{x_{\mathrm{FRU}}}{K_{\mathrm{FRU}} + x_{\mathrm{FRU}}} \tag{5.49}$$

$$r^{\mathrm{kin}}_{\mathrm{M},2} = k_{r,2}\,\frac{x_{\mathrm{FRU}}}{K_{\mathrm{FRU}} + x_{\mathrm{FRU}}}\,\frac{x_{\mathrm{AMC}}}{K_{\mathrm{AMC}} + x_{\mathrm{AMC}}} \tag{5.50}$$

$$r^{\mathrm{kin}}_{\mathrm{M},3} = k_{r,3}\,\frac{x_{\mathrm{FRU}}}{K_{\mathrm{FRU}} + x_{\mathrm{FRU}}}\,\frac{x_{\mathrm{AMC}}}{K_{\mathrm{AMC}} + x_{\mathrm{AMC}}}\,\frac{m_{\mathrm{PHB}}}{K_{\mathrm{PHB}} + x_{\mathrm{PHB}}} \tag{5.51}$$

Model parameters for the lumped hybrid cybernetic model are given in Table 5.5 and are obviously the same as in the full hybrid cybernetic model, except for the new lumped mode a new $k_{r,2}$ was estimated from experimental data of experiment `Ralst01FruSingle`.

Figure 5.9 show the simulation of the lumped hybrid cybernetic model in comparison with the full hybrid cybernetic model and the four experimental data sets `Ralst01FruSingle` - `Ralst04FruSingle`.

Although the model, especially the yield space is reduced significantly, the lumped hybrid cybernetic model is still in good agreement with the experimental data.

Table 5.5.: Model parameters for the lumped hybrid cybernetic model of *R. eutropha*.

Parameter	Value
$\mathbf{k_r}$	$[0.21\ \ 0.63\ \ 0.52]^{\mathrm{T}}$ [1/h]
$\mathbf{k_e}$	$[0.10\ \ 0.10\ \ 0.10]^{\mathrm{T}}$ [1/h]
$\boldsymbol{\alpha}$	$0.01\,\mathbf{k_e}$ [1/h]
$\boldsymbol{\beta}$	$[5.0\ \ 5.0\ \ 5.0]^{\mathrm{T}}$ [1/h]
K_{AMC}	0.01 [g/l]
K_{FRU}	0.06 [g/l] [45]
K_{PHB}	0.05 [g_{PHB}/g_{DW}]

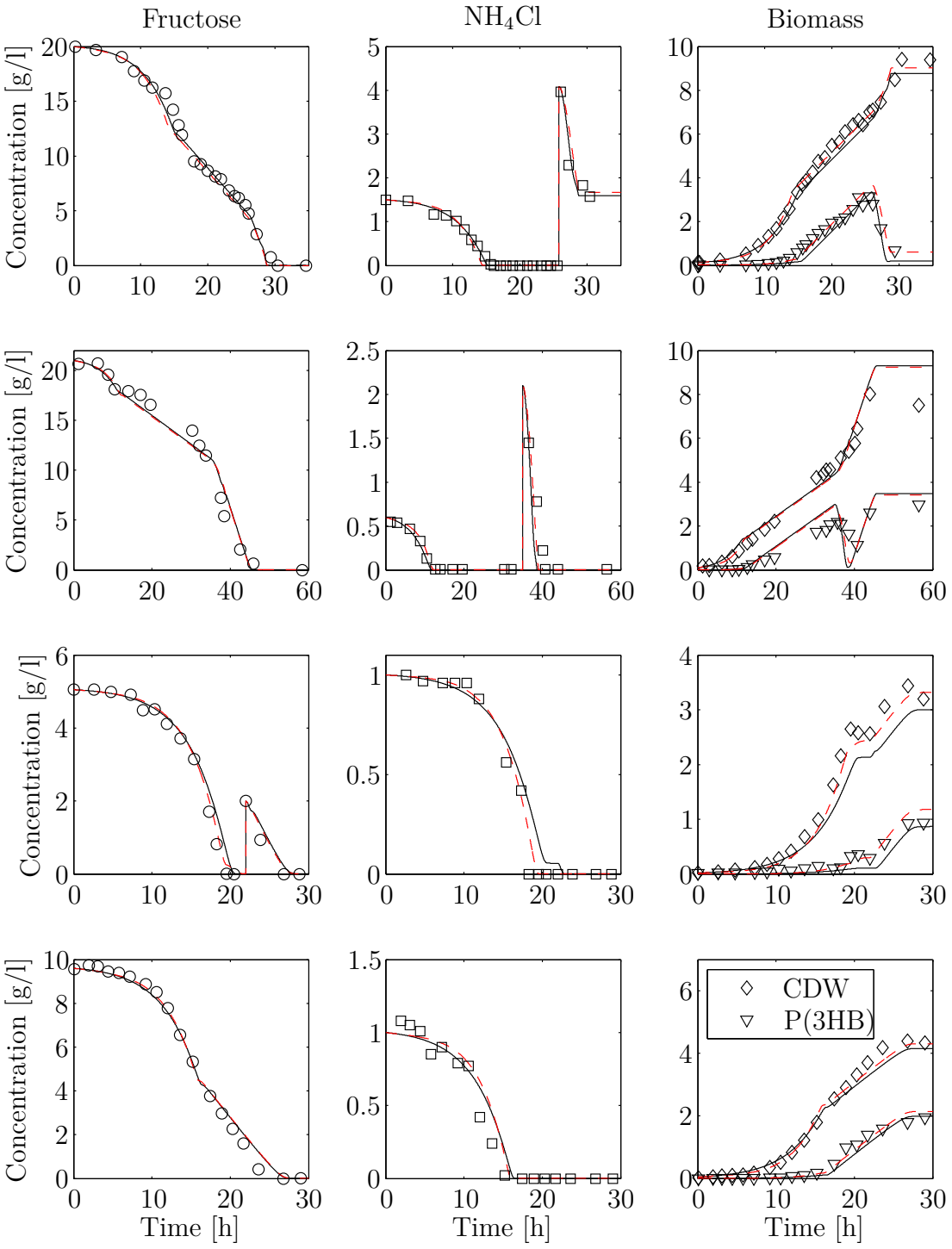

Figure 5.9.: Simulation of the lumped hybrid cybernetic model (solid black line) in comparison with the full hybrid cybernetic model (dashed red line) and experimental data sets `Ralst01FruSingle` (top row) - `Ralst04FruSingle` (bottom row).

5.3.2. Enzyme Levels as Algebraic Constraints

The systems equation in the system (5.6) - (5.9) has the form

$$\mathbf{y}' = \mathbf{f}(\mathbf{y}, t) \quad , \tag{5.52}$$

which we could generalize to the form

$$\mathbf{M}(\mathbf{y}, t)\, \mathbf{y}' = \mathbf{f}(\mathbf{y}, t) \quad , \tag{5.53}$$

where the mass matrix $\mathbf{M}$ is defined as the identity matrix

$$\mathbf{M} = \begin{bmatrix} 1 & 0 & 0 & 0 & 0 & 0 & 0 & 0 & 0 \\ 0 & 1 & 0 & 0 & 0 & 0 & 0 & 0 & 0 \\ 0 & 0 & 1 & 0 & 0 & 0 & 0 & 0 & 0 \\ 0 & 0 & 0 & 1 & 0 & 0 & 0 & 0 & 0 \\ 0 & 0 & 0 & 0 & 1 & 0 & 0 & 0 & 0 \\ 0 & 0 & 0 & 0 & 0 & 1 & 0 & 0 & 0 \\ 0 & 0 & 0 & 0 & 0 & 0 & 1 & 0 & 0 \\ 0 & 0 & 0 & 0 & 0 & 0 & 0 & 1 & 0 \\ 0 & 0 & 0 & 0 & 0 & 0 & 0 & 0 & 1 \end{bmatrix} \quad . \tag{5.54}$$

If quasi stationarity for the enzyme levels is assumed, the mass matrix $\mathbf{M}$ will have the form

$$\mathbf{M} = \begin{bmatrix} 1 & 0 & 0 & 0 & 0 & 0 & 0 & 0 & 0 \\ 0 & 1 & 0 & 0 & 0 & 0 & 0 & 0 & 0 \\ 0 & 0 & 1 & 0 & 0 & 0 & 0 & 0 & 0 \\ 0 & 0 & 0 & 1 & 0 & 0 & 0 & 0 & 0 \\ 0 & 0 & 0 & 0 & 0 & 0 & 0 & 0 & 0 \\ 0 & 0 & 0 & 0 & 0 & 0 & 0 & 0 & 0 \\ 0 & 0 & 0 & 0 & 0 & 0 & 0 & 0 & 0 \\ 0 & 0 & 0 & 0 & 0 & 0 & 0 & 0 & 0 \\ 0 & 0 & 0 & 0 & 0 & 0 & 0 & 0 & 0 \end{bmatrix} \tag{5.55}$$

and the system of differential equations will change to a system of differential and

algebraic equations (DAE), where the former differential equations for the enzyme levels are now algebraic constraints.

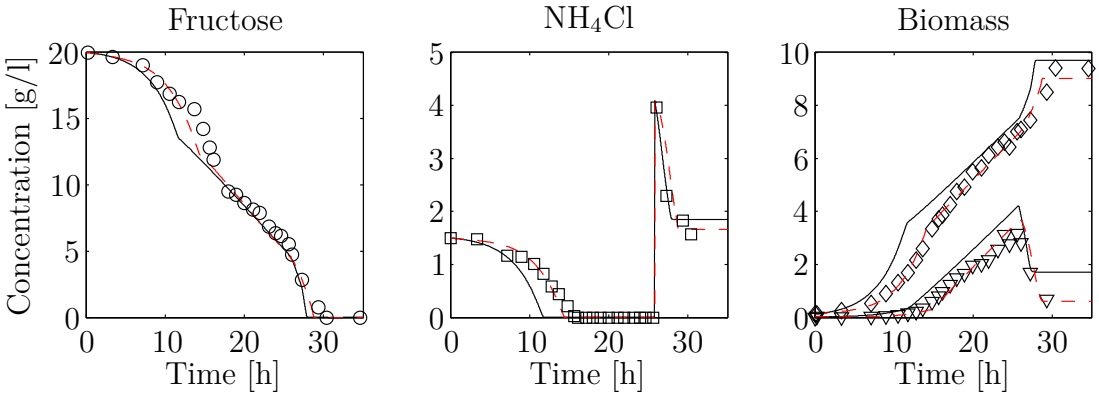

Figure 5.10.: Simulation of the hybrid cybernetic model with enzyme levels as algebraic constraints (solid black line) in comparison with the full hybrid cybernetic model (dashed red line) and experimental data set `Ralst01FruSingle`.

Figure 5.10 shows the simulation of the HCM-DAE system in comparison with the experimental data. It can be seen that the simulation is qualitatively in agreement with the data. However, the simulation is slightly too fast.

The biggest disadvantage of DAE systems is to find a good initial guess for consistent initial conditions. This is often very challenging.

5.3.3. Approximation of Enzyme Levels

Under the assumption that dynamics of enzyme levels are very fast compared to reaction kinetics, they can be assumed as quasi stationary (qss), e.g.:

$$\left.\frac{\mathrm{d}e_i}{\mathrm{d}t}\right|_{\mathrm{qss}} = \alpha_i + u_i\, r_{E,i}\, b - \beta_i\, e_i^{\mathrm{qss}} - e_i^{\mathrm{qss}}\, \mu \stackrel{!}{=} 0 \tag{5.56}$$

This leads to:

$$e_i^{\mathrm{qss}} = \frac{\alpha_i + r_{E,i}\, b\, u_i}{\beta_i + \mu} \tag{5.57}$$

Since in the rate equations $\mathbf{r_M}$ the relative enzyme level is used, it is convenient to rewrite equation (5.57) as relative enzyme level:

$$(e_i^{\mathrm{rel}})^{\mathrm{qss}} = \frac{e_i^{\mathrm{qss}}}{e_i^{\max}} = \frac{\alpha_i + r_{E,i}\, b\, u_i}{\beta_i + \mu} \frac{\beta_i + \mu_i}{\alpha_i + k_{e,i}} \tag{5.58}$$

Since $\alpha_i << k_{e,i}$ the constitutive enzyme synthesis rate α_i can be neglected:

$$(e_i^{\mathrm{rel}})^{\mathrm{qss}} = \frac{r_{E,i}}{\beta_i + \mu} \frac{\beta_i + \mu_i}{k_{e,i}}\, b\, u_i \tag{5.59}$$

The growth rate due to the ith active mode μ_i is obviously less or equal the overall growth rate μ, e.g. $\mu_i \leq \mu$. However the maximal growth rate of this system was estimated to $\mu^{\max} = 0.31\ \mathrm{h}^{-1}$, which is in agreement with [45]. Since β_i is more than ten times larger than $\mu^{\max}$, we can argue that:

$$\beta_i + \mu_i \approx \beta_i + \mu \tag{5.60}$$

The ith enzyme is synthesized if there is sufficient substrate for the ith active mode available. In this case the ith enzyme synthesis rate $r_{E,i}$ corresponds to $k_{e,i}$

$$r_{E,i} \to k_{e,i} \quad . \tag{5.61}$$

For this case we can therefore argue, that

$$\frac{r_{E,i}}{\beta_i + \mu} \frac{\beta_i + \mu_i}{k_{e,i}} \approx 1 \quad . \tag{5.62}$$

For low substrate concentration the enzyme synthesis rate is close to zero and therefore $r_{E,i} << k_{e,i}$. However, in this case no resources are allocated to this reaction and $u_i = 0$. This means, in this case the value of $\frac{r_{E,i}}{k_{e,i}}$ plays no role.

We can therefore conclude, that the concentration of relative enzyme levels e_i^{rel} can be approximated with the cybernetic control variable u_i:

$$(e_i^{\mathrm{rel}})^{\mathrm{qss}} = b\, u_i \quad . \tag{5.63}$$

To check this conclusion the relative enzyme levels e_i^{rel} of the full (un-reduced) model can be compared with the corresponding cybernetic control variables u_i. This is done for the simulation in Figure 5.4 (top row) and presented in Figure 5.11.

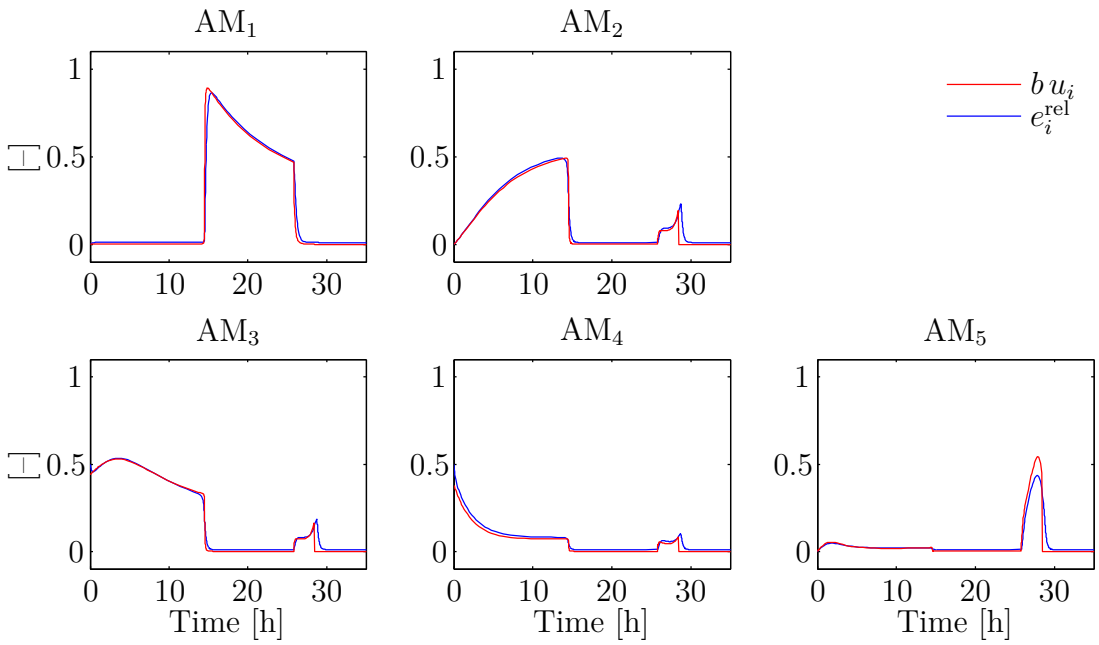

Figure 5.11.: Comparison of dynamic relative enzyme levels e_i^{rel} (blue line) with their quasi steady state approximation $(e_i^{\text{rel}})^{\text{qss}} = b\,u_i$ (red line).

As seen in Figure 5.11 the relative enzyme levels e_i^{rel} follow their quasi steady state approximations $b\,u_i$ very closely, which confirms the arguments above. The relative enzyme levels can be therefore substituted, which will reduce the given system of nine ODEs to a reduced system with only four ODEs

$$\frac{\mathrm{d}}{\mathrm{d}t}\begin{bmatrix} x_{\text{FRU}} \\ x_{\text{AMC}} \end{bmatrix} = \mathbf{S_s Z}\,\mathrm{diag}(\mathbf{v})\,\mathrm{diag}(\mathbf{u})\,\mathbf{r}_{\mathbf{M}}^{\text{kin}}\,b\,c \tag{5.64}$$

$$\frac{\mathrm{d}}{\mathrm{d}t} m_{\text{PHB}} = \mathbf{S_{m,s}Z}\,\mathrm{diag}(\mathbf{v})\,\mathrm{diag}(\mathbf{u})\,\mathbf{r}_{\mathbf{M}}^{\text{kin}}\,b - \mu\,m_{\text{PHB}} \tag{5.65}$$

$$\frac{\mathrm{d}c}{\mathrm{d}t} = \mu\,c \tag{5.66}$$

For the reduced system new *returns on investment* have to be calculated. Although the metabolic objective function $\phi(\mathbf{y})$ remains the same, the vector $\mathbf{q}$ is reduced

to

$$\mathbf{q} = \frac{\partial \phi(\mathbf{y})}{\partial \mathbf{y}} = \begin{bmatrix} -1 & 0 & -1.4 & 0 \end{bmatrix}^{\mathrm{T}} \tag{5.67}$$

The matrices $(\mathbf{B_v})_-$ and $(\mathbf{B_u})_-$ compute to

$$(\mathbf{B_v^T})_- = \begin{bmatrix} -1\, u_1^\circ\, b\, r_1^{\mathrm{kin}}\, c & * & 0 & * \\ -1\, u_2^\circ\, b\, r_2^{\mathrm{kin}}\, c & * & 0 & * \\ -1\, u_3^\circ\, b\, r_3^{\mathrm{kin}}\, c & * & 0 & * \\ -1\, u_4^\circ\, b\, r_4^{\mathrm{kin}}\, c & * & 0 & * \\ -1\, u_5^\circ\, b\, r_5^{\mathrm{kin}}\, c & * & -1.08\, u_5^\circ\, b\, r_5^{\mathrm{kin}}\, c & * \end{bmatrix} \tag{5.68}$$

$$(\mathbf{B_u^T})_- = \begin{bmatrix} -1\, v_1^\circ\, r_1^{\mathrm{kin}}\, c & * & 0 & * \\ -1\, v_2^\circ\, r_2^{\mathrm{kin}}\, c & * & 0 & * \\ -1\, v_3^\circ\, r_3^{\mathrm{kin}}\, c & * & 0 & * \\ -1\, v_4^\circ\, r_4^{\mathrm{kin}}\, c & * & 0 & * \\ -1\, v_5^\circ\, r_5^{\mathrm{kin}}\, c & * & -1.08\, v_5^\circ\, r_5^{\mathrm{kin}}\, c & * \end{bmatrix} \tag{5.69}$$

As argued in [96] the reference control inputs v_i° in $(\mathbf{B_u^T})_-$ correspond to the unregulated network state, e.g. $v_i^\circ = 1\ \forall i$. Since in this reduced system the synthesis of enzymes is omitted it is not required to penalize (or reward) enzyme synthesis with the weighting matrix R. The *return on investment* $\mathbf{p_u}$ is therefore calculated according the *unweighted* greedy policy

$$\mathbf{p_u} = (\mathbf{B_u^T})_- \mathbf{q} = \mathrm{diag}(\mathbf{f_c})\, \mathrm{r_M^{kin}}\, c \quad , \tag{5.70}$$

which can be simplified to

$$\mathbf{p_u} = \mathrm{diag}(\mathbf{f_c})\, \mathrm{r_M^{kin}} \quad , \tag{5.71}$$

since c will cancel out in equation (3.29).

The reference control inputs u_i° in $(\mathbf{B_v^T})_-$ also correspond to the unregulated network state. However, $u_i^\circ = 1\ \forall i$ is in contradiction with the postulation that $\sum \mathbf{u} = 1$ [43]. Instead of that, all resources are allocated equally, e.g $u_1^\circ = u_2^\circ = ... = u_{n_r}^\circ = \frac{1}{n_r}$.

The *return on investment* $\mathbf{p_v}$ according to the greedy policy equals to

$$\mathbf{p_v} = (\mathbf{B_v^T})_- \, \mathbf{q} = \mathrm{diag}(\mathbf{f_c}) \, \mathrm{r_M^{kin}} \, \frac{b}{n_r} \, c \quad , \tag{5.72}$$

which can be simplified to

$$\mathbf{p_v} = \mathrm{diag}(\mathbf{f_c}) \, \mathrm{r_M^{kin}} \quad , \tag{5.73}$$

since c, n_r and b will cancel out in equation (3.29).

Model parameters are the same as in the full hybrid cybernetic model, except the parameters for enzyme dynamics, which are not needed in this reduced approach. However, as seen in Figure 5.12 the model is still in good agreement with the experimental data.

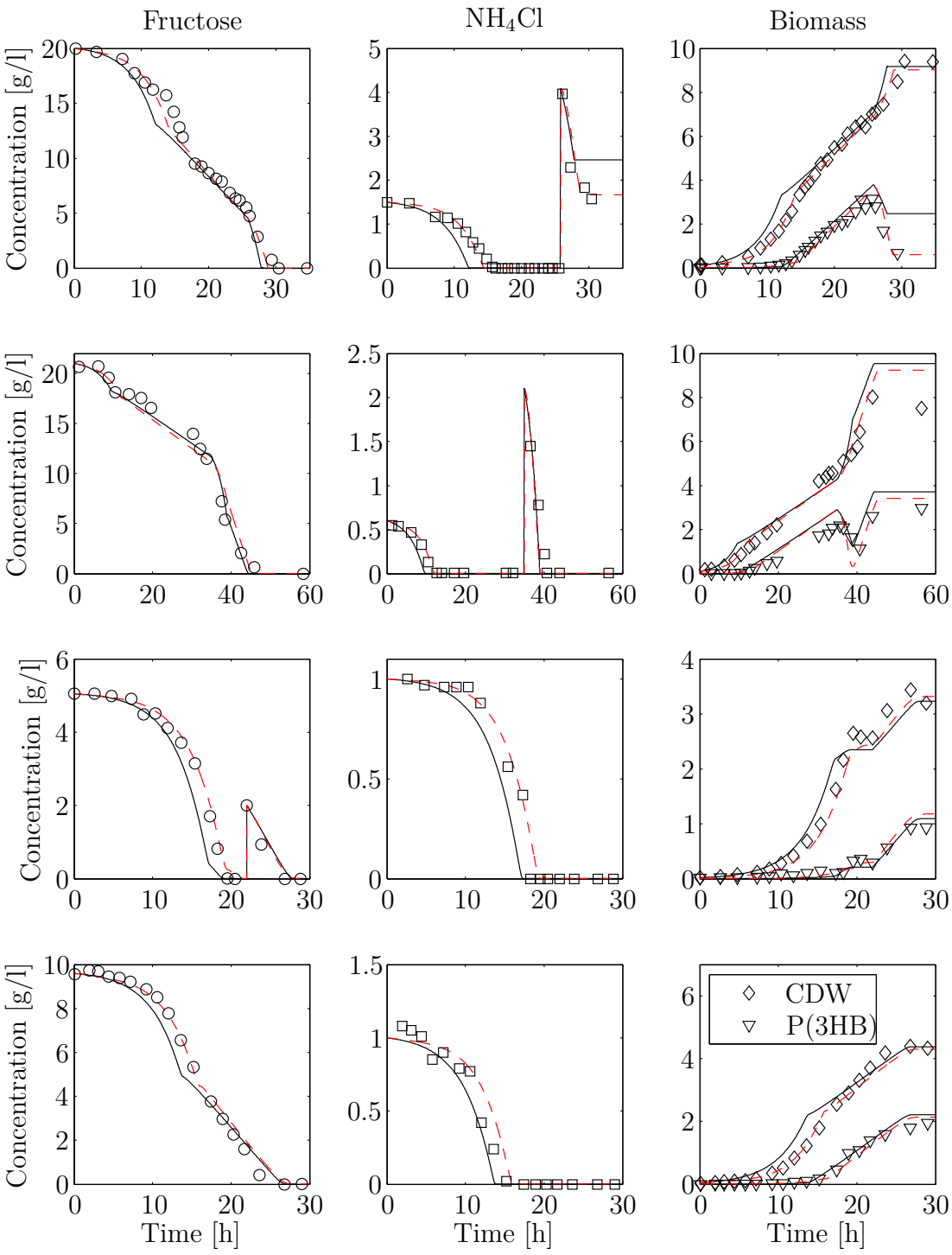

Figure 5.12.: Simulation of the reduced system with approximated enzyme levels (solid black line) in comparison with the full hybrid cybernetic model (dashed red line) and experimental data sets `Ralst01FruSingle` (top row) - `Ralst04FruSingle` (bottom row).

5.3.4. Combination of Lumped Modes with Approximation of Enzyme Levels

As seen in the sections above lumping of active modes and approximation of enzyme levels are reasonable reductions and are still in good agreement with the experimental data. It is therefore reasonable to combine the lumping of active modes with the approximation of enzyme levels.

In section 5.3.1 three active modes were lumped into a new single active mode. Two of these modes (AM_3 and AM_4) only metabolize fructose to non-PHB biomass, whereas the third mode (AM_2) metabolizes also fructose, but synthesizes a small additional amount of PHB besides the non-PHB biomass. The lumped mode will therefore utilize fructose into non-PHB biomass and a very small amount of PHB.

With regard to a simplified reduced model, it is reasonable to neglect active mode (AM_2) and only lumped the active modes AM_3 and AM_4. PHB will then still synthesized via the active mode AM_1 and metabolized via active mode AM_5. The modes of this model will then correspond to the three main processes: PHB synthesis (AM_1), PHB metabolization (AM_5) and synthesis of non-PHB biomass (AM_3, AM_4 lumped). Parameter of the lumped HCM with approximated enzyme levels are the same as in the full HCM, except the k_r value of the new lumped mode had to be estimated from experimental data to $k_r = 0.84$ 1/h. The active modes AM_2, AM_3 and AM_4 are lumped according the weighting vector $\mathbf{w}$:

$$\begin{bmatrix} -1.00 & -1.00 & -1.00 \\ -0.25 & -0.11 & -0.29 \\ 0.06 & 0.00 & 0.00 \\ 0.60 & 0.24 & 0.62 \end{bmatrix} \underbrace{\begin{bmatrix} 0.00 \\ 0.64 \\ 0.46 \end{bmatrix}}_{\mathbf{w}} = \begin{bmatrix} -1.00 \\ -0.20 \\ 0.00 \\ 0.42 \end{bmatrix} \tag{5.74}$$

The stoichiometry of the resulting active mode is very close to the lumped HCM in section 5.3.1.

Parameters for enzyme dynamics are not needed.

As seen in Figure 5.13 the model is in good agreement with the experimental data.

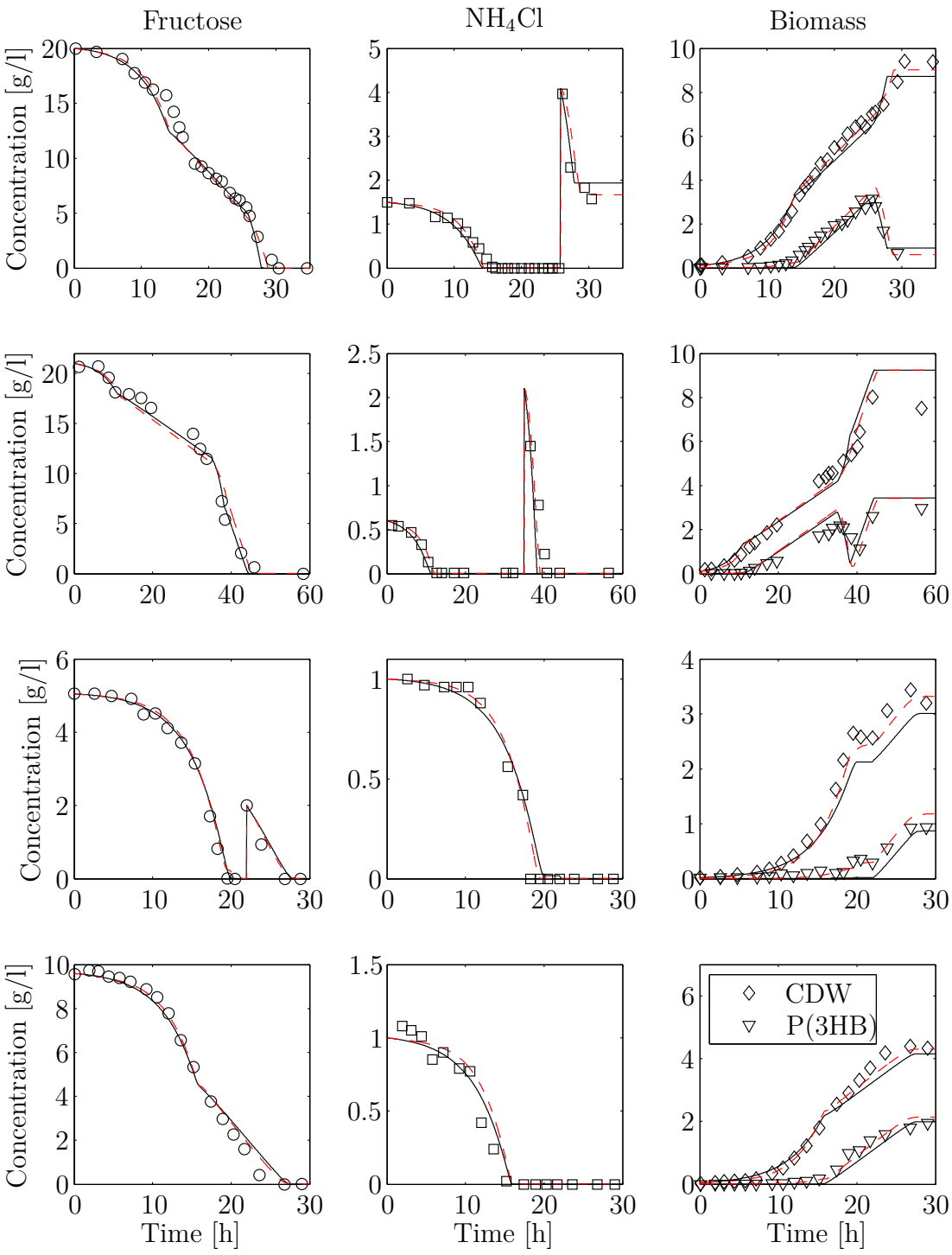

Figure 5.13.: Simulation of lumped hybrid cybernetic model with approximated enzyme levels (solid black line) in comparison with the full hybrid cybernetic model (dashed red line) and experimental data sets `Ralst01FruSingle` (top row) - `Ralst04FruSingle` (bottom row).

5.3.5. Comparison of the Reduced Models

In the sections above different types of reduced models are discussed. All of these models are more or less in good agreement with experimental data. However, these models have a different number of adjustable parameters. To compare these models in an objective way, a parameter is needed which not only includes the quality of the fit with experimental data, but also the number of parameters. If two different models can represent experimental data in the same quality, the model with less parameters is preferable.

An often used parameter for model comparison is the Fisher parameter F [1], which is related to the Fisher's test and allows for a proper statistical evaluation of rival models with different number of parameters:

$$F = \frac{(n-l)}{(n-1)} \frac{\sum_{i=1}^{n} (q_{\mathrm{exp},i} - \bar{q}_{\mathrm{exp}})^2}{\sum_{i=1}^{n} (q_{\mathrm{exp},i} - q_{\mathrm{mod},i})^2} \tag{5.75}$$

where n is the number of data points and l the number of adjustable parameters in. The index *mod* is for the model data and the index *exp* is for the experimental data. The bar represents the average value. A higher value of F suggests a better model. F increases with decreasing number of model parameters, with reduced model error $(q_{\mathrm{exp},i} - q_{\mathrm{mod},i})^2$ and with a wider range of data $(q_{\mathrm{exp},i} - \bar{q}_{\mathrm{exp}})^2$.

Since, the reduced models above are compared to the same experimental data, the Fisher parameter can be reduced to

$$F = \frac{(n-l)}{\sum_{i=1}^{n} (q_{\mathrm{exp},i} - q_{\mathrm{mod},i})^2} \tag{5.76}$$

Figure 5.14 shows the comparison of the Fisher parameter F for the full HCM and all reduced models (except DAE). The Fisher parameters of all models are very close to each other for each experiment.The values for experiment 4 are rather small since in this experiment there are less data points than in the other experiments.

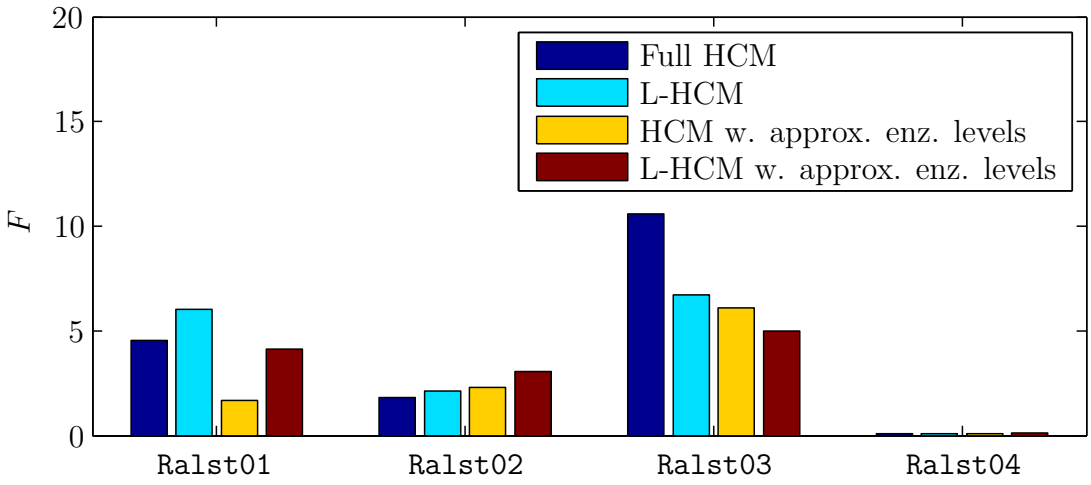

Figure 5.14.: Fisher parameter of the full hybrid cybernetic model and the reduced models for the experimental data sets `Ralst01FruSingle` - `Ralst04FruSingle`.

5.4. Population Balance Models

To describe cell to cell variance on a macroscopic scale, population balance models [64] are used. In the following, population balance models are formulated, which characterize the cells heterogeneity with respect to the intracellular amount of P(3HB) and which are based on the hybrid cybernetic model as described in Chapter 5.2. Since states of the single cell model of the hybrid cybernetic model will translate into internal coordinates of the population balance model, a reduced cybernetic model, as described in Chapter 5.3 is used, to reduce complexity.

In the hybrid cybernetic model, biomass is described as cell dry weight (c), where P(3HB) is a compartment of the cell dry weight. For formulation of the population balance model it is convenient to reformulate the model, such that both compartments P(3HB) and non-P(3HB) biomass are considered separately.

Concentration of P(3HB) is then defined as:

$$x_{\mathrm{P(3HB)}} = m_{\mathrm{P(3HB)}}\, c \tag{5.77}$$

and the concentration of the remaining compartment of non-P(3HB) biomass BIO as

$$x_{\mathrm{BIO}} = c - x_{\mathrm{P(3HB)}} \quad . \tag{5.78}$$

Concentration of P(3HB) $x_{\mathrm{P(3HB)}}$ and non-P(3HB) biomass BIO x_{BIO} will then translate into the internal coordinates of a two-dimensional population balance model.

5.4.1. Two-dimensional Population Balance Model

Based on the lumped hybrid cybernetic model with approximated enzyme levels the following population balance model can be formulated:

$$\frac{\partial n(t,\mathbf{x_c})}{\partial t} + \nabla_{\mathbf{x_c}} \left\{ \Pi\, \mathbf{r_L}\, n(t,\mathbf{x_c}) \right\} = a(\mathbf{x_c},\mathbf{x_s})\, n(t,\mathbf{x_c}) \quad . \tag{5.79}$$

Here n is the number density distribution with respect to the intracellular concentrations of P(3HB) and BIO ($\mathbf{x_c} = \left[x_{\mathrm{BIO}}\ x_{\mathrm{P(3HB)}}\right]^{\mathrm{T}}$). The rate $a(\mathbf{x_c},\mathbf{x_s})$ describes sources and sinks as a result of cell division and cell death. It is assumed that this rate depends on $\mathbf{x_c}$ and the substrates in the reactor $\mathbf{x_s} = [x_{\mathrm{FRU}}\ x_{\mathrm{AMC}}]^{\mathrm{T}}$.

The three reaction rates of the lumped active modes from Chapter 5.3.4 translate into the fluxes

$$\mathbf{r}_{\mathrm{L}} = \left[r_{\mathrm{L}}^{\mathrm{BIO}}\ r_{\mathrm{L}}^{\mathrm{P(3HB)_+}}\ r_{\mathrm{L}}^{\mathrm{P(3HB)_-}} \right]^{\mathrm{T}} \tag{5.80}$$

with

- $r_{\mathrm{L}}^{\mathrm{BIO}}$: flux in the direction of BIO synthesis
- $r_{\mathrm{L}}^{\mathrm{P(3HB)_+}}$: flux in the direction of P(3HB) synthesis
- $r_{\mathrm{L}}^{\mathrm{P(3HB)_-}}$: flux in the direction of P(3HB) metabolization

The fluxes are regulated via cybernetic control variables:

$$\mathbf{r}_{\mathrm{L}} = \mathrm{diag}(\mathbf{v})\, \mathrm{diag}(\mathbf{u})\, b\, \mathbf{r}_{\mathrm{L}}{}^{\mathrm{kin}} \quad . \tag{5.81}$$

For low ammonium chloride concentration and high fructose concentration synthesis of P(3HB) is favored, while non-P(3HB) biomass BIO is increasing and P(3HB) is decreasing when there is sufficient ammonium chloride available.

P(3HB) distribution among the cells can be measured via flow cytometry of stained cells. To the best of the authors knowledge it is not possible so far to determine

the distribution of the non-P(3HB) biomass BIO among the cells. The model has therefore no practical relevance, since it is not possible to compare this model with experimental data. However, the model was studied theoretically in the Diploma thesis of Philipp Paetzold [58], which was advised by the present author. Results were also published in [17].

Furthermore the direct flow cytometric measurement of the intracellular P(3HB) content in *R. eutropha* has crucial disadvantages, e.g. a complex staining procedure and the cells may not be usable afterwards for additional analysis steps. In contrast, measurements of the forward scatter which is correlated to cell size are relatively simple and have little effect on the cells viability. For this reason a reduced population balance model by correlating size and intracellular P(3HB) content is presented in the following section.

5.4.2. One-dimensional Population Balance Model

In the experiment `Ralst05FruParallel` in Chapter 4 the intracellular amount of P(3HB) is measured using flow cytometric analysis of BODIPY stained cells. It was already argued that cell internal P(3HB) is correlated to cell size, which is correlated to forward scatter.

In Figure 5.15 (top row) the mean values of the fluorescence intensity distribution and the forward scatter distribution are plotted and a linear correlation can be observed. Furthermore, the mean values of the forward scatter distribution show the same course as experimental P(3HB) data in Figure 5.15 (bottom row).

Motivated by these observations a linear relationship is assumed, which makes direct computation of the P(3HB) distribution from measurement of the size distribution possible. A corresponding one-dimensional population balance equation can be constructed [16]

$$\begin{aligned} \frac{\partial n(l,t)}{\partial t} + \frac{\partial}{\partial l}\left\{ r_1^{\mathrm{P(3HB)_+}}\, n(l,t)\right\} = \\ -(r_1^{\mathrm{BIO}} + r_1^{\mathrm{P(3HB)_-}})\, S(l)\, n(l,t) \\ + \int_{l_{\min}}^{l_{\max}} (r_1^{\mathrm{BIO}} + r_1^{\mathrm{P(3HB)_-}}) S(l^*)\, p(l,l^*)\, n(t,l^*)\, \mathrm{d}l^* \quad . \end{aligned} \tag{5.82}$$

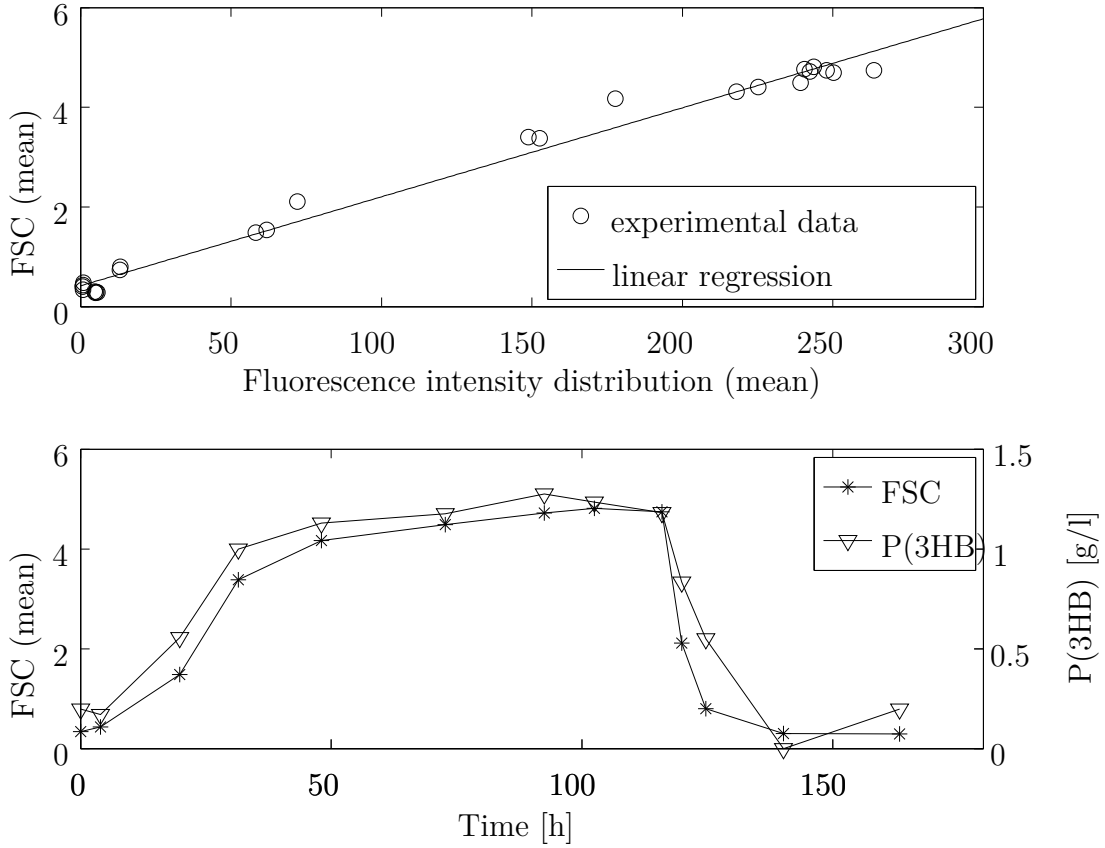

Figure 5.15.: Mean values of forward scatter and fluorescence intensity distributions show linear correlation (top row) and mean values of the forward scatter distribution show same course as experimental P(3HB) data (bottom row).

Here it is assumed that each cell grows due to P(3HB) production in the absence of ammonium chloride with the rate $r_{\mathrm{l}}^{\mathrm{P(3HB)_+}}$. In addition, the cells divide in presence of ammonium chloride by consuming either fructose or P(3HB) as carbon source with the rates $r_{\mathrm{l}}^{\mathrm{BIO}}$ or $r_{\mathrm{l}}^{\mathrm{P(3HB)_-}}$, respectivly. The partition mechanism is described by the beta distribution p and division probability distribution S according to Mantzaris et al. [51].

The reaction rates $\mathbf{r}_{\mathrm{l}}$ are again regulated by cybernetic control variables:

$$\mathbf{r}_{\mathrm{l}} = \mathrm{diag}(\mathbf{v})\,\mathrm{diag}(\mathbf{u})\,b\,\mathbf{r}_{\mathrm{l}}^{\mathrm{kin}} \quad , \tag{5.83}$$

with rates characterizing the following subprocesses:

- Cell division by utilizing fructose and ammonium chloride

$$r^{\text{kin}}_{\text{l,BIO}} = k_{\text{l,BIO}} \frac{x_{\text{FRU}}}{K_{\text{FRU}} + x_{\text{FRU}}} \frac{x_{\text{AMC}}}{K_{\text{AMC}} + x_{\text{AMC}}} \quad . \tag{5.84}$$

- Growth by P(3HB) synthesis

$$r^{\text{kin}}_{\text{l,P(3HB)}_+} = k_{\text{l,P(3HB)}_+} \frac{l\, x_{\text{FRU}}}{K_{\text{FRU}} + x_{\text{FRU}} + K_I\, l^2} \quad . \tag{5.85}$$

- Cell division by metabolizing P(3HB) and ammonium chloride

$$r^{\text{kin}}_{\text{l,P(3HB)}_-} = k_{\text{l,P(3HB)}_-} \frac{x_{\text{AMC}}}{K_{\text{AMC}} + x_{\text{AMC}}} (l - l_{\min})^{1.5} \quad . \tag{5.86}$$

It is assumed, that the rate of cell division depends on cell size. The characteristic length l is correlated to the forward scatter, which also depends on the cell volume. However, in fact, the forward scatter depends on the area which is hit by the light beam. To correlate this area with the cell volume it is therefore neccessary to include the exponent $3/2 = 1.5$ in equation (5.86).

The population balance equation describing the size distribution of the cell culture is coupled to the concentrated dynamics of the external substrates.

Utilization of external substrates are described by

$$\frac{\mathrm{d}x_{\text{FRU}}}{\mathrm{d}t} = -\int_{l_{\min}}^{l_{\max}} \Pi_{\text{FRU}}\, \mathbf{r}_{\text{l}}\, n(l,t)\, \mathrm{d}l \tag{5.87}$$

for fructose and

$$\frac{\mathrm{d}x_{\text{AMC}}}{\mathrm{d}t} = -\int_{l_{\min}}^{l_{\max}} \Pi_{\text{AMC}}\, \mathbf{r}_{\text{l}}\, n(l,t)\, \mathrm{d}l \tag{5.88}$$

for ammonium chloride, with $\Pi = [\Pi_{\text{FRU}}\ \Pi_{\text{AMC}}]^{\text{T}}$ being the stoichiometric matrix.

The overall system is numerically solved using a finite volume scheme the for discretization of the population balance equation [51]. In Figure 5.16 the comparison of simulation results with experimental data is shown. Initial conditions for the simulation are the experimental data at $t = 19.8$ h. In the first 116 hours fructose concentration was high and ammonium chloride concentration was low (see Figure

5.17). During this phase P(3HB) content increases and forward scatter distribution shifts to higher values as seen in Figure 5.16. At $t = 116$ h ammonium chloride was added and the organisms switches to P(3HB) metabolization, which results in a shift of forward scatter distribution to lower values as can be observed in Figure 5.16.

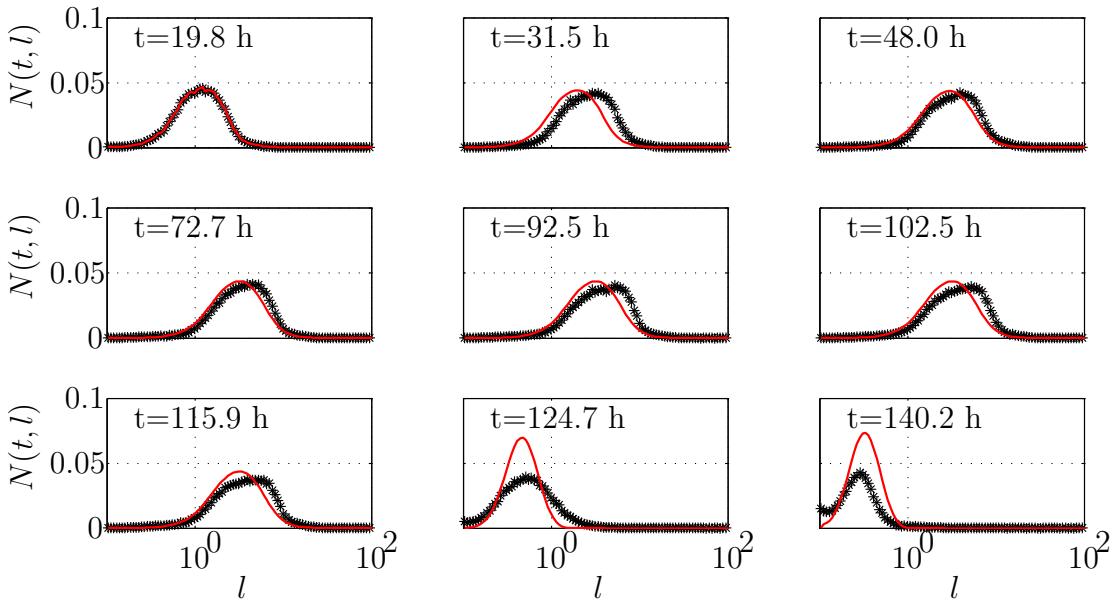

Figure 5.16.: Simulation results (red line) of one-dimensional population balance model in comparison with experimental forward scatter distribution (black $*$).

The model can represent the available experimental data until ammonium chloride is added and P(3HB) is metabolized. From that time point the model slightly differs from the experimental data. However, the shifting of the peak is in good agreement, only the number of cells can not be represented by the model for later time points. This might be due to neglected cell death in the population balance model.

Furthermore, the model is still not validated with additional independent experimental data and the presented experimental data have a poor resolution in the forward scatter distribution. Any conclusions are therefore still speculative.

Therefore, further experiments are needed to improve and validate the model. So far, it could only be shown, that correlation of cell size with P(3HB) content is a promising option for a fast method to model and determine cell to cell variance of

P(3HB) content, since no complex staining procedure is needed.

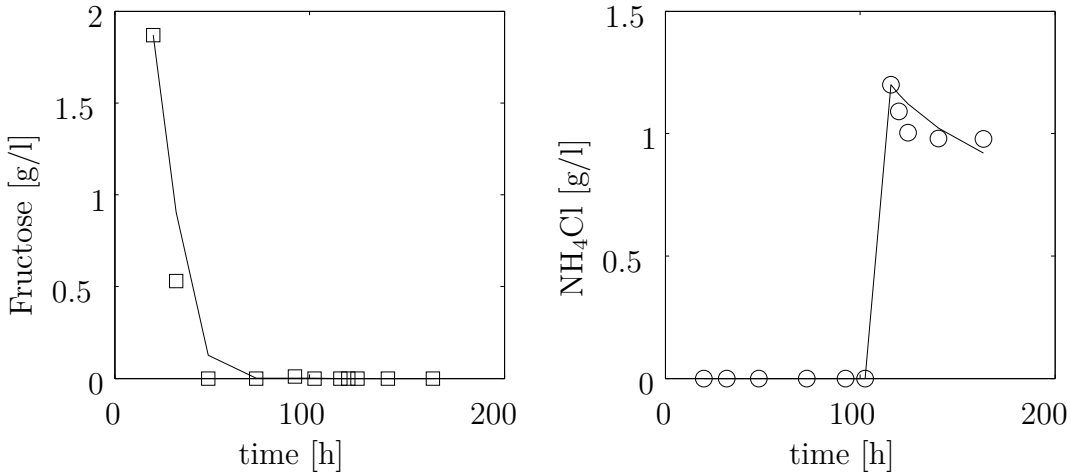

Figure 5.17.: Simulation results (black solid line) of one-dimensional population balance model and experimental data (Fructose: □, NH4Cl: ○). Substrate concentration in medium at $t = 0$ h: Fructose: 3 g/l, NH4Cl: 0.1 g/l. NH4Cl pulse at $t = 116$ h: ≈ 1.3 g/l.

5.5. Conclusion and Summary

Based on a metabolic network a hybrid cybernetic model was developed, which describes the synthesis and metabolization of P(3HB) in *R. eutropha*. The concept of the hybrid cybernetic modeling approach was extended to include internal metabolites, which have slow dynamics. Parameters were estimated from experiments, which include all three main processes (growth, synthesis of P(3HB) and metabolization of P(3HB)) in one single experiment. The model was validated with different and independent additional experiments.

Nonlinear analysis of the model reveals a region of multi-stationarity, which is rather small and is therefore not relevant from a practical point of view. This is in agreement with experimental observations.

It was then shown, that the model can be reduced without loosing much accuracy. The reduced model could therefore be used to formulate a population balance model. To the authors knowledge, this is the first time the cybernetic modeling approach was coupled with population balance modeling.

Starting point was a two-dimensional population balance model with two internal coordinates, which are P(3HB) and non-P(3HB) biomass, respectively. Although cell internal P(3HB) amount can be measured by flow cytometry, to the best of the authors knowledge, there is no way to estimate the distribution of non-P(3HB) biomass among single cells. The two-dimensional population balance model could in fact be used for simulation, but has therefore little practical relevance.

In contrast to that, a one-dimensional population model was formulated, which relates the cell size by means of forward scatter to cell internal P(3HB) concentration. An additional advantage is, that cells do not have to be stained in a complex procedure, which might harm the cells or can at least alter them.

6. *Rhodospirillum rubrum*

R. rubrum is a much more complex organism than *R. eutropha*. To examine whether similar modeling approaches as they were formulated for *R. eutropha* can be applied to *R. rubrum* it is neccessary in a first step to perform similar experiments with *R. rubrum*. Allthough *R. rubrum* is a facultative photosynthetic bacterium, experiments were performed under aerobic and dark conditions.

Fortunately there are already a few experiments with *R. rubrum* growing on fructose available in literature [67, 68], which will presented here for convenience in a consistent way with the experiments in Chapter 4.

In contrast to *R. eutropha* it was observed that cells of *R. rubrum* stained with Nile red show a bimodal distribution under the microscope (data not shown) when growing on acetate as sole carbon source. Some cells were full with P(3HB), but others were almost empty. To verify this, own experiments with *R. rubrum* growing on acetate as carbon source were performed.

Based on these experimental findings it is discussed whether the modeling approaches for *R. eutropha* can be adapted to *R. rubrum*.

6.1. *R. rubrum* Growing on Fructose

Experiments with *R. rubrum* growing on fructose were done by C. Rudolf during her PhD. For convenience, the results are presented here according to [67, 68] in a consistent way with the experiments in Chapter 4. Cultivation conditions for these experiments may vary from the conditions described in Chapter 2.3.

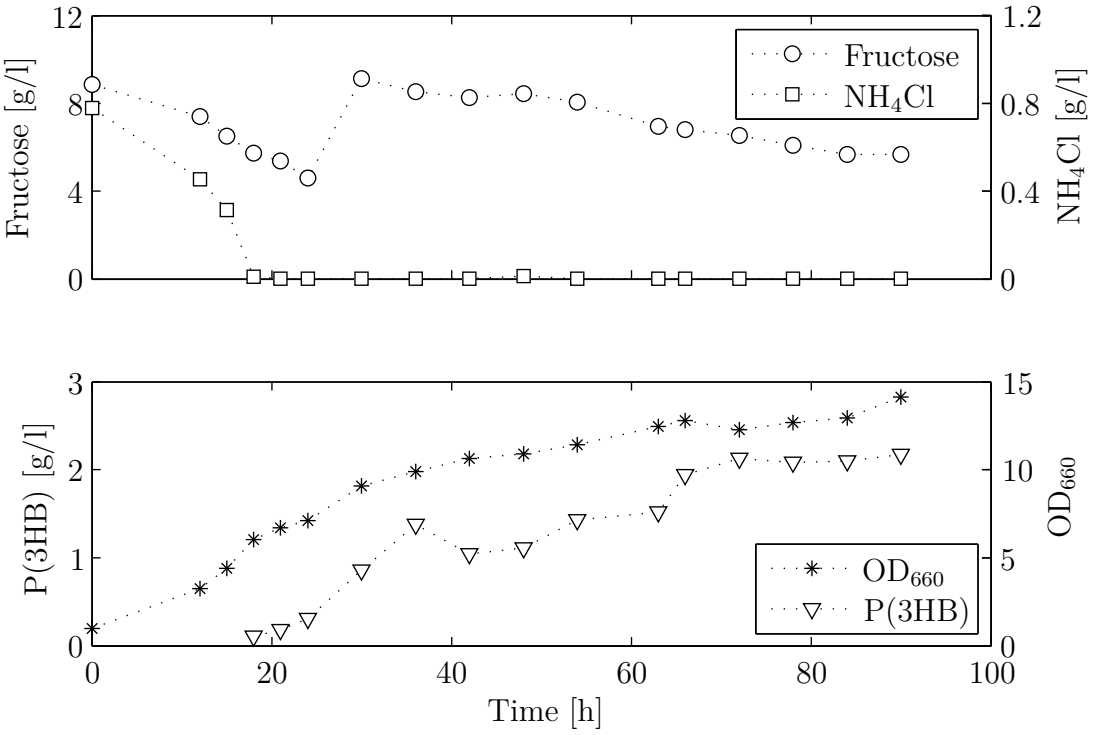

Figure 6.1.: Time course of experiment `Rhod01FruSingle`.

6.1.1. Rhod01FruSingle

In the beginning of this experiment (see Figure 6.1) both substrates fructose (carbon) and ammonium (nitrogen) are available. Cell growth is monitored via optical density at 660 nm. During the first 20 hours both substrates are consumed and biomass is increasing. After 20 hours the nitrogen source is depleted and external carbon source fructose is now stored into internal carbon resevere material P(3HB). After approximately 30 hours more fructose is added to the fermenter to maintain a longer P(3HB) synthesis.

After 37 hours P(3HB) concentration drops in Figure 6.1. P(3HB) can be metabolized, when cells are able to grow and devide, which is usually only the case if a nitrogen source is available. However, this is not the case at this time point. It can be therefore concluded, that the P(3HB) concentration at t=37 hours might be an outlyer.

6.1.2. Rhod02FruSingle

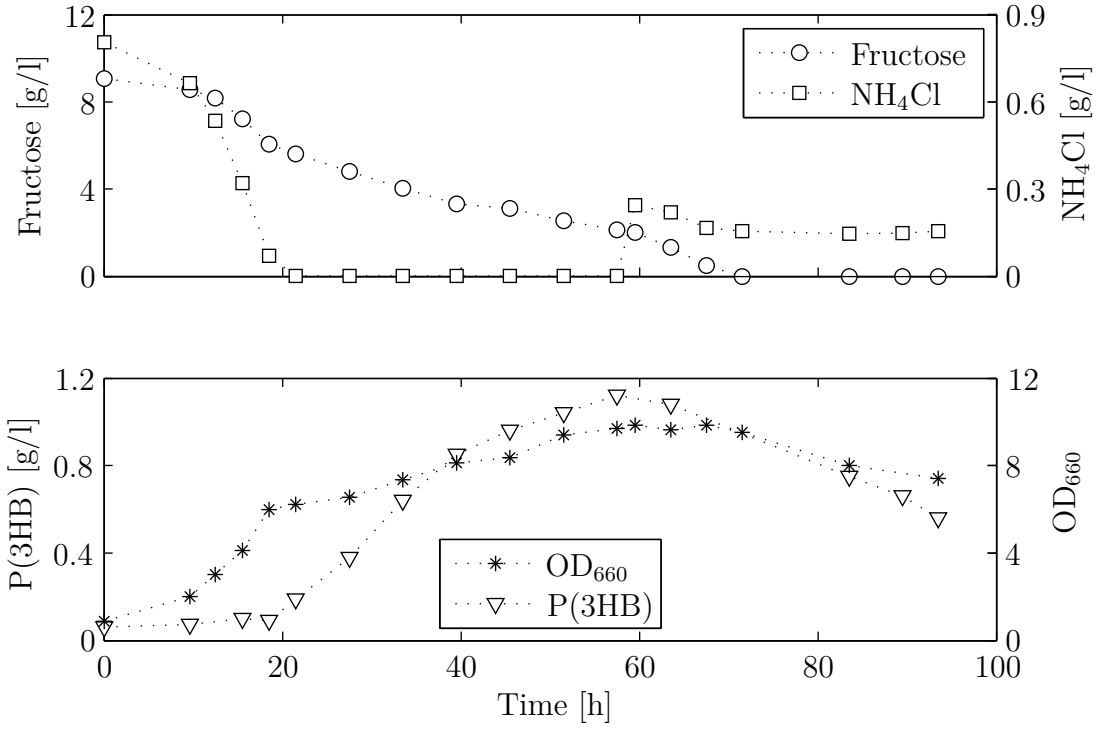

Figure 6.2.: Time course of experiment `Rhod02FruSingle`.

In the beginning, again both substrates are available (see Figure 6.2) and optical density increases due to cell growth. Ammonium is depleted after 20 hours. From this time point external carbon source fructose is stored into internal carbon reserve material P(3HB). Optical density is increasing linear between 20 and 60 hours.

At time point t=60 h new ammonium is added and P(3HB) is now decreasing, since it can be metabolized when ammonium is available. Although new non-P(3HB) biomass is now synthesized (e. g. new cells are formed), the optical density is decreasing. This gives the hint, that optical density is not linear correlated to cell dry weight, but depends also on the fraction of P(3HB) to non-P(3HB) biomass, as it is the case for *R. eutropha* and described in Chapter 2.4.3. Assuming a linear correlation between optical density and cell dry weight might lead to inaccurate results.

6.2. *R. rubrum* Growing on Acetate

As mentioned above, in contrast to *R. eutropha* it was observed that cells of *R. rubrum* stained with Nile red show a bimodal distribution under the microscope when growing on acetate as sole carbon source. To validate and quantify this, the following experiment was performed.

6.2.1. Rhod03AceFlask

R. rubrum was grown in a shaking flask with sodium acetate as single carbon source. Cell growth was monitored with optical density (Figure 6.3) and is increasing until 50 hours. At approximately t=52 h new sodium actetate was added and optical density increases again until 70 hours.

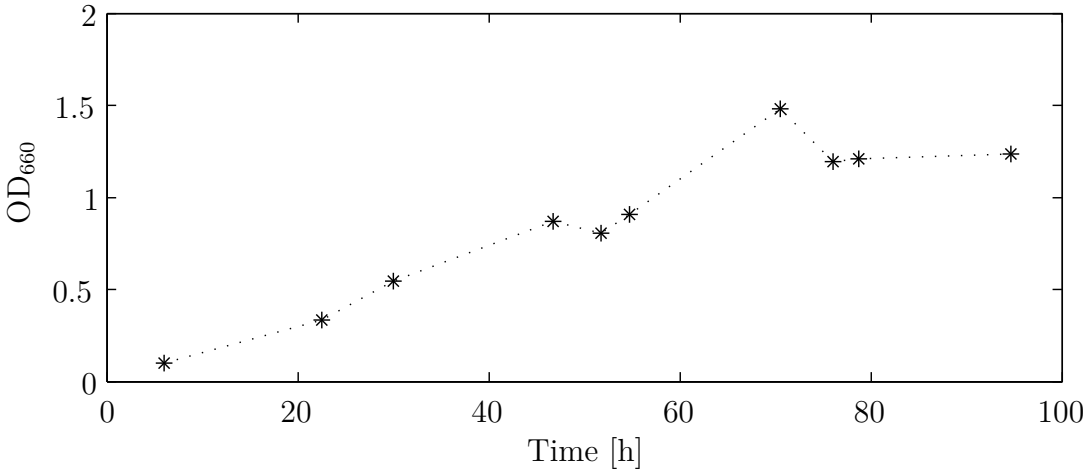

Figure 6.3.: Time course of experiment `Rhod03AceFlask`, optical density.

Samples were analyzed via flow cytometry. P(3HB) within the cells were stained with Nile red and fluorescence intensity was measured. Figure 6.4 shows the temporal evolution of the fluorescence distribution, which is correlated to P(3HB). In general the distribution is shifting to higher values of the fluorescence distribution, which means, that P(3HB) concentration is increasing. After 70 hours the distribution shifts back, which implies a decreasing P(3HB) concentration.

However, it is remarkable, that the distribution is bi-modal. The initial distribution already looks like two overlapping distributions. From 6 hours the peak on

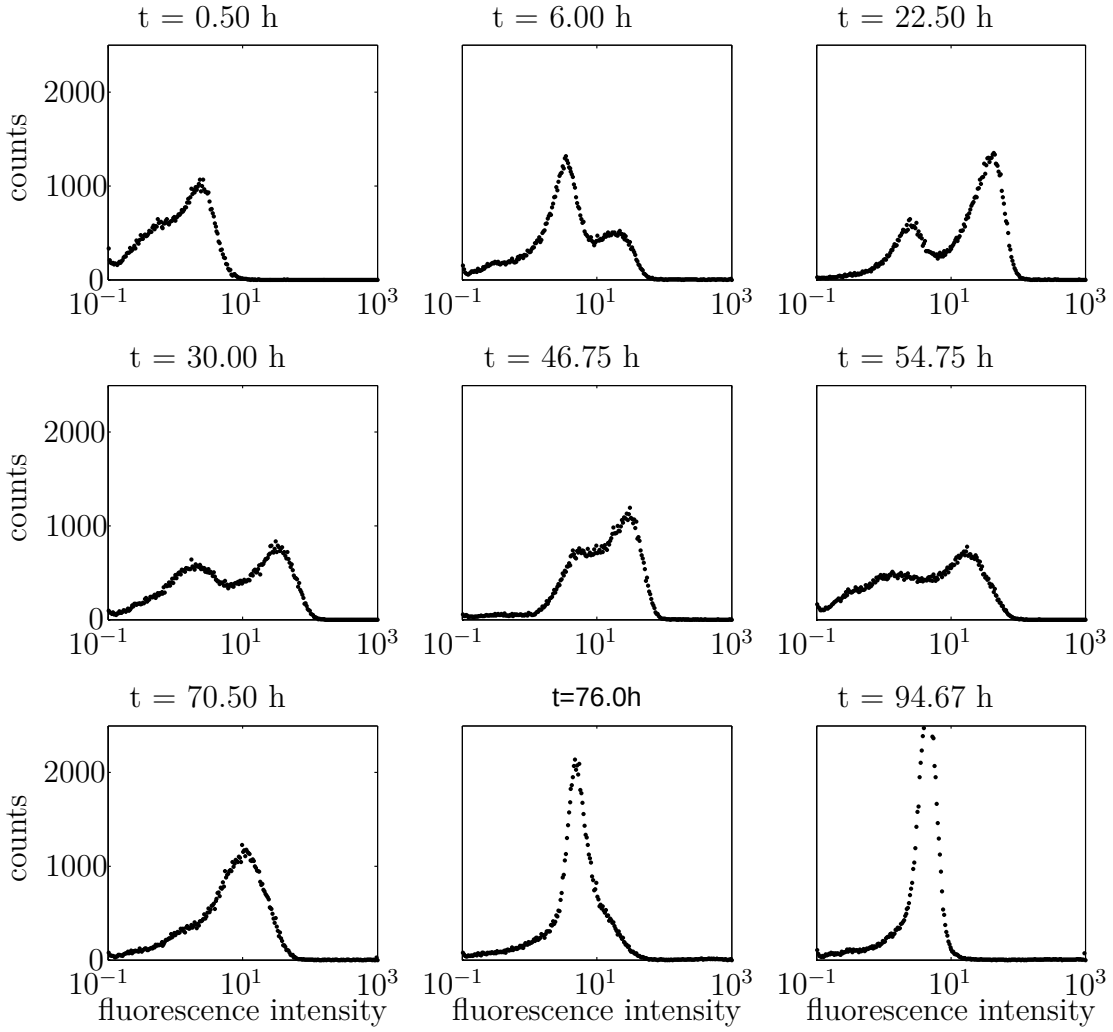

Figure 6.4.: Flow cytometry measurement of experiment `Rhod03AceFlask`, fluorescence intensity.

the right side of the distributions increases, while the left peak seems to be shifting towards the right peak, where both nearly merge after 70 hours. Only one merged peak is then shifting back.

This can also be observed in the forward scatter in Figure 6.5. The forward scatter is correlated to cell size. Cells with accumulated P(3HB) are bigger than cells without P(3HB). Although, the initial distribution in forward scatter looks uni-modal, a second peak is appearing after 6 hours and increasing. After 50 hours the distribution looks uni-modal again. However, resolution of the forward scatter is pretty poor and a bi-modal distribution might be longer observable at higher

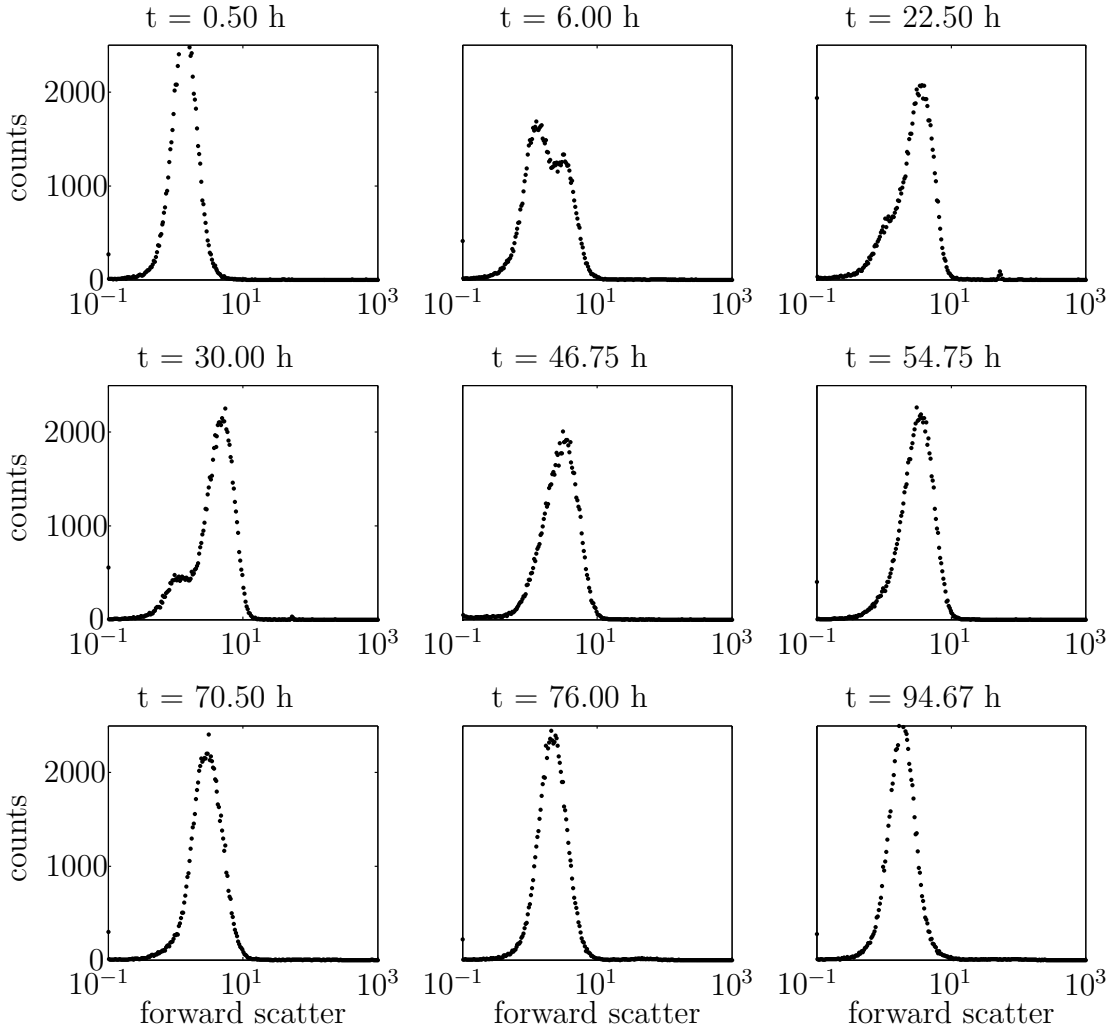

Figure 6.5.: Flow cytometry measurement of experiment `Rhod03AceFlask`, forward scatter.

resolution.

Figure 6.6 additionally shows a two-dimensional histogram of the fluorescence intensity versus forward scatter at the four time points between 6 and 47 hours. Two groups of cells can be clearly identified. And it can also clearly be seen that cells with higher fluorescence intensity (e.g. higher P(3HB) concentration) have higher forward scatter values (e.g. have higher cell size or volume).

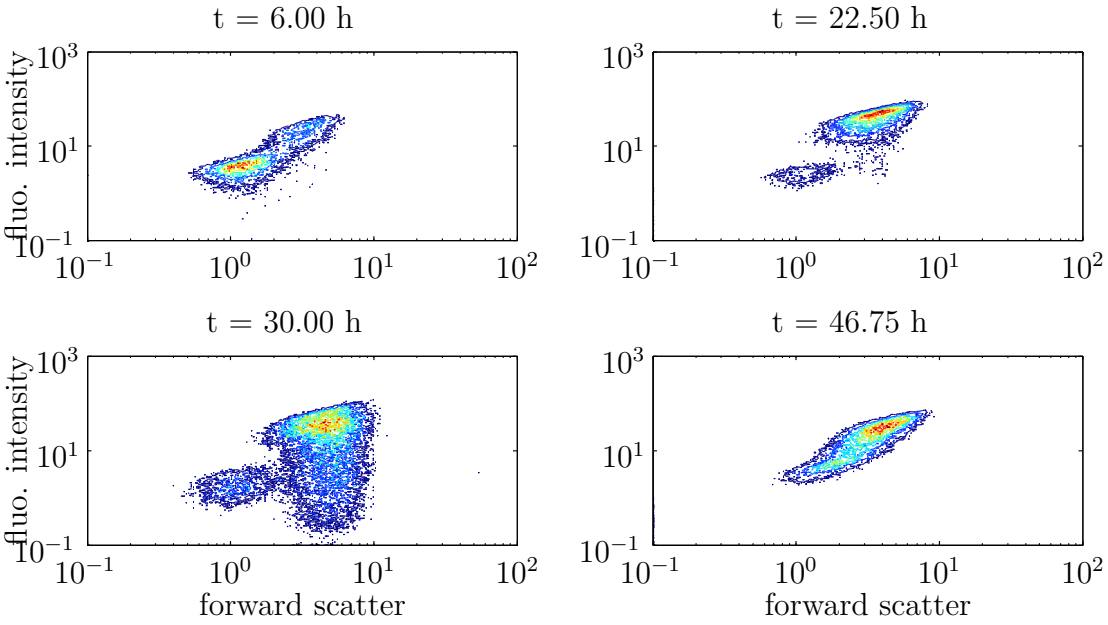

Figure 6.6.: 2D flow cytometry measurement of experiment `Rhod03AceFlask`, fluorescence intensity vs forward scatter.

6.3. Modeling the Production of Poly(3-hydroxybutyrate) in *R. rubrum*

Although *R. rubrum* is a much more complex organism than *R. eutropha*, the experimental results are very similar to those in Chapter 4. Both organisms synthesize P(3HB) under excess carbon source or lack of a nitrogen source, and metabolize P(3HB) when nitrogen limitation is removed. It is therefore feasible to discuss similar modeling approaches for *R. rubrum* as they are formulated for *R. eutropha* in Chapter 5. For that, the following steps have to be conducted:

1. Construction of a metabolic network and metabolic yield analysis
2. Formulation of a hybrid cybernetic model
3. Nonlinear analysis of the model
4. Model reduction
5. Population balance modeling based on the reduced model

For *R. rubrum* growing on fructose, this is straight forward. However, *R. rubrum* growing on actetate shows a bimodal P(3HB) distribution in contrast to *R. eutropha* where no bimodal distributions are observed so far. A population balance model for *R. rubrum* growing on acetate, which can describe this bimodal distribution, is therefore an interesting task. This bimodal distribution suggests a bistable region, which is larger than the bistable region observed for *R. eutropha* as described in Chapter 5.2.3.

6.3.1. Metabolic Network

For *R. rubrum* a metabolic network was recently published [29]. This network contains of 144 reactions, 119 internal metabolites and 14 external metabolites. This network has still a moderate complexity. However, calculation of elementary modes is already challenging.

A systematic way to calculate elementary modes in larger networks, is to divide the network in disjoint subnetworks. The most simple way is to chose, for example, two reactions, e. g. substrate uptakes, and divide the network in four disjoint subnetworks, which are

no.	reaction 1	reaction 2
1	0	0
2	0	1
3	1	0
4	1	1

where 0 means reaction **does not** take place, and 1 means reaction **does** take place.

By choosing n reactions (preferable uptake reactions) every network can be divided into 2^n disjoint subnetworks. Choosing uptake reactions is reasonable since most of the disjoint subnetworks have then a reduced number of substrate uptakes, which is useful if not all substrates are available to the organism.

Since *R. rubrum* is a facultative photosynthetic bacterium, it is reasonable to chose the reaction `Photo` from the metabolic network in [29] to devide the network into subnetworks which function under dark conditions and subnetworks which do not.

Furthermore the substrate uptake reactions for fructose (`Fru_up`) and acetate (`Ac_up`) are reasonable choices, since these are the substrates already used in Chapter 6. Additionally succinate is an important and often used carbon substrate for *R. rubrum* and oxygen has also an important influence on bacterial growth.

Therefore, for dividing the metabolic network of *R. rubrum* the following five uptake reactions were chosen:

- `O2_up`: oxygen uptake reaction
- `Photo`: uptake reaction necessary for photo synthesis
- `Fru_up`: fructose uptake reaction
- `Suc_up`: succinate uptake reaction
- `Ac_up`: acetate uptake reaction

From these five reactions follow $2^5 = 32$ disjoint subnetworks, which were analysed from M. Berger during her pre-diploma thesis [4]. The total network has more then 7 million elementary modes. However, the experiments in Chapter 6 are performed under aerob and dark conditions, which reduces the number of needed elementary modes to less than 4 million. Under these conditions there are less than 2 million elementary modes, where *R. rubrum* grows on fructose as single carbon source and less than 46.000 elementary modes, where *R. rubrum* grows on acetate as single carbon source.

Although the number of needed elementary modes could be reduced significantly, it is still to large for reasonable dynamic modeling. This subset of elementary modes need to be be further reduced with knowledge of experimental yield data by metabolic yield analysis. Unfortunately, the experiments in Chapter 6 only provide optical density as biomass equivalent. This is not sufficient to calculate cell dry weight (see Chapter 2.4.3), which is necessary for a reasonable metabolic yield analysis. Hence, further experiments are needed for dynamic modelling of P(3HB) formation in *R. rubrum* with fructose and/or acetate, which therefore was clearly beyond the scope of this work.

7. Conclusions

This thesis focuses on the dynamic mathematical modeling of poly(3-hydroxybutyrate) synthesis and metabolization in microorganisms, in particular *R. eutropha* and *R. rubrum*. Existing models in literature usually neglect metabolization of poly(3-hydroxybutyrate) or have fitted the model to experimental data without significant metabolization of poly(3-hydroxybutyrate).

By neglecting metabolization of poly(3-hydroxybutyrate) cell internal regulation might be of no importance, but becomes crucial if metabolization of poly(3-hydroxybutyrate) is included into dynamic modeling. The organism needs to switch between growth, synthesis of poly(3-hydroxybutyrate) and metabolization of poly(3-hydroxybutyrate). A mathematical model therefore needs to include cell internal regulation, which is able to switch between theses processes.

Since cell internal regulation is usually very complex and often not fully understood, in this thesis a hybrid cybernetic modeling approach is used. This approach is extended to include cell internal metabolites with slow dynamics.

Available experimental data from literature usually neglect metabolization of poly(3-hydroxybutyrate) or only focus on certain subprocesses. Therefore own experiments with different carbon substrates were performed, which include all three subprocesses in a single experiment: growth, synthesis and metabolization of poly(3-hydroxybutyrate).

The hybrid cybernetic model was formulated for *R. eutropha* growing on fructose as single carbon source. However, other substrates e.g. acetate and glucose were studied experimentally and show similar behaviour as fructose. The dynamic model can therefore be easily adapted to these carbon substrates.

A non-linear analysis of the model reveals that metabolization of poly(3-hydroxybutyrate) is in fact crucial and has to be included into dynamic modeling. Additionally, a

small region of multiplicity was detected.

The formulated model still neglects cell to cell variance w.r.t. intracellular compounds, in particular the amount of poly(3-hydroxybutyrate). In contrast, heterogeneity can be described within the framework of population balance modeling. Therefore, based on the cybernetic model a population balance model is formulated. Although the formulated cybernetic model has a moderate complexity, the translation of the states c, $m_{\mathrm{P(3HB)}}$ and $\mathbf{e}$ into internal coordinates of the population balance equations, makes the population balance model computationally challenging. Therefore different reductions of the cybernetic model are discussed and compared. The population balance model is then based on a reduced cybernetic model.

First, a population balance model is formulated, which consideres the two main compartments P(3HB) and non-P(3HB) biomass as internal coordinates. It combines the cybernetic modeling approach with population balance modeling.

However, measurement of the non-P(3HB) biomass distribution is so far hardly possible. This limits the practical use of such a two-dimensional population balance model. On the other hand, it turned out, that the amount of P(3HB) is nicely correlated to the forward scatter of flow cytometry, which in turn is correlated to cell size. Based on this correlation a one-dimensional population balance model is formulated with cell size as internal coordinate of the population balance equation. Change of cell size depends on synthesis and metabolization of poly(3-hydroxybutyrate). Cell size can easily be measured even without complex cell staining.

It is shown that the one-dimensional population balance model can in principle represent the experimental observations. However, the resolution of the measured forward scatter is unfortunately rather poor. For validation and even improvement of the one-dimensional population balance model better data from flow cytometry is needed.

For *R. rubrum* a few experimental data exist in literature, which include synthesis as well as metabolization of poly(3-hydroxybutyrate). Since these data show the same behaviour than the experimental data for *R. eutropha*, the modeling approach can in principle be easily adapted to *R. rubrum*. However, *R. rubrum* has a much higher metabolic complexity. Therefore, additional experiments are needed for a

proper model formulation. This was beyond the scope of the present thesis and is an interesting topic for future work.

Additionally, data from flow cytometry for *R. rubrum* show existence of bi-modal distribution in cell internal amount of poly(3-hydroxybutyrate). This gives hint of a potential bi-stability.

As an interesting and surprising side result of this thesis, it is shown that *R. eutropha* is able to grow on glucose as single carbon source without previous mutagenic treatment, which is in contradiction to literature.

Furthermore it is made clear, that only monitoring optical density is not sufficient to estimate cell dry weight. Although this is a very common procedure in biology, this might lead to incorrect data under certain conditions, e.g. during accumulation of storage compounds. Instead, knowledge of all cell compartments, which influences optical density is crucial. Once a proper correlation is known, it allows the estimation of certain experimental data which might be difficult to measure, e.g. concentration of poly(3-hydroxybutyrate).

The main focus of this thesis was the mathematical modeling of the yield of P(3HB). By optimizing yield in industrial processes, biopolymers will become cheaper in future and thereby possibly a substitute for convectional synthetic polymers.

However, a big advantage of synthetic polymers is their wide variety in properties. Although there are already several biopolymers with different properties know, mathematical models which combine metabolism with polymer properties are still rare or even missing. Therefore the next step is to extend the formulated model to more advanced polymers and to include polymer properties, which depend on chain length and structure. *R. eutropha* for instance is able to synthesize not only P(3HB), but also P(3HB-3HV) and other polymers, depending on environmental conditions and availability of certain carbon substrates. By combining the cybernetic metabolic model with polymerization kinetics one might be able in future to adjust the desired polymer properties already during the fermentation process.

Bibliography

[1] S. L. Ajnazarova and V. V. Kafarov. *Methods for Experimental Optimization in Chemical Technology*. Vishaia Shkola, Moscow, 1985.

[2] M. Aragno, A. Walther-Mauruschat, F. Mayer, and H. G. Schlegel. Micromorphology of gram-negative Hydrogen bacteria - I. Cell morphology and flagellation. *Archives of Microbiology*, 114(2):93–100, 1977.

[3] D. K. A. Barnes, F. Galgani, R. C. Thompson, and M. Barlaz. Accumulation and fragmentation of plastic debris in global environments. *Philosophical Transactions of the Royal Society B: Biological Sciences*, 364(1526):1985–1998, 2009.

[4] M. Berger. Synthese und Analyse eines metabolischen Netzwerkes für Rhodospirillum rubrum. Master's thesis, Otto-von-Guericke Universität, Magdeburg, 2010. (supervised by: A. Franz).

[5] S. Böttger. Sensitivitätsanalyse kybernetischer Modelle. Master's thesis, Otto-von-Guericke Universität, Magdeburg, 2012. (supervised by: A. Franz).

[6] H. Brandl, E. J. Knee Jr, R. C. Fuller, R. A. Gross, and R. W. Lenz. Ability of the phototrophic bacterium Rhodospirillum rubrum to produce various poly(beta-hydroxyalkanoates): Potential sources for biodegradable polyesters. *International Journal of Biological Macromolecules*, 11(1):49–55, 1989.

[7] D. H. Davis, M. Doudoroff, R. Y. Stanier, and M. Mandel. Proposal to reject the genus Hydrogenomonas: Taxonomic implications. *International Journal of Systematic Bacteriology*, 19(4):375–390, 1969.

[8] J. G. B. Derraik. The pollution of the marine environment by plastic debris: A review. *Marine Pollution Bulletin*, 44(9):842–852, 2002.

[9] P. Dhurjati, D. Ramkrishna, M. C. Flickinger, and G. T. Tsao. A cybernetic

view of microbial-growth: Modeling of cells as optimal strategists. *Biotechnology and Bioengineering*, 27(1):1–9, 1985.

[10] I. Disli, A. Kremling, and A. Kienle. A model based analysis of multiple steady states in continuous cell cultures. In *Proceedings MATHMOD 09 Vienna - Full Papers CD Volume*, 2009.

[11] Y. Doi. *Microbial Polyesters*. VCH Publishers, Inc., 1990.

[12] Y. Doi, M. Kunioka, Y. Nakamura, and K. Soga. Nuclear magnetic resonance studies on unusual bacterial copolyesters of 3-hydroxybutyrate and 4-hydroxybutyrate. *Macromolecules*, 21(9):2722–2727, 1988.

[13] Y. Doi, A. Tamaki, M. Kunioka, and K. Soga. Biosynthesis of an unusual copolyester (10 mol % 3-hydroxybutyrate and 90 mol % 3-hydroxyvalerate units) in Alcaligenes eutrophus from pentanoic acid. *Journal of the Chemical Society, Chemical Communications*, pages 1635–1636, 1987.

[14] Y. Doi, A. Tamaki, M. Kunioka, and K. Soga. Production of copolyesters of 3-hydroxybutyrate and 3-hydroxyvalerate by alcaligenes eutrophus from butyric and pentanoic acids. *Applied Microbiology and Biotechnology*, 28(4-5):330–334, 1988.

[15] L. Ferraz, A. Bonomi, R. A. M Piccoli, F. M. Kapritchkoff, W. Schmidell, R. C. P. Alli, C. Y. Takano, M. N. Mattos, V. Oliveira V., and Fontolan. Cybernetic structured modeling of the production of polyhydroxyalkanoates by Alcaligenes eutrophus. *Brazilian Journal of Chemical Engineering*, 16(2):205–212, 1999.

[16] A Franz, R. Dürr, and A. Kienle. Population Balance Modeling of Biopolymer Production in Cellular Systems. In *Proceedings of the 19th IFAC World Congress*, pages 1705 – 1710, Cape Town, South Africa, 2014.

[17] A. Franz, H. Grammel, R. Rehner, P. Paetzold, and A. Kienle. Multiscale Modeling of Biopolymer Production in Multicellular Systems. In *Proceedings to the 7th Vienna International Conference on Mathematical Modeling - MATHMOD 2012*, pages 320 – 325, 2012.

[18] A. Franz, R. Rehner, A. Kienle, and H. Grammel. Rapid selection of glucose-utilizing variants of the polyhydroxyalkanoate producer Ralstonia eutropha

H16 by incubation with high substrate levels. *Letters in Applied Microbiology*, 54(1):45–51, 2012.

[19] C. J. Gadgil, P. J. Bhat, and K. V. Venkatesh. Cybernetic model for the growth of Saccharomyces cerevisiae on melibiose. *Biotechnology Progress*, 12(6):744–750, 1996.

[20] K. G. Gadkar, F. J. Doyle, T. J. Crowley, and J. D. Varner. Cybernetic model predictive control of a continuous bioreactor with cell recycle. *Biotechnology Progress*, 19(5):1487–1497, 2003.

[21] J. Gagneur and S. Klamt. Computation of elementary modes: a unifying framework and the new binary approach. *BMC Bioinformatics*, 5:1–21, 2004.

[22] F. Galgani, J. P. Leaute, P. Moguedet, A. Souplet, Y. Verin, A. Carpentier, H. Goraguer, D. Latrouite, B. Andral, Y. Cadiou, J. C. Mahe, J. C. Poulard, and P. Nerisson. Litter on the sea floor along European coasts. *Marine Pollution Bulletin*, 40(6):516–527, 2000.

[23] R. Ghosh, A. Hardmeyer, I. Thoenen, and R. Bachofen. Optimization of the Sistrom culture medium for large-scale batch cultivation of Rhodospirillum rubrum under semiaerobic conditions with maximal yield of photosynthetic membranes. *Applied and Environmental Microbiology*, 60(5):1698–1700, 1994.

[24] DSMZ GmbH. Rhodospirillaceae medium (modified). `http://www.dsmz.de/microorganisms/medium/pdf/DSMZ_Medium27.pdf`, 2007.

[25] DSMZ GmbH. Mineral medium for chemolithotrophic growth (h-3). `http://www.dsmz.de/microorganisms/medium/pdf/DSMZ_Medium81.pdf`, 2011.

[26] G. Gottschalk, H. G. Schlegel, and U. Eberhardt. Verwertung von Fructose durch Hydrogenomonas H16(I.). *Archiv für Mikrobiologie*, 48(1):95–108, 1964.

[27] R. A. Gross and B. Kalra. Biodegradable polymers for the environment. *Science*, 297(5582):803–807, 2002.

[28] M. J. Guardia, A. Gambhir, A. F. Europa, D. Ramkrishna, and W. S. Hu. Cybernetic modeling and regulation of metabolic pathways in multiple steady states of hybridoma cells. *Biotechnology Progress*, 16(5):847–853, 2000.

[29] O. Hädicke, H. Grammel, and S. Klamt. Metabolic network modeling of redox balancing and biohydrogen production in purple nonsulfur bacteria. *BMC Systems Biology*, 5, 2011.

[30] E. Heinzle and R. M. Lafferty. A kinetic model for growth and synthesis of poly-β-hydroxybutyric acid (PHB) in Alcaligenes eutrophus H 16. *European Journal of Applied Microbiology and Biotechnology*, 11(1):8–16, 1980.

[31] K. D. Jones and D. S. Kompala. Cybernetic model of the growth dynamics of Saccharomyces cerevisiae in batch and continuous cultures. *Journal of Biotechnology*, 71(1-3):105–131, 1999.

[32] T. Katoh, D. Yuguchi, H. Yoshii, H. D. Shi, and K. Shimizu. Dynamics and modeling on fermentative production of poly(β-hydroxybutyric acid) from sugars via lactate by a mixed culture of Lactobacillus delbrueckii and Alcaligenes eutrophus. *Journal of Biotechnology*, 67(2-3):113–134, 1999.

[33] S. Khanna and A. K. Srivastava. Recent advances in microbial polyhydroxyalkanoates. *Process Biochemistry*, 40(2):607–619, 2005.

[34] S. Khanna and A. K. Srivastava. A simple structured mathematical model for biopolymer (PHB) production. *Biotechnology Progress*, 21(3):830–838, 2005.

[35] S. Khanna and A. K. Srivastava. Computer simulated fed-batch cultivation for over production of PHB: A comparison of simultaneous and alternate feeding of carbon and nitrogen. *Biochemical Engineering Journal*, 27(3):197–203, 2006.

[36] S. Khanna and A. K. Srivastava. Optimization of nutrient feed concentration and addition time for production of poly(β-hydroxybutyrate). *Enzyme and Microbial Technology*, 39(5):1145–1151, 2006.

[37] H. Y. Kim, J. S. Park, H. D. Shin, and Y. H. Lee. Isolation of glucose utilizing mutant of Alcaligenes eutrophus, its substrate selectivity, and accumulation of poly-β-hydroxybutyrate. *Journal of Microbiology*, 33(1):51–58, 1995.

[38] J. I. Kim, J. D. Varner, and D. Ramkrishna. A hybrid model of anaerobic E. coli GJT001: combination of elementary flux modes and cybernetic variables. *Biotechnology Progress*, 24(5):993–1006, 2008.

[39] S. Klamt, J. Saez-Rodriguez, and E. D. Gilles. Structural and functional

analysis of cellular networks with CellNetAnalyzer. *BMC Systems Biology*, 1, 2007.

[40] Steffen Klamt. *Strukturelle Analyse von Stoffwechselnetzen illustriert am bakteriellen Redox- und Zentralstoffwechsel*. PhD thesis, Universtät Stuttgart, 2005.

[41] D. S. Kompala. Cybernetic modeling of spontaneous oscillations in continuous cultures of Saccharomyces cerevisiae. *Journal of Biotechnology*, 71(1-3):267–74, 1999.

[42] D. S. Kompala, D. Ramkrishna, N. B. Jansen, and G. T. Tsao. Investigation of bacterial-growth on mixed substrates: Experimental evaluation of cybernetic models. *Biotechnology and Bioengineering*, 28(7):1044–1055, 1986.

[43] D. S. Kompala, D. Ramkrishna, and G. T. Tsao. Cybernetic modeling of microbial growth on multiple substrates. *Biotechnology and Bioengineering*, 26(11):1272–1281, 1984.

[44] C. König, I. Sammler, E. Wilde, and H. G. Schlegel. Konstitutive Glucose-6-phosphat-Dehydrogenase bei Glucose verwertenden Mutanten von einem kryptischen Wildstamm. *Archives of Microbiology*, 67:51–57, 1969.

[45] C. König and H. G. Schlegel. Langfristiges organotrophes Wachstum von Hydrogenomonas H16 im Chemostaten. *Archives of Microbiology*, 62:41–55, 1968.

[46] M. V. Kumar, K. P. Zeyer, A. Kienle, and S. Pushpavanam. Conceptual analysis of the effect of kinetics on the stability and multiplicity of a coupled bioreactor-separator system using a cybernetic modeling approach. *Industrial & Engineering Chemistry Research*, 48(24):10962–10975, 2009.

[47] J. H. Law and R. A. Slepecky. Assay of poly-β-hydroxybutyric acid. *Journal of Bacteriology*, 82(1):33–36, 1961.

[48] J. H. Lee, H. C. Lim, and J. Hong. Application of nonsingular transformation to on-line optimal control of poly-β-hydroxybutyrate fermentation. *Journal of Biotechnology*, 55(3):135–150, 1997.

[49] N. S. Makkar and L. E. Casida. Cupriavidus necator gen. nov., sp. nov.: a

nonobligate bacterial predator of bacteria in soil. *International Journal of Systematic Bacteriology*, 37(4):323–326, 1987.

[50] M. Mangold, A. Kienle, E. D. Gilles, and K. D. Mohl. Nonlinear computation in DIVA - Methods and applications. *Chemical Engineering Science*, 55(2):441–454, 2000.

[51] N. V. Mantzaris, P. Daoutidis, and F. Srienc. Numerical solution of multivariable cell population balance models: I. Finite difference methods. *Computers and Chemical Engineering*, 25(11-12):1411–1440, 2001.

[52] J. Monod. The growth of bacterial cultures. *Annual Review of Microbiology*, 3:371–394, 1949.

[53] C. J. Moore. Synthetic polymers in the marine environment: A rapidly increasing, long-term threat. *Environmental Research*, 108(2):131–139, 2008.

[54] A. Mulchandani, J. H. T. Luong, and C. Groom. Substrate-inhibition kinetics for microbial-growth and synthesis of poly-beta-hydroxybutyric acid by Alcaligenes eutrophus ATCC-17697. *Applied Microbiology and Biotechnology*, 30(1):11–17, 1989.

[55] A. A. Namjoshi, W. S. Hu, and D. Ramkrishna. Unveiling steady-state multiplicity in hybridoma cultures: The cybernetic approach. *Biotechnology and Bioengineering*, 81(1):80–91, 2003.

[56] A. A. Namjoshi and D. Ramkrishna. Multiplicity and stability of steady states in continuous bioreactors: dissection of cybernetic models. *Chemical Engineering Science*, 56(19):5593–5607, 2001.

[57] PlasticsEurope Association of Plastics Manufactors. Plastics - the Facts 2013: An analysis of European latest plastics production, demand and waste data. `http://www.plasticseurope.org/cust/documentrequest.aspx?DocID=59108`, October 2013.

[58] P. Paetzold. Populationsdynamische Modellierung der Polyhydroxybuttersäure (PHB)Synthese in Ralstonia eutropha. Master's thesis, Otto-von-Guericke Universität, Magdeburg, 2012. (supervised by A. Franz).

[59] M. A. Pinto and C. D. Immanuel. Modelling and bifurcation studies of a two-

stage continuous bioreactor for the production of poly-beta-hydroxybutyrate (PHB). In *AIChE Annual Meeting*, 2005.

[60] M. A. Pinto and C. D. Immanuel. Sensitivity of bifurcation traits to model parameters in poly-beta-hydroxy butyrate production. In *ADCHEM*, 2006.

[61] Y. Poirier, C. Nawrath, and C. Somerville. Production of polyhydroxyalkanoates, a family of biodegradable plastics and elastomers, in bacteria and plants. *Biotechnology (N.Y.)*, 13(2):142–150, 1995.

[62] P. Raje and A. K. Srivastava. Updated mathematical model and fed-batch strategies for poly-β-hydroxybutyrate (PHB) production by Alcaligenes eutrophus. *Bioresource Technology*, 64(3):185–192, 1998.

[63] D. Ramkrishna. *A Cybernetic Perspective of Microbial Growth*, chapter 8, pages 161–178. American Chemical Society, 1983.

[64] D. Ramkrishna. *Population Balances. Theory and Applications to Particulate Systems in Engineering*. Academic Press, 2000.

[65] D. Ramkrishna, D. S. Kompala, and G. T. Tsao. Are microbes optimal strategists. *Biotechnology Progress*, 3(3):121–126, 1987.

[66] A. I. Roussos and C. Kiparissides. A bivariate PBE approach for the description of microbial PHB production processes. In *Proc. 4th International Conference on Population Balance Modelling*, pages 207–225, Berlin, Germany, 2010.

[67] C. Rudolf. *Untersuchungen zum biotechnologischen Potenzial des fakultativ photosynthetischen Bakteriums Rhodospirillum rubrum und dessen Zentralstoffwechsel*. PhD thesis, Otto-von-Guericke Universität, Magdeburg, 2013.

[68] C. Rudolf and H. Grammel. Fructose metabolism of the purple non-sulfur bacterium Rhodospirillum rubrum: Effect of carbon dioxide on growth, and production of bacteriochlorophyll and organic acids. *Enzyme and Microbial Technology*, 50(4-5):238–246, 2012.

[69] F. H. Schmidt. Die enzymatische bestimmung von Glucose und Fructose nebeneinander. *Klinische Wochenschrift*, 39(23):1244–1247, 1961.

[70] S. Schuster and C. Hilgetag. On elementary flux modes in biochemical reaction systems at steady state. *Journal of Biological Systems*, 2(2):165–182, 1994.

[71] A. A. Shah, F. Hasan, A. Hameed, and S. Ahmed. Biological degradation of plastics: A comprehensive review. *Biotechnology Advances*, 26(3):246–265, 2008.

[72] L. Shang, D. Di Fan, M. I. Kim, J. D. R. Choi, and H. N. Chang. Modeling of poly(3-hydroxybutyrate) production by high cell density fed-batch culture of Ralstonia eutropha. *Biotechnology and Bioprocess Engineering*, 12(4):417–423, 2007.

[73] M. Shimao. Biodegradation of plastics. *Current Opinion in Biotechnology*, 12(3):242–247, 2001.

[74] H.-S. Song, J. A. Morgan, and D. Ramkrishna. Systematic development of hybrid cybernetic models: application to recombinant yeast co-consuming glucose and xylose. *Biotechnology and Bioengineering*, 103(5):984–1002, 2009.

[75] H.-S. Song and D. Ramkrishna. Reduction of a set of elementary modes using yield analysis. *Biotechnology and Bioengineering*, 102(2):554–568, 2009.

[76] H.-S. Song and D. Ramkrishna. Prediction of metabolic function from limited data: Lumped hybrid cybernetic modeling (L-HCM). *Biotechnology and Bioengineering*, 106(2):271–284, 2010.

[77] H.-S. Song and D. Ramkrishna. Cybernetic models based on lumped elementary modes accurately predict strain-specific metabolic function. *Biotechnology and Bioengineering*, 108(1):127–140, 2011.

[78] B. Sonnleitner, E. Heinzle, G. Braunegg, and R. M. Lafferty. Formal kinetics of poly-β-hydroxybutyric acid (PHB) production in Alcaligenes eutrophus H 16 and Mycoplana rubra R 14 with respect to the dissolved oxygen tension in ammonium-limited batch cultures. *European Journal of Applied Microbiology and Biotechnology*, 7(1):1–10, 1979.

[79] J. V. Straight and D. Ramkrishna. Cybernetic modeling and regulation of metabolic pathwaysgrowth on complementary nutrients. *Biotechnology Progress*, 10(6):574–587, 1994.

[80] P. Suriyamongkol, R. Weselake, S. Narine, M. Moloney, and S. Shah. Biotech-

nological approaches for the production of polyhydroxyalkanoates in microorganisms and plants - A review. *Biotechnology Advances*, 25(2):148–175, 2007. cited By (since 1996) 62.

[81] R. C. Thompson, C. J. Moore, F. S. Vom Saal, and S. H. Swan. Plastics, the environment and human health: Current consensus and future trends. *Philosophical Transactions of the Royal Society B: Biological Sciences*, 364(1526):2153–2166, 2009.

[82] R. C. Thompson, S. H. Swan, C. J. Moore, and F.S. Vom Saal. Our plastic age. *Philosophical Transactions of the Royal Society B: Biological Sciences*, 364(1526):1973–1976, 2009.

[83] M. Tohyama and K. Shimizu. Control of a mixed culture of Lactobacillus delbrueckii and Ralstonia eutropha for the production of PHB from glucose via lactate. *Biochemical Engineering Journal*, 4(1):45–53, 1999.

[84] C. T. Trinh, A. Wlaschin, and F. Srienc. Elementary mode analysis: A useful metabolic pathway analysis tool for characterizing cellular metabolism. *Applied Microbiology and Biotechnology*, 81(5):813–826, 2009.

[85] B. G. Turner and D. Ramkrishna. Revised enzyme-synthesis rate expression in cybernetic models of bacterial-growth. *Biotechnology and Bioengineering*, 31(1):41–43, 1988.

[86] P. Vandamme and T. Coenye. Taxonomy of the genus Cupriavidus: a tale of lost and found. *International Journal of Systematic and Evolutionary Microbiology*, 54(6):2285–2289, 2004.

[87] M. Vaneechoutte, P. Kämpfer, T. De Baere, E. Falsen, and G. Verschraegen. Wautersia gen. nov., a novel genus accomodating the phylogenetic lineage including Ralstonia eutropha and related species, and proposal of Ralstonia [Pseudomonas] syzygii (Roberts et al. 1990) comb. nov. *International Journal of Systematic and Evolutionary Microbiology*, 54(2):317–327, 2004.

[88] A. von Kamp and S. Schuster. Metatool 5.0: fast and flexible elementary modes analysis. *Bioinformatics*, 22(15):1930–1931, 2006.

[89] J. Weber, A. Kayser, and U. Rinas. Metabolic flux analysis of Escherichia coli in glucose-limited continuous culture. II. Dynamic response to famine

and feast, activation of the methylglyoxal pathway and oscillatory behaviour. *Microbiology*, 151:707–716, 2005.

[90] E. Wilde. Untersuchungen über Wachstum und Speicherstoffsynthese von Hydrogenomonas. *Archiv für Mikrobiologie*, 43(2):109–137, 1962.

[91] S. T. Wu, Y. C. Lin, and J. R. Too. Continuous production of poly(3-hydroxybutyrate-co-3-hydroxyvalerate): Effects of C/N ratio and dilution rate on HB/HV ratio. *Korean Journal of Chemical Engineering*, 26(2):411–416, 2009.

[92] E. Yabuuchi, Y. Kosako, I. Yano, H. Hotta, and Y. Nishiuchi. Transfer of two Burkholderia and an Alcaligenes species to Ralstonia gen. nov.: Proposal of Ralstonia pickettii (Ralston, Palleroni and Doudoroff 1973) comb. nov., Ralstonia solanacearum (Smith 1896) comb. nov. and Ralstonia eutropha (Davis 1969) comb. nov. *Microbiology and Immunology*, 39(11):897–904, 1995.

[93] S. Yoo and W. S. Kim. Cybernetic model for synthesis of poly-beta-hydroxybutyric acid in Alcaligenes eutrophus. *Biotechnology and Bioengineering*, 43(11):1043–1051, 1994.

[94] J. Young, K. Henne, J. Morgan, A. Konopka, and D. Ramkrishna. Cybernetic modeling of metabolism: towards a framework for rational design of recombinant organisms. *Chemical Engineering Science*, 59(22-23):5041–5049, 2004.

[95] J. D. Young, K. L. Henne, J. A. Morgan, A. E. Konopka, and D. Ramkrishna. Integrating cybernetic modeling with pathway analysis provides a dynamic, systems-level description of metabolic control. *Biotechnology and Bioengineering*, 100(3):542–559, 2008.

[96] J. D. Young and D. Ramkrishna. On the matching and proportional laws of cybernetic models. *Biotechnology Progress*, 23(1):83–99, 2007.

[97] S. T. Yu, C. C. Lin, and J. R. Too. PHBV production by Ralstonia eutropha in a continuous stirred tank reactor. *Process Biochemistry*, 40(8):2729–2734, 2005.

A. Appendix

A.1. Media for Cultivation

Table A.1.: Composition of LB medium.

Name	Molecular formula	Concentration
Tryptone		10 g/l
Yeast extract		5 g/l
Sodium chloride	NaCl	5 g/l

Table A.2.: Composition of mineral medium for *R. eutropha* [25].

Name	Molecular formula	Concentration
Carbon source		varied
Ammonium chloride	NH_4Cl	varied
Potassium dihydrogen phosphate	KH_2PO_4	2.30 g/l
Sodium hydrogenphosphate dihydrate	$Na_2HPO_4 \times 2\ H_2O$	2.90 g/l
Magnesium sulfate heptahydrate	$MgSO_4 \times 7\ H_2O$	0.50 g/l
Calcium chloride dihydrate	$CaCl_2 \times 2\ H_2O$	0.01 g/l
Ammonium iron(III) citrate	$C_6H_8O_7 \times xFe \times xH_3N$	0.05 g/l
Trace element solution SL-6	(see Table A.3)	5.00 ml/l

Table A.3.: Composition of trace element solution SL-6 [24].

Name	Molecular formula	Concentration
Zinc sulfate heptahydrate	$ZnSO_4 \times 7\ H_2O$	0.10 g/l
Manganese chloride tetrahydrate	$MnCl_2 \times 4\ H_2O$	0.03 g/l
Boric acid	H_3BO_3	0.30 g/l
Cobalt chloride hexahydrate	$CoCl_2 \times 6\ H_2O$	0.20 g/l
Copper(II) chloride dihydrate	$CuCl_2 \times 2\ H_2O$	0.01 g/l
Nickel(II) chloride hexahydrate	$NiCl_2 \times 6\ H_2O$	0.02 g/l
Sodium molybdate dihydrate	$Na_2MoO_4 \times 2\ H_2O$	0.03 g/l

Table A.4.: Composition of mineral medium for *R. rubrum* [23].

Name	Molecular formula	Concentration
Potassium dihydrogen phosphate	KH_2PO_4	2.96 g/l
Dipotassium hydrogenphosphate	K_2HPO_4	4.44 g/l
p-aminobenzoic acid	$C_7H_7NO_2$	2.85 mg/l
Sodium chloride	NaCl	120 mg/l
Vitamin solution	(see Table A.5)	10 ml/l
Ammonium chloride	NH_4Cl	varied
Carbon source		varied

Table A.5.: Composition of vitamin solution for mineral medium for *R. rubrum*.

Name	Molecular formula	Concentration
Nitrilotriacetic acid	$C_6H_9NO_6$	20 g/l
Aspartic acid	$C_4H_7NO_4$	4 g/l
Glutamic acid	$C_5H_9NO_4$	10 g/l
Potassium hydroxide	KOH	22 g/l
Magnesium sulfate heptahydrate	$MgSO_4 \times 7\ H_2O$	58.9 g/l
Ferrous sulfate heptahydrate	$FeSO_4 \times 7\ H_2O$	0.2 g/l
Nicotinic acid	$C_6H_5NO_2$	0.1 g/l
Thiamine	$C_{12}H_{18}Cl_2N_4OS$	50 mg/l
Biotin	$C_{10}H_{16}N_2O_3S$	2 mg/l
Calcium chloride dihydrate	$CaCl_2 \times 2\ H_2O$	6.6 g/l
Trace element solution	(see Table A.6)	20 ml/l

Table A.6.: Composition of trace element solution for mineral medium for *R. rubrum*.

Name	Molecular formula	Concentration
Ethylenediaminetetraacetic acid	$C_{10}H_{16}N_2O_8$	50 g/l
Zinc sulfate heptahydrate	$ZnSO_4 \times 7\ H_2O$	22 g/l
Manganese chloride tetrahydrate	$MnCl_2 \times 4\ H_2O$	5.1 g/l
Boric acid	H_3BO_3	11.4 g/l
Ferrous sulfate heptahydrate	$FeSO_4 \times 7\ H_2O$	5 g/l
Cobalt chloride hexahydrate	$CoCl_2 \times 6\ H_2O$	1.6 g/l
Copper sulfate pentahydrate	$CuSO_4 \times 5\ H_2O$	1.1 g/l
Ammonium molybdate tetrahydrate	$2(NH_4)_6Mo_7O_{24} \times 4\ H_2O$	1.1 g/l

A.2. Metabolic Reactions of *R. eutropha*

No.	Reaction
1	FRU + PEP + ATP $\longrightarrow$ F16P + PYR + ADP
2	F16P $\longrightarrow$ F6P
3	F16P $\longrightarrow$ 2 G3P
4	AMC $\longrightarrow$ NH_3
5	G6P + 2 NADP $\longrightarrow$ Rl5P + CO_2 + 2 NADPH
6	Rl5P $\longleftrightarrow$ R5P
7	Rl5P $\longleftrightarrow$ X5P
8	X5P + R5P $\longleftrightarrow$ S7P + G3P
9	S7P + G3P $\longleftrightarrow$ E4P + F6P
10	X5P + E4P $\longleftrightarrow$ G3P + F6P
11	F6P $\longrightarrow$ G6P
12	G3P + NAD + ADP $\longleftrightarrow$ 3PG + NADH + ATP
13	3PG $\longleftrightarrow$ PEP
14	PEP + ADP $\longrightarrow$ PYR + ATP
15	OXA + ATP $\longrightarrow$ PEP + ADP + CO_2
16	PYR $\longrightarrow$ AcCoA + Form
17	PYR + NAD $\longrightarrow$ AcCoA + NADH + CO_2
18	AcCoA + OXA $\longrightarrow$ ISC
19	ISC + NADP $\longrightarrow$ αKG + NADPH + CO_2
20	αKG + NAD $\longrightarrow$ SucCoA + NADH + CO_2
21	SucCoA + ADP $\longleftrightarrow$ SUC + ATP
22	SUC + FAD $\longleftrightarrow$ MAL + FADH
23	MAL + NAD $\longrightarrow$ OXA + NADH
24	PYR + ATP $\longrightarrow$ OXA + ADP
25	ISC $\longrightarrow$ SUC + GOX
26	AcCoA + GOX $\longrightarrow$ MAL
27	NH_3 + αKG + NADPH $\longrightarrow$ GLUT + NADP
28	GLUT + NH_3 + ATP $\longrightarrow$ GLUM + ADP
29	2 AcCoA $\longleftrightarrow$ AcAcCoA

30 AcAcCoA + NADPH $\longrightarrow$ P(3HB) + NADP

31 P(3HB) + NAD $\longrightarrow$ ACE + NADH

32 ACE + SucCoA $\longrightarrow$ AcAcCoA + SUC

33 SUC $\longrightarrow$ SUCx

34 2 NADH + O_2 + 4 ADP $\longrightarrow$ 2 NAD + 4 ATP

35 2 FADH + O_2 + 2 ADP $\longrightarrow$ 2 FAD + 2 ATP

36 0.21 G6P + 0.07 F6P + 0.9 R5P + 0.36 E4P + 0.13 G3P + 1.5 3PG + 0.52 PEP + 2.83 PYR + 3.74 AcCoA + 1.79 OXA + 8.32 GLUT + 0.25 GLUM + 41.1 ATP + 8.26 NADPH + 3.12 NAD $\longrightarrow$ BIO + 7.51 αKG + 2.61 CO2 + 41.1 ADP + 8.26 NADP + 3.12 NADH

All stoichiometric coefficients are given in mmol, except BIO is given in g.

Declaration of Honor

I hereby declare that I produced this thesis without prohibited external assistance and that none other than the listed references and tools have been used.

I did not make use of any commercial consultant concerning graduation. A third party did not receive any nonmonetary perquisites neither directly nor indirectly for activities which are connected with the contents of the presented thesis.

All sources of information are clearly marked, including my own publications.

In particular I have not consciously:

- Fabricated data or rejected undesired results,
- Misused statistical methods with the aim of drawing other conclusions than those warranted by the available data,
- Plagiarized data or publications,
- Presented the results of other researchers in a distorted way.

I do know that violations of copyright may lead to injunction and damage claims of the author and also to prosecution by the law enforcement authorities. I hereby agree that the thesis may need to be reviewed with an electronic data processing for plagiarism.

This work has not yet been submitted as a doctoral thesis in the same or a similar form in Germany or in any other country. It has not yet been published as a whole.

Magdeburg, July 14th, 2015

André Franz